UNIVERSIDAD AUTÓNOMA DE MADRID

ESCUELA POLITÉCNICA SUPERIOR

PROYECTO FIN DE CARRERA

CHARACTERIZATION OF ULTRASOUND TRANSDUCERS

Ingeniería de Telecomunicación

Helia Relaño Iborra

Abril 2014

CHARACTERIZATION OF ULTRASOUND TRANSDUCERS

Helia Relaño Iborra

TUTOR: Morten Fischer Rasmussen
PONENTE: Daniel Ramos Castro

Escuela Politécnica Superior
Universidad Autónoma de Madrid
Abril 2014

Resumen

El presente proyecto investiga el proceso de caracterización de transductores de ultrasonidos. Su objetivo principal es evaluar la viabilidad de un método simplificado para realizar una caracterización de este tipo centrada en las propiedades acústicas de dichos dispositivos.

Con este fin se ha estudiado un experimento consistente en la medición del campo de presión generado por una matriz de transductores de ultrasonidos. A partir de los datos obtenidos de dicho experimento, se han derivado los parámetros que caracterizan a los 32x32 elementos de esta matriz, tales como su patrón de radiación, directividad y ángulo de aceptación. En esta memoria se recogen los métodos desarrollados para obtener estos parámetros, así cómo los resultados obtenidos que, además, son comparados con otras investigaciones en curso para evaluar su validez.

Tras esta información de los datos experimentales, se ha procedido a desarrollar modelos teóricos con el propósito de optimizar la configuración del experimento estudiado de modo que sea posible obtener de forma precisa los atributos de una matriz de transductores a partir de él haciendo un uso óptimo de los recursos computacionales y de tiempo. La validez de estos modelos se ha evaluado frente a los efectos del ruido. Finalmente, basándose en los resultados obtenidos tanto del análisis experimental como de los del proceso de modelización, se proponen una serie de recomendaciones para desarrollar este tipo de experimentos.

Este proyecto pone de manifiesto las posibilidades de utilizar mediciones del campo de presión para llevar a cabo el complejo proceso de caracterización de transductores de ultrasonidos, abordando tanto el potencial como las debilidades de dicho método.

Palabras Clave: *ultrasonidos, transductores, CMUT, caracterización, directividad, campo de presión*

Abstract

This project investigates the process of characterization of ultrasound transducers. The main objective is to assess the feasibility of a simplified method to perform such a characterization, focusing on the acoustical properties of these devices.

In order to do so an experimental measurement of the pressure field generated by an ultrasound transducer array is studied. From the obtained data parameters such as the radiation pattern, the directivity and the angle of acceptance are determined for the elements of a 32x32 ultrasound probe. The methods to obtain these parameters are described in this report and the obtained results are compared with other current researches to assess their validity.

After obtaining the aforementioned information from the measurement, models are developed to optimize the experimental set-up in order to allow accurate identification of the attributes of transducer arrays making optimal use of time and computational resources. It is also studied the strength of these models against noise and bias. Finally, a series of recommendations are outlined based on the results from the experimental analysis and the modelization process.

The study brings light to the possibilities of using a pressure field measurement to carry out the complex process of characterizing ultrasound transducers while addressing both the potency and the weaknesses of such a methodology.

Keywords: *ultrasounds, transducers, CMUT, characterization, directivity, pressure field*

Acknowledgements

This project could have never been possible without the guidance and assistance of Professor Jørgen Arendt Jensen and Morten Fischer Rasmussen. I deeply appreciate the opportunity you have given me of working in the Center for Fast Ultrasound at the Technical University of Denmark, and all the help and support you have offered me throughout this months. Thank you specially Morten for all the enriching discussions and the continuous help.

I would also like to take a moment to thank my teachers in Universidad Autónoma de Madrid, from whom I first learnt what engineering was about. I am specially grateful to Daniel Ramos for his guidance in every step of this project, as well as to José María Martínez for his patience and efficiency. Also thanks to Jorge López de Vergara, my Erasmus coordinator, who made the transition to DTU so smooth and fulfilling. To Irene and everyone in the International Relations Office: thanks for helping so many of us to study abroad, I could not be happier that I chose to.

I cannot forget to thank Carlos Moreno. I already suspected it, but you have proven to me what a wonderful human being you are time and time again during this past months. Thanks for helping out whenever I needed you. To my other fellow "telecos": Ricardo Landriz, I am so immensely lucky to have had you as a partner, thanks for four years of hard work, for teaching me so much and for becoming a great friend in the process (Also, thanks for your help with all the paperwork!). Eva, Rodri and Jaime, thanks for the good times and for sharing the daily joys and frustrations.

Nina Dupont and Luca Fianchisti, I cannot find the appropriate words to thank you, but luckily we have learnt to understand each other in a mixture of languages and gestures, so I will try: thank you for keeping me healthy and sane, for the food and the conversations and for always making me laugh. You have become my family in Denmark, and I don't say that lightly.

Speaking of which, I would not be writing this lines if it wasn't for my beautiful parents Jorge and Diana, so thank you for raising me to become the person I am today, for supporting me, and for being an inspiration every day. To my brother and the rest of my crazy family: thank you for reminding me of my roots.

Finally I would like to thank my lovely friends in Spain, the amazing people I have met here in Denmark and every person that has contributed to this project in any extent. Thank you. Tak. Gracias.

Helia Relaño Iborra . Lyngby, Denmark. March 24, 2014.

Table of Contents

List of Figures

List of Tables

Glossary

List of symbols

c	Speed of sound [m s^{-1}]
f	Frequency [Hz]
k	Wave number
p	Pressure [Pa]
r	Radial distance in spherical coordinate system [m]
v	Particle velocity [m s^{-1}]
x, y, z	Cartesian coordinates
Z	Impedance [kg m^{-2}]
κ	Compressibility [Pa^{-1}]
λ	Wavelength [m]
ρ	Density [kg m^{-3}]
θ	Polar angle in spherical coordinate system [radian]
φ	Azimuth angle in spherical coordinate system [radian]
ω	Angular frequency [radians/s]

Abbreviations

1D	One dimensional
2D	Two dimensional
3D	Three dimensional
AC	Alternating Current
CMUT	Capacitive Micromachined Ultrasound Transducers
dB	Decibel
DC	Direct Current
PMUT	Piezoelectric Micromachined Ultrasound Transducers
PSF	Point Spread Function
PZT	Lead Zirconate Titanate
RANSAC	Random Sample Consensus Algorithm
SNR	Signal to Noise Ratio
ToF	Time of Flight

CHAPTER 1

Introduction

Human hearing covers a frequency range between 20 and 20.000 Hz. Beyond that threshold human beings cannot perceive sound waves and sounds are defined as Ultrasounds. Ultrasound signals have many different uses: from range finding with Sonar to motion sensors or material testing. One of the fields where they have been of special use is medical imaging.

Ultrasound imaging systems are one of the most used nowadays in the field of medical imaging. The main element in such systems is the ultrasound probe, that generates, and commonly also receives, the ultrasound signal. Analysing and defining the properties of the transducer probe is a key part in the design and optimization of medical ultrasound systems and thus the importance of characterizing ultrasound transducers.

The main goal in the design process of an ultrasound probe should be to obtain a high degree of quality in the final medical image, but the factors that affect the image quality are broader than just the transducer probe design. That is the reason why other characteristics of the transducers are used to assess their performance such as bandwidth, angle of acceptance, directivity or frequency response; and not only imaging tests. It is necessary to know and characterize the fields created by ultrasound transducers in order to design the best suited for different medical imaging techniques.

However, the process of characterizing these devices is not trivial and it involves a number of complex measurements. This project aims to assess the potency of using a single pressure field measurement to gather the relevant information needed to characterize an ultrasound transducer, focusing on its acoustic properties. In the present study a method for characterizing ultrasound transducer arrays is investigated, based on ultrasound field measurements and the use of models.

To put this investigation in context with the historical findings and current research, this chapter will briefly summarize the history and the state of the art of the characterization of ultrasound transducers. Consequently the objectives, purpose and scope of this project will be addressed at length.

1.1 Historical Review

Transmission of ultrasound waves dates back to the early 20th century. In the beginning its main application was underwater transmission to detect submarines, and it was used widely during World War I [21]. Concurrently the piezoelectric effect, i. e. the electro-mechanical transformation produced in

crystalline materials that was discovered in the late 19th century by Pierre and Jacques Curie, was being thoroughly investigated leading to the development of the first ultrasound transducers by Paul Langevin using quartz crystals, although the first transducers were not used until World War II.

Between 1939 and 1945, other uses of ultrasounds were being investigated. One of the main applications was flaw detection in materials, as well as the measurement of materials thickness. Also further investigation was put into piezoelectric materials with the use of ferroelectrics (materials with a spontaneous electric polarization), that rapidly became the most popular choice in the development of ultrasonic transducers.

After World War II, the knowledge gained in the ultrasounds research field was used to study physical phenomena such as magnetoacoustic oscillation in metals, the effect of dislocations and impurities on sound wave propagation and spin-phonon and nuclear spin interactions in solids, among thers. A more comprehensive list of the applications of ultrasound in physics and pertinent explanations can be found in [21].

One of the most important applications of ultrasound is its use in the medical field. From the beginning, two main uses of ultrasound waves in the medical field were investigated. On the one hand, low intensity ultrasounds was proven to allow differentiation between distinct kinds of soft tissue, leading to the development of acoustic imaging systems. At the same time, the potential of high intensity ultrasound for medical interventions was researched.

The first investigations on the interactions of ultrasounds with live tissue can be found as early as the 1920s, [22], and the research has been carried out steadily since then, although it was not until the decades of the sixties and seventies when doctors and hospitals started to regard ultrasound as a valid diagnostic and treatment tool. Some of the research areas included the investigation of the irreversible effects of ultrasound on tissue and the potential dangers of ultrasound radiation in humans. These studies led to the definition of ultrasound imaging as a non-invasive technique. In comparison with X-rays or nuclear imaging techniques, ultrasound imaging was solely based on the nature of the human tissue, and the change in impedance between different types of tissue.

Throughout the years, techniques to apply ultrasounds on isolated tissue, *in vitro*, and in living tissue, i.e. *in vivo*, have been developed, as well as *Doppler imaging* that allows the recording of velocities of moving objects, which makes it relevant to assess the flow of blood through the human body. Color images and flow representation systems were developed in the mid eighties and in the nineties 3D imaging was made possible using ultrasounds. Some of the most common and well-known procedures that use ultrasounds are the imaging of the developing foetus and the imaging of the heart.

Since the beginning of the development of these techniques an special effort was made to involve the medical community and physicians in the process of the development of better ultrasound systems. More and more compact systems are being build and the ease of usage of such systems has improved through the years. Today ultrasound imaging can be performed in a doctor's office or even transported between different rooms in a hospital.

This relative simplicity of the technique, together with its non-invasive nature, has allowed the ultrasound imaging technique to be accepted by the medical community as a useful tool and made it one of the most

popular imaging techniques nowadays.

References [1], [2] and [22] give a more thorough overview of the history of medical ultrasound.

1.2 State of the Art

Transducer arrays have been in the center of the medical ultrasound research for many years. Both capacitive and piezoelectric transducer arrays have been investigated for various applications and purposes, as shows the extensive literature on the topic. Different piezoelectric materials, like quartz, lead zirconate titanate (PZT), zinc oxide or aluminum nitride, have been investigated. Although PZT is the most popular choice, studies like [5] have tried to analyse transducers that use other materials, taking advantage of lower fabrication costs.

In the last 20 years the interest in characterizing ultrasound transducers and transducer arrays has been focusing on Capacitive Micromachined Ultrasound Transducers (CMUTs) [4]-[7]. Since their invention in 1994 in Stanford University [12], CMUTs have become an interesting alternative to the traditional piezoelectric transducers. *"CMUT technology is not simply a low-cost replacement of piezoelectric transducer technology. Many features inherent in CMUT technology enable revolutionary advances in ultrasound imaging"*, [8]. Consequently, comparative studies between both technologies have been carried out as function of different parameters. For instance in [4], Meyner et al. compared two arrays, one CMUT and one Piezoelectric Micromachined Ultrasound Transducer (PMUT), in terms of electrical impedance, electroacoustic-performances, and radiation patterns, concluding that CMUT arrays have a better bandwidth but a lower pulse sensitivity.

Studies to prove the viability of CMUTs as the natural evolution of transducer technologies have been performed ever since they were presented in the nineties, when they were proposed as efficient broadband ultrasonic transducers. Haller et al. developed the first micromachined ultrasonic transducer, [12], and already showed the future projection of such devices in terms of the bandwidth (around four times better than that of a piezoelectric transducer) and the possibilities of integration with control electronics. Other advantages found in these early works were the lower temperature sensibility and the shorter pulse length.

CMUTs allow the fabrication of large arrays of transducers with relative ease and a low cost [10]. CMUTs consist of two-plate electrodes (capacitor cells) that are biased with a continuous voltage (DC). When an alternating current (AC) excites them, they produce a vibration that, in turn, generates the needed acoustic waves. The reciprocal phenomenon also takes place, meaning that if the biased electrode receives an ultrasound signal it generates a current output due to the capacitance change, [8]. The process of design and fabrication has been covered in many articles in the last years, focusing on different materials, and techniques, [10]-[12].

In the 2000s different investigations proved the viability of CMUTs for ultrasound imaging. In [8] Oralkan et al. showed imaging results for wired phantoms using 1-D transducer arrays, the Point Spread Function (PSF), was used to measure the effects of the wide-band transducers in B-scan mode images. Axial resolution (the ability of the system to distinguish between objects closely placed in the axial direction) was shown to improve at shorter ultrasonic pulses. Signal to Noise Ratio improvements were also shown.

However, imaging results are not only dependent on the transducer characteristics, since they are also dependent on the signal processing applied and on the electronics of the ultrasound system. That is why other tests are performed in order to assess the quality of transducer arrays by means of determining electrical impedance, electro-acoustic performance, radiation pattern, heating of the array, etc.

Such experiments for the whole array are presented in, among others, [4]. Other investigations both have evaluated characteristics of the array and of each single isolated element. In [6], Jin et al. presented a set of experiments, and compared the results with models based on the electrical equivalent circuit of a CMUT. This model was also addressed and investigated in [11]. Both investigations showed good agreement between measurements and models, pointing to this model as a relevant tool for designing and implementing transducer arrays.

Different experimental set-ups have been used to evaluate the characteristics of the transducer arrays: echoes can be generated by reflecting surfaces in order to assess the emitting/receiving performance, or a hydrophone can be used to measure the pressure field generated by the transducer [4], [6].

Other studies have focused in different applications, like dual modality high frequency operations [4], underwater applications [5], operations under high pressures [9] orvolumetric imaging [11], among others. The set up for characterization does not broadly vary, even if the final use of the transducer changes, and the procedure of design and characterization, using models and finite element simulation, remains somehow unchanged no matter the application.

Another important line of investigation that is being followed by a number of researchers in recent years is that of the crosstalk phenomenon. It refers to the interaction between elements of a transducer array and has been shown to affect the directivity and radiation pattern of the array. This phenomenon has also been shown to increase the acoustic noise in measurements performed with transducer arrays and in the resulting images, [23], [24]. [6]-[8], and [16] have acknowledged this and have been able to shown deviations from measured to modelled results in terms of crosstalk.

In general, the process of design, fabrication, characterization and integration of ultrasound transducers has been researched thoroughly in the last two decades. Special relevance has been given to the possibilities that microelectronics have brought to the table and the development of accurate models that can predict the behaviour of these devices that are key to the development of robust ultrasound imaging systems.

1.3 Motivation

As seen in the previous sections, ultrasound transducers have been widely studied and developed from a multidisciplinary perspective that has involved many scientific fields, like chemistry, electronics, acoustics and medicine in the past century and still does in the present.

The literature discussed above shows, first of all, the extreme importance that has been given to the adequate characterization of ultrasound transducers. A sharp analysis of the characteristics of such elements is decisive for the acquisition of valid data that can lead to good quality ultrasound images. Secondly, it

shows it is a research field that is being pursued currently, with articles and findings published in the last 20 years, but also plenty of them recently (up to even 2013).

The intention of this project is then to further investigate within this area, with the aim of finding a compact way to characterize ultrasound transducer arrays. Since characterization is a difficult process that needs of highly skilled and experienced professionals, as shown in [4]-[16] and others, this work aspires to find a less arduous procedure that still allows characterizing ultrasound transducers.

According to the Dictionary of Cambridge, Characterization is *"the way in which something is described by stating its main qualities"*, [25]. So when one is faced with a project such as *Characterization of Ultrasound transducers* the first thing that should be taken into consideration is, precisely, what are the main qualities of Ultrasound transducers, and how can those qualities be determined and stated.

Ultrasound transducers' characterization is a difficult task, since transducers are complex electromechanical devices, thus involving a combination of electrical and mechanical components, [27]. As it can be found in literature, there are many parameters that define ultrasound transducers based on their acoustic, electrical or chemical properties. In this project the focus will be on the acoustic parameters, based on pressure field measurements. Other characteristics such as electrical impedance, transmit and receive response or heating of the devices are out of the scope of this project. Reference is made to [4]-[16], [21] and [23]-[24], that present experiments to determine some of these parameters.

1.4 Objectives

The main goal of the present project is to define a characterization procedure of the acoustical properties of ultrasound transducers based on a pressure field measurement.

For this purpose two main objectives are pursued. The first one is to find how much information can be gathered from a measurement performed on an emitting transducer array. With this goal in mind data measured in June 2012 will be processed in order to estimate the array element positions, the directivity of these elements, their radiation patterns and their angle of acceptance.

The second objective will be to develop models to represent a measuring set-up, and test their behaviour in the presence of noise and with the modification of different set-up parameters to design an optimal experiment that could potentially gather all the data needed to accurately determine ultrasound transducers' properties.

1.5 Structure

After this introductory chapter, the theory needed to understand the methods and results of this project will be introduced in **Chapter 2**.

Consequently, **Chapter 3** deals with characterization parameters and the methods to obtain them from pressure field measurements' data.

Chapter 4 is dedicated to present models of experimental set-ups and the different tests these models were subjected to in order to assess the possibilities that different arrangements offer in terms of efficiency and accuracy.

Finally **Chapter 5** will summarize the results and conclusions reached in this investigation, and also will point out the research possibilities left open for further development in this research area.

CHAPTER 2

Theoretical Background

2.1 Medical Ultrasound Systems

Ever since the discovery of the possibilities of ultrasound for diagnostic imaging it has become one of the most popular imaging techniques, due to its non invasiveness as well as its portability and ease of use.

From the users point of view, i.e. the medical professional, ultrasound systems are compact, fast and easy to use, while giving images that can help monitor and diagnose cardiology problems, cancer cysts, pregnancies and blood flow among other conditions. Figure 2.1 illustrates such a system.

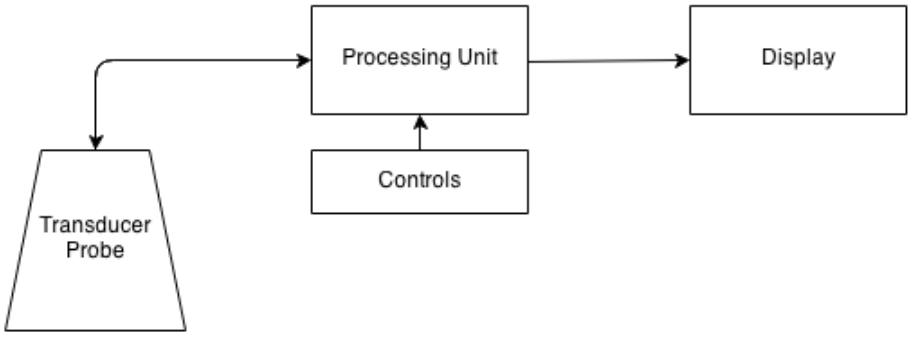

Figure 2.1 – Medical Ultrasound System

The functioning principle is that the transducer generates ultrasound signals that travel through the patient's body generating echoes by scattering and by reflection due to the difference in characteristics of the tissues of the human body they encounter. These echoes are received back in the transducer and are later processed by the imaging system that then displays a 2D grayscale image of the human body.

This project focuses on the first part of ultrasound imaging systems, the transducer probe. The processing of the ultrasound signal and the imaging techniques that render the final ultrasound diagnostic image are left out of its scope.

2.2 Ultrasound Physics

2.2.1 Ultrasound Waves

Ultrasounds are sounds of higher frequency than that of the audible region of human beings, that is to say with frequencies over 20 kHz. They are described by the theory of acoustics. Ultrasound waves propagate by compression and expansion of the material they are travelling in, manifesting themselves as pressure fluctuations where no mass displacement occurs. Generally when dealing with medical ultrasound, the waves are longitudinal, meaning that the expansion and compression happens in the same direction as that of propagation of the wave, although research is being conducted on the possibilities ultrasonic transverse waves could offer in the medical field.

The speed of such waves is dependent on the material they are propagating in and is defined as:

$$c = \sqrt{\frac{1}{\kappa\rho}} \tag{2.1}$$

Where κ is the compressibility of the material and ρ its density. The characteristic impedance of a medium is given by the speed of sound in the medium and its density as:

$$Z = \kappa\rho \tag{2.2}$$

The characteristic impedance relates, for longitudinal waves, the acoustic pressure to the particle velocity generated through the wave's transmission:

$$p = Zv \tag{2.3}$$

The acoustic pressure is defined as the time-varying pressure deviation of the static ambient (barometric) pressure of the medium, [3].

Waves are defined by the linearised wave equation [3], that can be expressed in terms of pressure as:

$$\nabla^2 p = \frac{1}{c^2}\frac{\partial^2 p}{\partial t^2} \tag{2.4}$$

Where ∇^2 is the 3D Laplacian operator given by:

$$\nabla^2 = \frac{\partial^2}{\partial x^2} + \frac{\partial^2}{\partial y^2} + \frac{\partial^2}{\partial z^2} \tag{2.5a}$$

$$\nabla^2 = \frac{1}{r^2}\frac{\partial}{\partial r}(r^2\frac{\partial}{\partial r}) + \frac{1}{r^2 sin\theta}\frac{\partial}{\partial\theta}(sin\theta\frac{\partial}{\partial\theta}) + \frac{1}{r^2 sin^2\theta}\frac{\partial^2}{\partial\varphi^2} \tag{2.5b}$$

Two coordinate systems are shown: linear and spherical coordinates, respectively. This is done because of the importance that both plane waves and spherical waves have when explaining wave propagation.

Plane waves vary only in one spatial direction and are the solutions to the 1D wave equation:

$$\frac{\partial^2 p}{\partial z^2} = \frac{1}{c^2}\frac{\partial^2 p}{\partial t^2} \tag{2.6}$$

The general solution of this equation is of the form:

$$p = f(ct - z) + g(ct + z) \tag{2.7}$$

Where f and g are continuous functions whose shape will be determined by the initial conditions given for the equation. They represent, respectively, an acoustic disturbance travelling in the z-direction with the speed c and a similar wave travelling at the same speed in the opposite direction. A particular solution that satisfies the wave equation is that of the harmonic plane wave that travels in the positive axial direction. It is defined as:

$$p(z,t) = p_0 exp(j(\omega t - kz)) \tag{2.8}$$

Here ω is the angular frequency, and k the wave number. These quantities are related as follows:

$$k = \frac{\omega}{c} = \frac{2\pi}{\lambda} \tag{2.9}$$

Where λ is the wavelength of the propagating plane wave.

On the other hand, spherical waves must satisfy the spherical wave equation given by:

$$\frac{1}{r}\frac{\partial^2}{\partial r^2}(rp) = \frac{1}{c^2}\frac{\partial^2 p}{\partial t^2} \tag{2.10}$$

The general solution has the form:

$$p = \frac{1}{r}f(r - ct) + \frac{1}{r}g(r + ct) \tag{2.11}$$

In this case f and g are referred to as outward travelling wave and inward travelling wave, respectively. It can be seen that the pressure of such waves is only dependent on time and on the radial distance from the source. The inward travelling wave in ultrasounds can cause problems when propagating into the ultrasound probe, that is why a great amount of research is made on investigating backing materials of the transducers, in order to attenuate or dampen this wave, [26]. A particular solution for the spherical wave equation is:

$$p(r,t) = p_0(r) exp(j(\omega t - kr)) \tag{2.12}$$

Spherical waves are of importance when describing pressure fields generated by ultrasound systems as well as other phenomena in ultrasound fields like scattering.

2.2.2 Propagation, Energy and Intensity

As waves travel through space, a change in energy is generated: the excited particles will have kinetic energy, whereas the particles not yet excited by the wave will present an amount of potential energy. The addition of the density of those energies gives the acoustic energy density:

$$w = w_k + w_p = \frac{1}{2}\rho v^2 + \frac{1}{2}\kappa p^2 \tag{2.13}$$

It is also interesting to characterize the energy that moves along with the wave. Such quantity is expressed by means of the acoustic intensity, or acoustic energy flux:

$$I = pv \tag{2.14}$$

The acoustic energy and the acoustic intensity are related by the principle of conservation of energy that states:

$$\frac{\partial I}{\partial x} + \frac{\partial w}{\partial t} = 0 \tag{2.15}$$

This relation also describes the way power propagates with acoustic waves.

A propagating wave is subject to attenuation due to the dissipation of thermal energy to the medium (absorption), to the generation of secondary spherical waves (scattering) and to mode conversion. The total attenuation effect depends on the medium of propagation and can be modelled by the amplitude attenuation factor , μ_a or its logarithmic equivalent, the attenuation coefficient α.

Given an acoustical wave $p(z,t) = A_0 f(ct - z)$ the amplitude of the travelling wave will depend on the spatial position as:

$$A_z = A_0 e^{-\mu_a z} \tag{2.16}$$

The absorption coefficient is defined as $\alpha = 20(log_{10}e)\mu_a$ and is dependent both on the material and on the frequency of the wave signal.

Scattering and reflection will not be treated in depth here, despite their importance in ultrasound medical imaging, because they are out of the scope of this project. Instead, in the following sections the more concrete background for this study, being the characteristics and properties of ultrasound transducers, will be discussed.

2.3 Ultrasound Transducers

The elements in charge of emitting ultrasound waves, and thus generating the resulting pressure field are the ultrasound transducers. They also produce the inverse effect, that is they generate an electrical signal when they receive an acoustic wave.

2.3.1 Piezoelectric Transducers

Piezoelectric materials are those that generate an electrical potential when they are subject to pressure and also suffer a displacement when they are exposed to an electric field. They act both as sensors and actuators, this means they are able to produce and detect acoustic waves. The most common material used in piezoelectric medical transducers is Lead zirconate titanate (PZT).

The behaviour of such materials can be characterized in terms of their transmitting constant d, which is the strain produced by a unit of electric field (in m/V) and their receiving constant g being the potential produced by a unit of stress (in V/(N/m)). For PZT, $d = 300 \times 10^{-12}$ m V^{-1} and $g = 2.5 \times 10^{-2}$ V/(N/m) [2].

Piezoelectric materials vibrate sinusoidally after their exposure to an electric field has ended. The frequency of that oscillation is known as the fundamental resonance frequency of the transducer, and is closely related to the thickness of the crystal:

$$f_0 = \frac{c_c}{2L_c} \tag{2.17}$$

Where c_c is the speed of sound in the transducer and L_c is the thickness of the transducer. The piezoelectric is backed by a highly absorbent epoxy to reduce the excessive vibrations. Also a matching layer is added to perform impedance matching between the piezoelectric element and the human skin, thus

maximizing the emission of energy, [1]. The design of this layers will depend on the final applications of the transducer.

2.3.2 Transducer Arrays

The simplest transducer system is known as a transducer probe. To allow real time imaging, this ultrasound beam must be scanned within the body. Modern systems use mechanical or electrical means to achieve this. It is in this category of electrical scanners that transducers arrays fall. They consist of multiple transducers that can be arranged in various manners to compose linear arrays, curved arrays or the phased arrays first developed in the early eighties.

When designing multi element piezoelectric transducers a trade-off must be reached between bandwidth and energy efficiency, [4]. This can be achieved by different backing of the transducers and multiple impedance matching layers.

The most common types of ultrasonic transducers are capacitive (CMUT) and piezoelectric (PMUT) micro ultrasonic transducers, [5]. Microfabricated transducers have become more and more popular with the advances of microelectronics.

As ultrasound propagation is assumed to be lineal the field generated by multiple piezoelectric elements can be calculated as the sum of the fields produced by each of them, as discussed in [17].

Many aspects can be used to define and characterize a transducer. Below, some of the chosen characterization parameters for this investigation are defined in order to facilitate the understanding of the following sections:

Radiation Pattern is defined as the spatial distribution of the ultrasound field generated when the transducer emits a signal, [4].

Directivity Pattern is defined as the distribution of the emitted energy in relation to the angle to the normal of the transducer face. It must be noted, that theoretically, it is a far-field concept, even so normally it is not measured far away from the transducer, [18].

Angle of acceptance is defined as the angle at which the emitted energy has decreased a specific amount compared to the maximum. Generally, when the energy is expressed in decibels (dB) the acceptance angle is the one relative to the -3 dB point, although sometimes it is interesting to research the -6 dB or -12 dB points, [20].

CHAPTER 3

Characterization Parameters

This chapter deals with the process of obtaining transducer's information from the data acquired from a measurement of the pressure field generated by an emitting ultrasound array. The analysis of this data would lead to the characterization of ultrasound transducers.

The parameters chosen to achieve the acoustic characterization of these devices are discussed in this section and the process to obtain their values is depicted. Firstly, the experimental set-up is described and consequently the steps for analysing and gathering information about a transducer are covered.

3.1 Description of the Experiment

The available data comes from measurements carried out in the Technical University of Denmark in June 2012. The measurements were performed in a water tank with an emitting 32x32 2D transducer array using a Onda HGL-0400 Hydrophone (see Appendix B for the data sheet of the device) to receive the signal.

The transducer array's layout is shown in Figure 3.1, it consists of 1024 elements distributed with a 0.3 mm separation. Additionally 3 rows are left without elements, as is shown in the diagram.

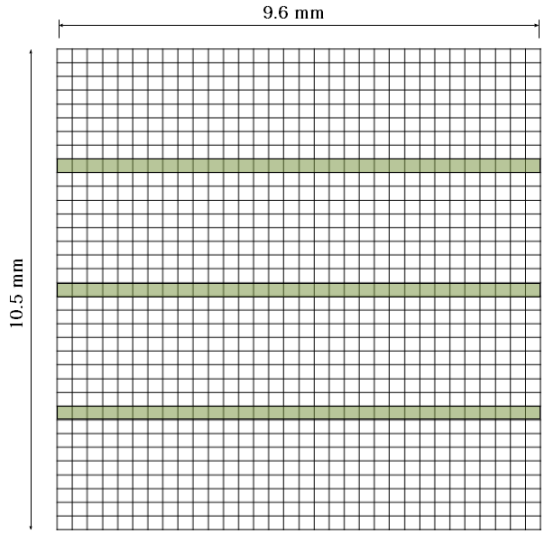

Figure 3.1 – Transducer array schematic. Shadowed rows indicate no presence of transducer elements

The information provided by the manufacturer of this transducer array can be found in Appendix A. It includes information about the elements' sensitivity and their typical impulse response, among other data. In this study the focus would be in the acoustic characterization of the device based on the data obtained for the experiment described in this section.

In this experiment the transducer array is placed inside the water tank as seen in Figure 3.2, while the hydrophone is moved around the tank to sample the generated field. By doing so a total of 643 measuring positions were used. These positions had two depths in the z-direction, 1 cm and 2 cm away from the transducer, with 329 and 324 measurement points in each plane, respectively. In the xy-plane the coordinates were distributed randomly between -20 mm and +20 mm in both x and y direction, where the center of coordinates was assumed to be the center of the transducer array.

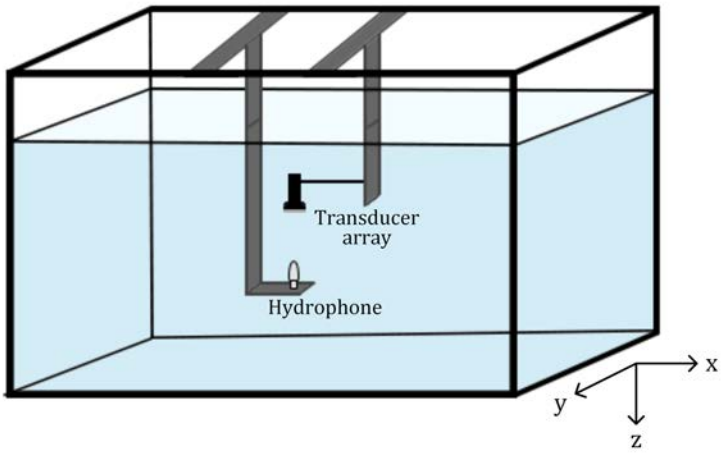

Figure 3.2 – Experiment set-up

For each position of the hydrophone, each element of the array emitted four periods of a sinusoidal signal with a 3.5 MHz frequency. Such a signal is plotted in Figure 3.3. Each of this signals was generated by applying a continuous (DC) voltage bias and a small AC signal to excite the element. Since the transducer array is a 32x32 array, the hydrophone performed 1024 measurements for each position.

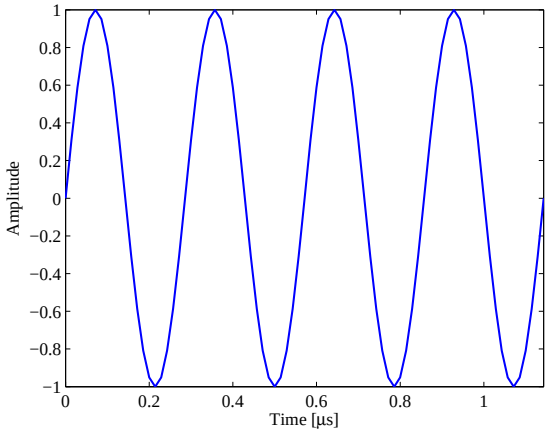

Figure 3.3 – Emitted wave

The received signal was measured with a sampling frequency of 70×10^6 samples/s and each position was assigned a set of coordinates that took the center of the transducer array as origin. For each position of the hydrophone the logged data includes the pressure measured in 1888 samples, the coordinates of the measuring position as well as information about the experiment such as the number of emissions or the samples of the emitted signal among other parameters.

It must be noted that the recorded signal, meaning the pressure wave received in the hydrophone, is actually an integration of the pressure received over the surface of the hydrophone, that has a circular ending with a 3 mm diameter, as it is shown in figure 3.4.

To sum it up, the data to analyse consists of 643 datasets, one for each hydrophone position, with those datasets composed of 1024 measurements each corresponding to one of the transducer array elements. The fact that each array element is recorded in a separate emission allows characterization of each single element within the array.

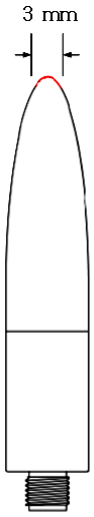

Figure 3.4 –
Diagram of the hydrophone used in measurements. Red line indicates the integration surface

3.2 Speed of Sound Calculation

In order to work with these data to obtain the characterization parameters, firstly a coordinate system must be established that includes both the array elements and the measurement positions. That is to say, the location of each element of the array must be determined by assigning them a unique coordinate. This will be achieved by making use of the time that the wave uses to travel from the transducer element to the hydrophone, also known as the time of flight.

Since the experiment was carried out in water it is important to establish at which speed the emitted ultrasound wave travelled in this medium to be able to calculate the time of flight. As it was defined in equation (2.1) the speed of sound in a medium is related to its density and compressibility. For water in normal conditions it is assumed to be 1480 m/s. However, the water in the tank was not kept under the same conditions throughout the whole set of measurements, the temperature of the water increased due to heating of the electronics involved and thus, the speed of sound cannot be assumed to be the same for all the measurements of the hydrophone.

Since the speed of sound is a key quantity to evaluate wave transmission, it is necessary to calculate the different speeds that were assumed for each measurement. A first problem involves the lack of temperature data, since only a small set of times and temperatures were logged in the course of the experiment. It becomes necessary to make some assumptions regarding the temperature conditions, specifically that the temperature increased linearly with time during the experiment's run. The logged temperatures and the assumed model can be seen in Figure 3.5.

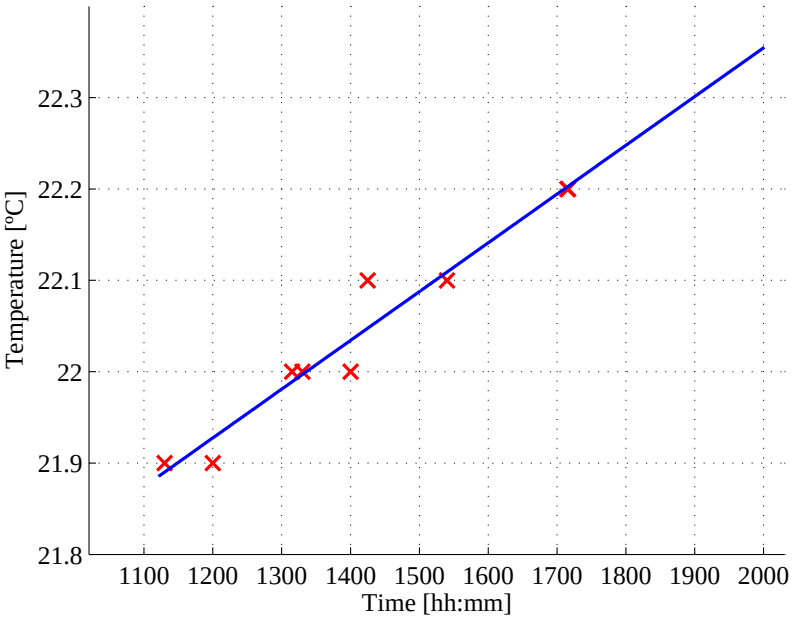

Figure 3.5 – Temperature model. Crosses indicate the logged temperatures during the experiment, and the blue line represents the model assumed for the temperature increase

"A simple and accurate formula" for the estimation of speed of sound in water was developed by J. Lubbers and R. Graaff in 1998, [14]. It relates the speed of sound , c, to the temperature of water, T, and can be condensed in the following equation:

$$c = 1405.03 + 4.624 \cdot \mathrm{T} - 3.83 \times 10^{-2} \cdot \mathrm{T}^2 \tag{3.1}$$

Using this model, 643 values for the speed of sound have been generated, one per measurement position. The estimated speed of sound in terms of both temperature and time of the measurements is plotted in Figure 3.6. As it can be seen in the figure the speed of sound variation through time is of around 2 $\mathrm{m\,s^{-1}}$.

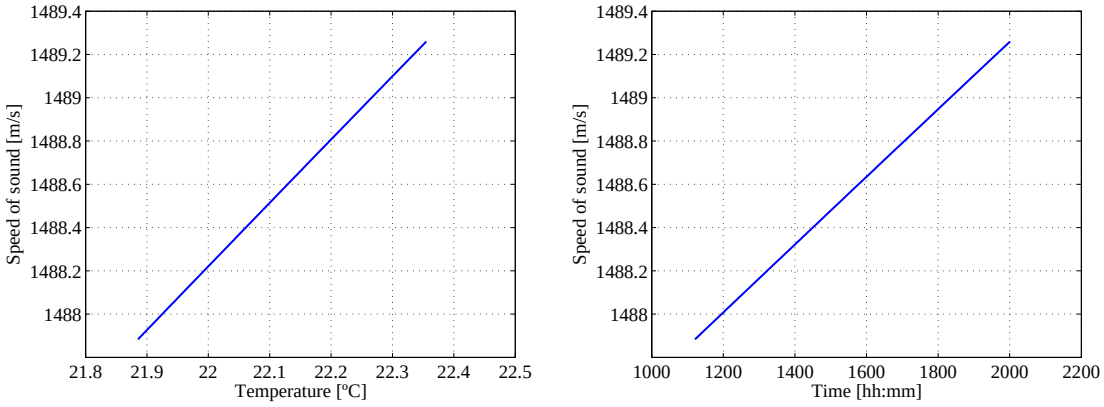

(a) In relation to temperature

(b) In relation to measurement time

Figure 3.6 – Speed of sound values

3.3 Time of Flight Calculation

As explained before, the only spatial references included in the data set are the coordinates of each of the measurement positions. In order to characterize the elements of the transducer array their positions must be estimated within the spatial coordinate system defined by the hydrophone positions.

To do so, the relation between speed, distance, and time, shown in equation 3.2 can be used.

$$d = t \cdot c \tag{3.2}$$

If the time it takes the wave to travel from the transducer to the hydrophone can be estimated, then a simple multiplication with the speed of sound values found in section 3.2 will allow finding the distances between the device and each of the array elements.

Two approaches were taken for this calculation and are described in the following sections. Figure 3.7 shows the steps taken in each of the methods followed:

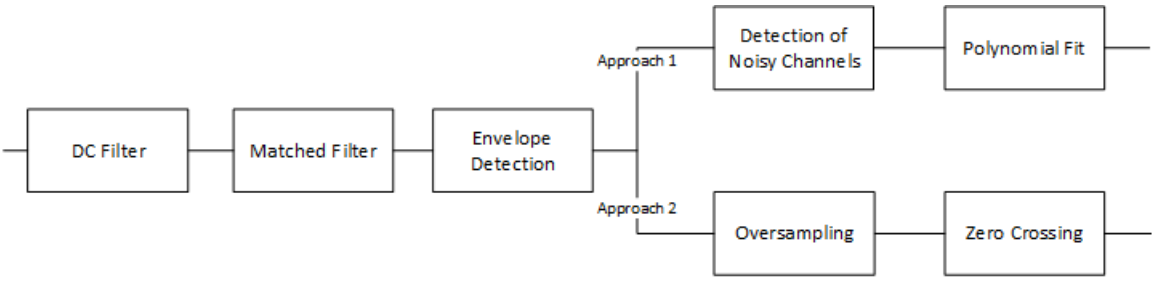

Figure 3.7 – Block diagram for the polynomial approximation of the time of flight

In both approaches the first steps include basic signal processing to make the data easier to process by getting rid of the continuous bias and minimizing the effects of noise. After that, a first rough value of the time of flight is estimated making use of the envelope of the signal. It is after this that the two methods diverge, one using a polynomial fitting strategy while the other uses a zero crossing methodology.

This process is applied for each of the 643 measurements and to al 1024 submeasurements in them corresponding to the 1024 elements of the array.

3.3.1 DC Filter and Matched Filter

The first step is to handle the data to make it easier to process. In that regard first a DC Filter is applied in order to get rid of the continuous bias of the signal, and then a matched filter is applied to reduce noise in the data.

DC filtering removes the continuous voltage that was used to bias the transducer element. The matched filtering improves the signal to noise ratio (SNR) by correlating the known emitted signal (see Figure 3.3) with the measured samples, in order to detect this signal in the hydrophone meadured data.

A filter is considered to be matched to a signal when its impulse response is a delayed and time reversed version of that signal. Let the original signal be denoted as $s(t)$, then the impulse response of its matched filter will be:

$$h(t) = s(T - t) \tag{3.3}$$

The the output signal of such a filter is, as linear systems' theory indicates, the convolution of the input signal with the impulse response of the filter.

$$\begin{aligned} r_{mf}(t) = r(t) * h(t) &= \int_{-\infty}^{\infty} r(\alpha)h(t-\alpha) \\ &= \int_{-\infty}^{\infty} r(\alpha)s(T-t+\alpha) \end{aligned} \tag{3.4}$$

Where $r(t)$ indicates the measured signal in the hydrophone and $r_{mf}(t)$ the signal after the matched filtering is performed. These derivations are also true in the case of the actual discrete signals gathered after the sampling of the continuous signal, $r[n]$. In this case the convolution is expressed as:

$$\begin{aligned} r_{mf}[n] = r[n] * h[n] &= \sum_{m=-\infty}^{\infty} r[m]h[n-m] \\ &= \sum_{-\infty}^{\infty} r[m]s(N-m+m) \end{aligned} \tag{3.5}$$

The effect of this process is illustrated in Figure 3.8 for measurement number 250, taken at the position with coordinates [-16.3, 2.0, 20.0] mm. It can be seen in the figure that the DC filtering does not affect the signal to noise ratio of the samples, but gets rid of the DC offset of the signal. The process of match-filtering does indeed improve this ratio by means of comparing and localizing the sent signal in the measured samples.

After this first treatment of the received signal the data is ready to be further investigated in order to find the time of flight, as will be discussed in the following sections.

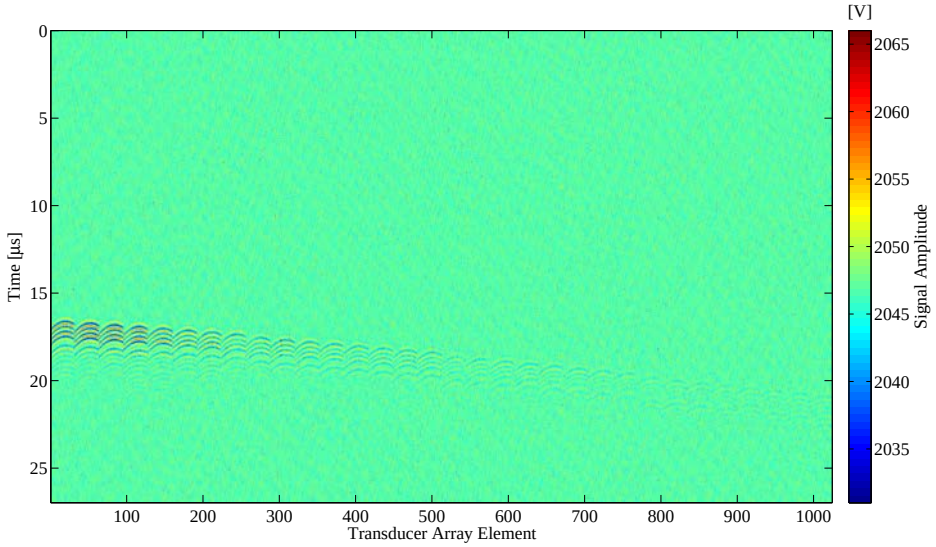

(a) Original Measurement

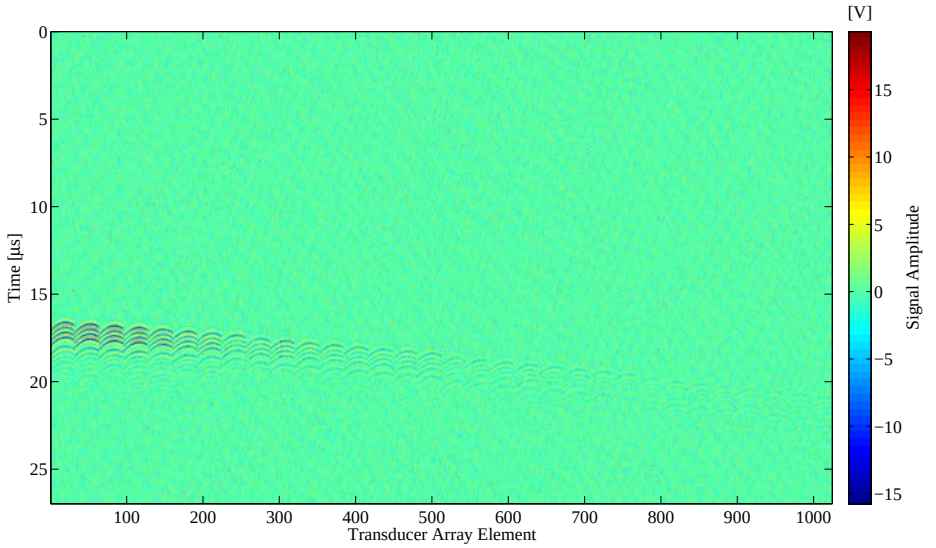

(b) Samples after DC Filtering

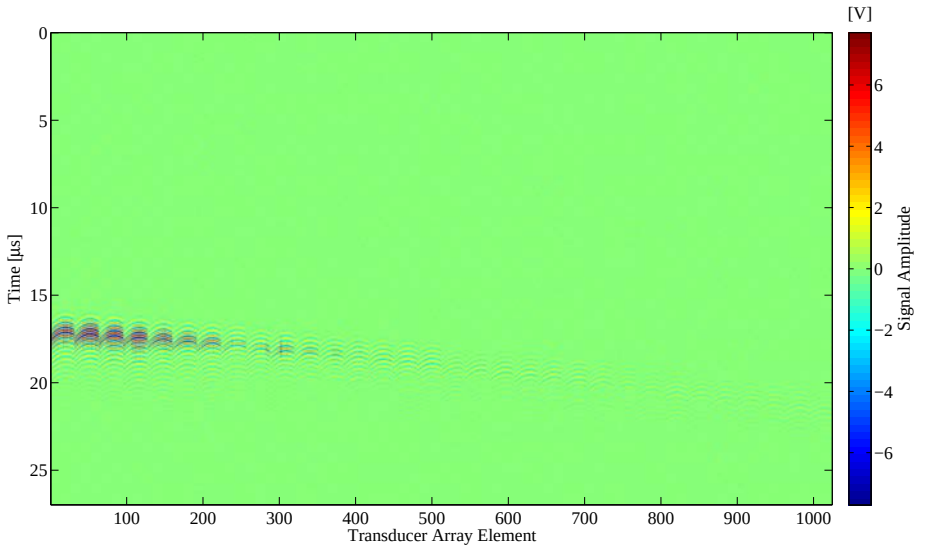

(c) Samples after matched filtering

Figure 3.8 – Samples obtained in measurement number 250 with coordinates [-16.3, 2, 20] mm

3.3.2 Rough Time of Flight Calculation

The time of flight denotes the time that takes the wave to travel from the transducer element to the hydrophone.

Because the measured signal is discrete the time of flight can be found in terms of a sample delay. A first value for the sample delay that the signal suffers travelling from the transducer to the hydrophone is calculated by detecting the maximum value of the correlation between emitted and received waves. This is done by detecting the maximum value of the envelope of the output of the matched filter described in the previous section.

The envelope detection process is carried out by generating the analytic signal of the input samples using the Hilbert transform. In general, the envelope, e_r of a given signal $r(t)$ is defined as:

$$e_r = \sqrt{r(t)^2 + \hat{r}(t)^2} \tag{3.6}$$

Where $\hat{r}(t)$ is the analytical signal of the input, defined as:

$$\hat{r}(t) = r(t) + jH(r)(t) \tag{3.7}$$

As it appear is equation 3.7 this is a complex signal whose real component is the original signal and whose imaginary component is the Hilbert transform of the original signal. Again, discrete-time analogous derivations of equations 3.6 and 3.7 can be made for the discrete signals sampled in the hydrophone.

The results of this process are shown in Figure 3.9. Element number 700 and hydrophone measurement position 250 have been chosen as illustration.

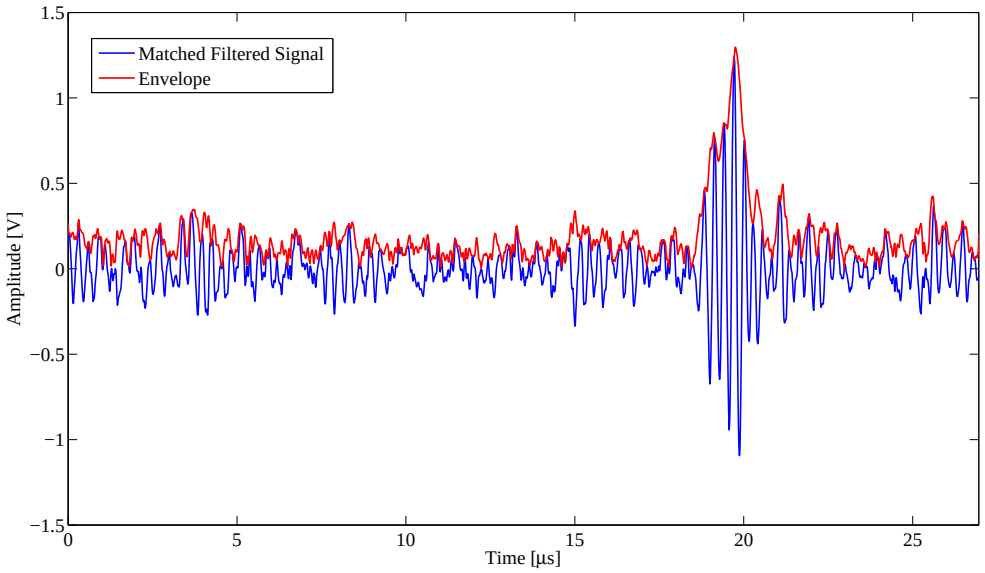

Figure 3.9 – Correlation of emitted and received signal, in blue, and the absolute value of its envelope, in red. For position 250 and transducer element 700

The sample at which this peak is found are considered as a first estimate of the sample delay of the signal. The transformation from samples to time is straightforward making use of the sampling frequency used during the measurements that is known to be 70×10^6 samples/s:

$$t = \frac{samples}{f_s} \tag{3.8}$$

The results for measurement position 250 are shown in Figure 3.10 for the 1024 transducer elements.

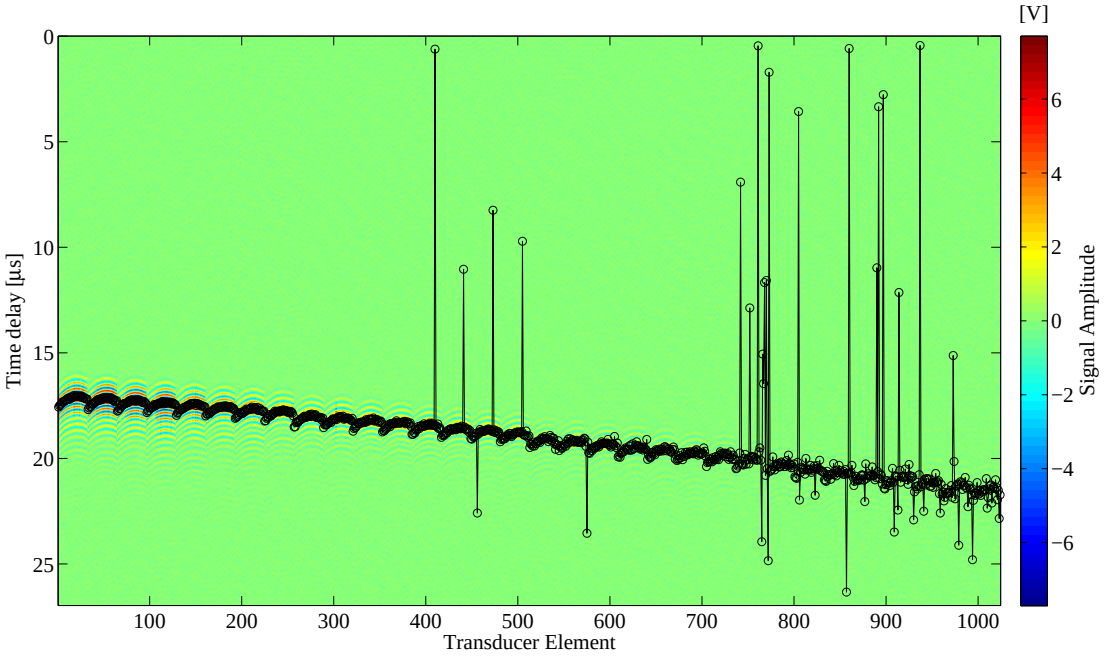

Figure 3.10 – Received signal and calculated time of flight for measurement 250

A close-up of the region of interest is shown in Figure 3.11. Both this one and Figure 3.10 show that the results obtained for the time of flight are not smooth and present a high degree of variabilty.

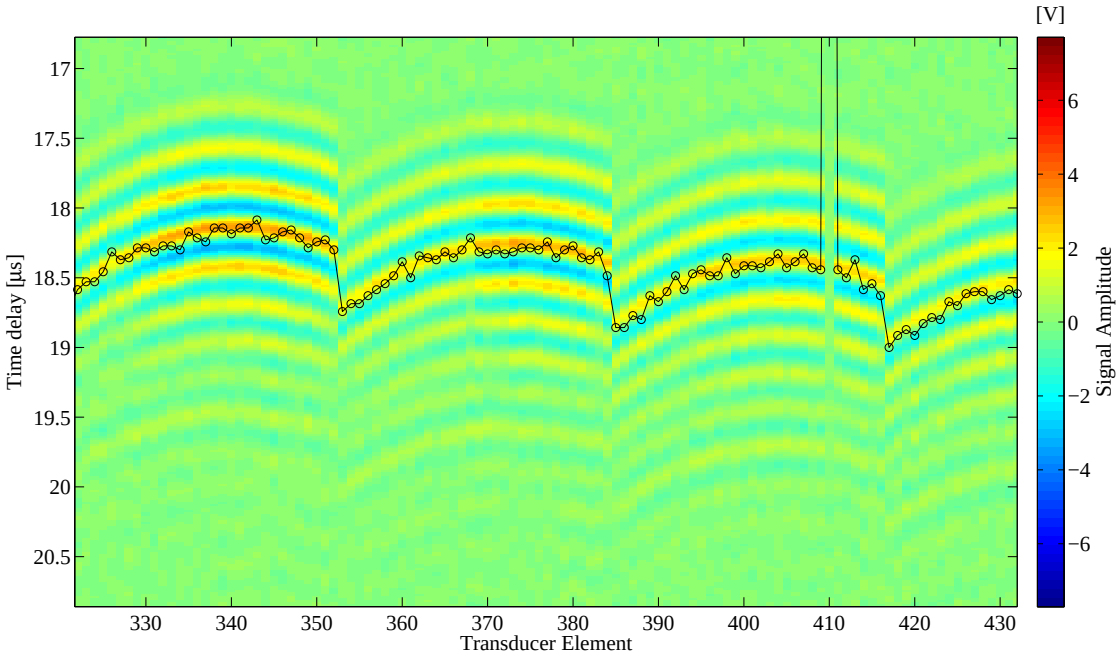

Figure 3.11 – Close-up of received signal and calculated Time of Flight for measurement 250

The lack of uniformity in the results indicate that further processing is needed to calculate an accurate value of the time of flight.

3.3.3 Polynomial Approximation

The first approach to calculate the values for the time of flight from each transducer element to the hydrophone for each measurement precisely is based on the fact that a pattern in the times of arrival for the signal can be detected for every 32 elements, as show figure 3.12.

These 32-element groups correspond to each of the rows of the transducers array. It can be observed that a second order curve could model the behaviour of the calculated time of flight for each of these groups, and thus a second order polynomial is fitted to the data values obtained in the first rough approximation explained in the previous section.

However, as it can be observed in Figure 3.10, some points are estimated outside the expected region for the time of flight values and using these data points when developing the polynomial model leads to inaccurate results.

The first step taken is to eliminate these points that fall outside the expected region from the polynomial fitting. This acceptance area is defined around the maximum and minimum expected values, as seen in Figure 3.13. Once the outer points have been detected, the remaining ones are used to define a model curve and then new time of flight values are assigned to each element based on this model. The results of this process can be seen in Figure 3.13 for measurement 250.

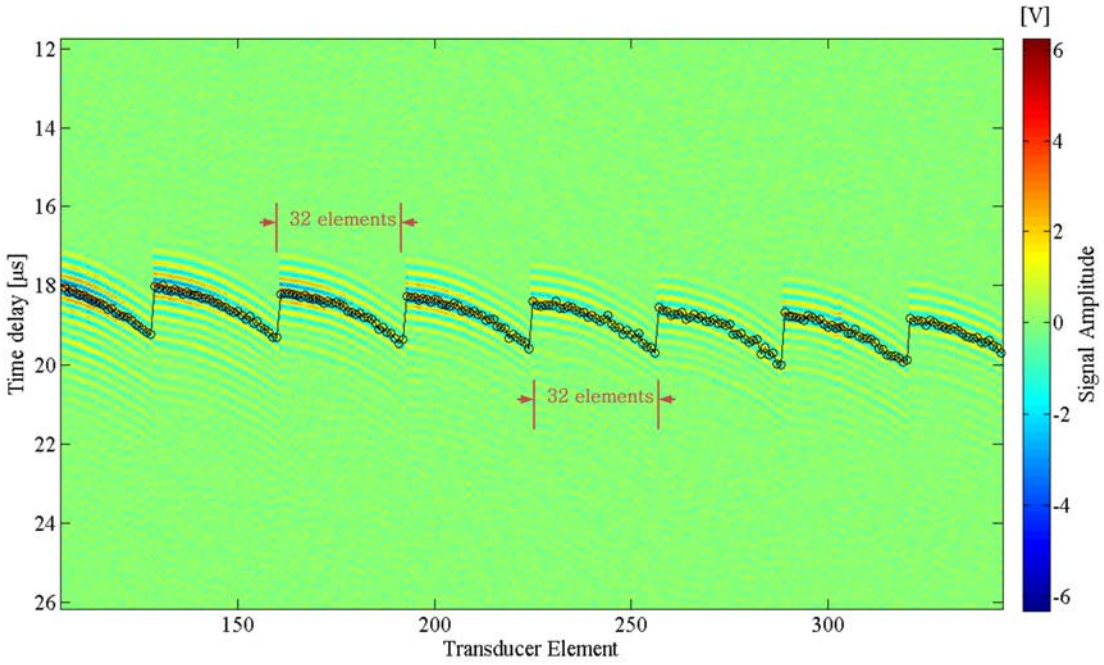

Figure 3.12 – Close-up of received signal and calculated time of flight for measurement 303

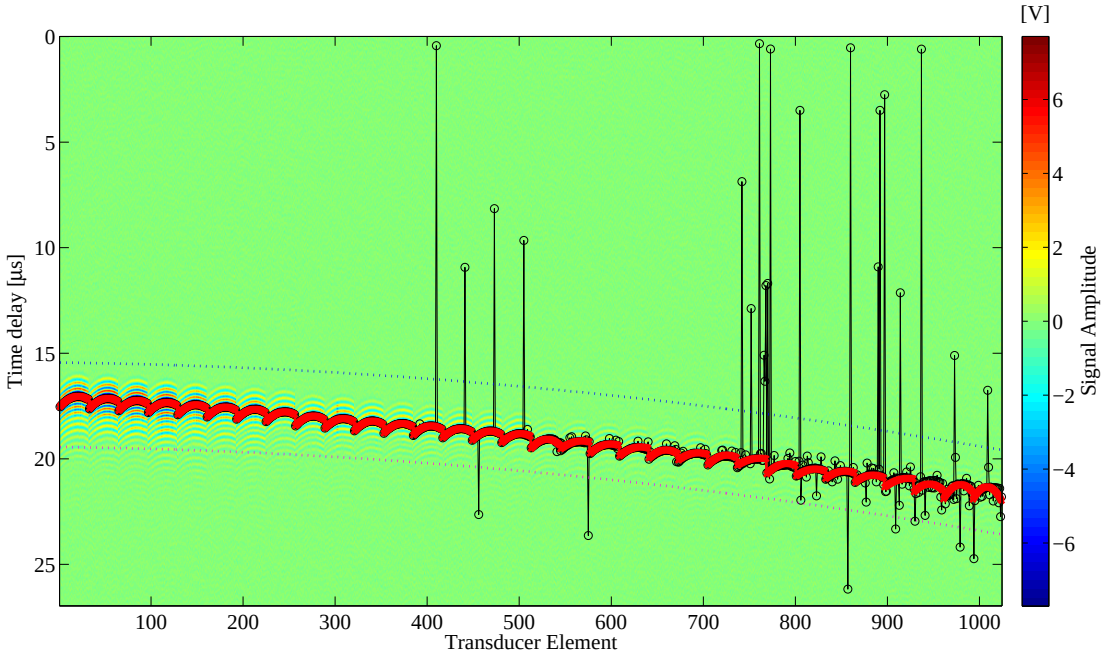

Figure 3.13 – Received signal, calculated time of flight (black) and fitted time of flight (red) for measurement 250. The dotted lines indicate the limits of the acceptance region

For the sake of clearness some close-ups of the most important phenomena observed when this approach was used are shown in Figure 3.14. These are:

Good Fit as it can be observed in Figure 4.16a, there are regions of the samples where the curve model is in

accordance with the first estimation of the time of flight, and the results are smoothly distributed.

Short-circuited elements When two adjacent elements are short-circuited, and thus emit the same signal, the model fails to assign them the same value, as shown in Figure 4.16b.

Dead Elements that is the elements of the transducer array that are not emitting any signal. As shown in Figure 4.16c, they are assigned a value in accordance to the model allotted to their group, meaning the model is unable to recognize dead elements.

Wrong fit there are groups of elements in which the modelled curve fails to accurately reflect the behaviour of the arriving signal, as shown in Figure 4.16d. This is mainly due to a poor original estimation of the time of flight. When the signal is weaker the SNR makes the original time values incorrect, which prevents a good model to be created from these points.

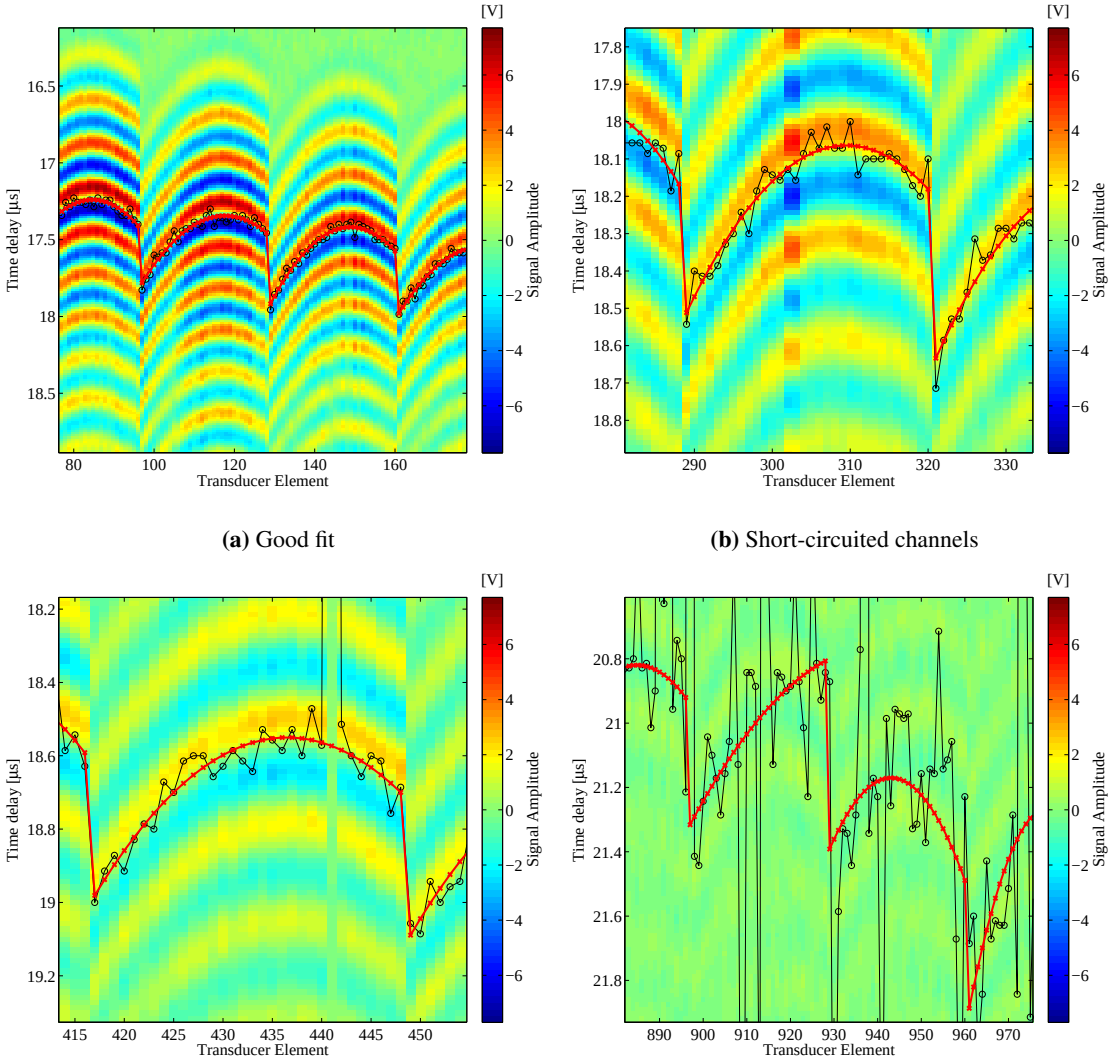

(a) Good fit

(b) Short-circuited channels

(c) Dead channel

(d) Wrong fit

Figure 3.14 – Close ups of different phenomena in time of flight calculation with polynomial fit for measurement number 250

A second round of polynomial fitting has also been tested. In this case the acceptance region for the data points to include in the model is hardened by adjusting it to the values of the first fit as shown in Figure 3.15

There is no improvement in terms of dead and short-circuited elements detection and a slight improvement is shown in the noisier elements, see Figure 3.16. However, it is not a significant improvement if compared with the computation time required to re-apply the time of flight estimation procedure.

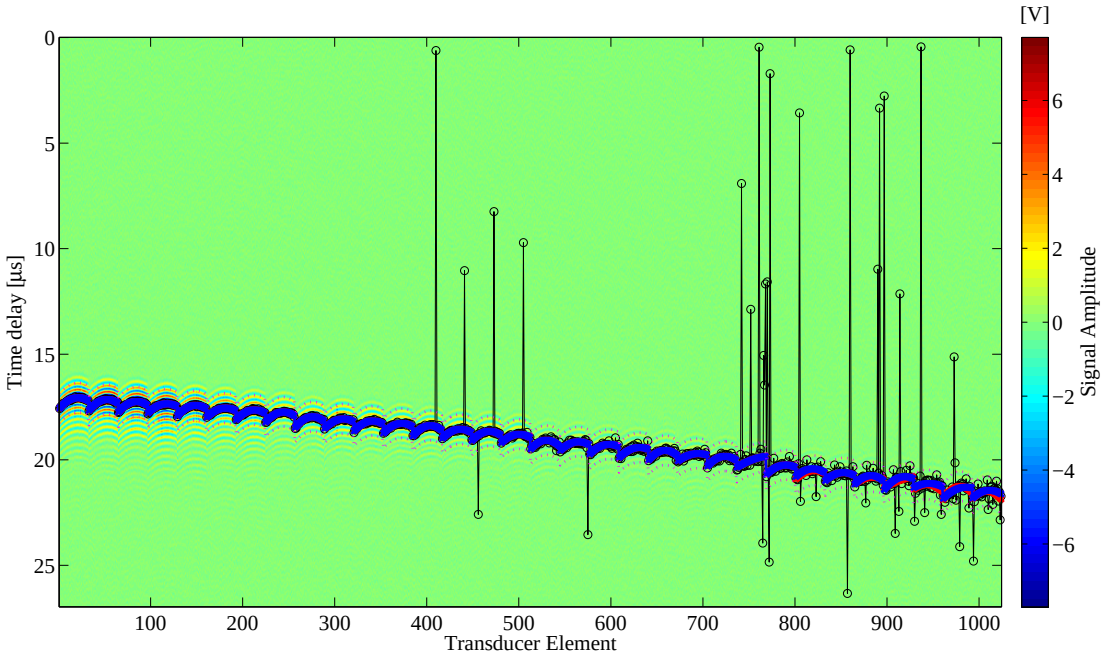

Figure 3.15 – Received signal, calculated time of flight (black), fitted time of flight (red) and second fitting results (blue) for measurement 250. The dotted lines indicate the limits of the acceptance region

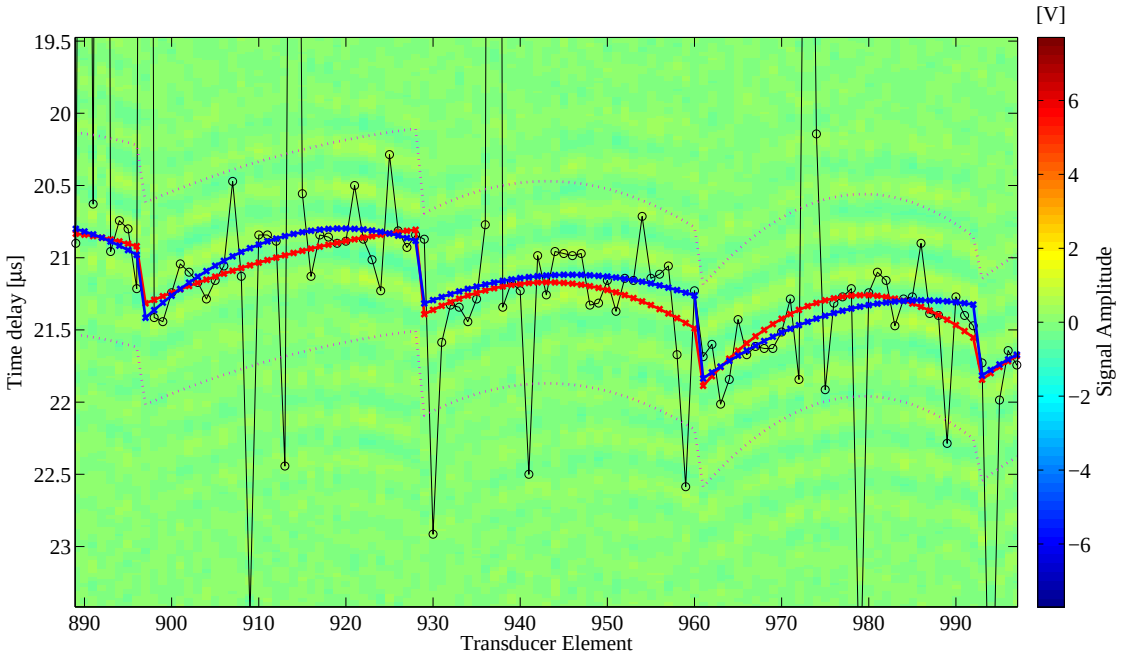

Figure 3.16 – Close up of the results after a seond polynomial fitting: Calculated time of flight (black), fitted time of flight (red) and second fitting results (blue) for measurement 250. The dotted lines indicate the limits of the acceptance region

3.3.4 Approximation based on Zero Crossing

A second approach to calculate the time of flight is, as shown in Figure 3.7, to adjust the estimated values of the time of flight to the nearest zero crossing of the signal. Like that, it is assured the convention for calculating these values is the same for all elements and measurements, in contrast to the polynomial fitting that assumed different models for each 32-element set.

In the zero crossing approach, after the first time of flight has been calculated, the received signal is upsampled in order to have more accuracy regarding the placement of the values. This is done in order to allow a sharper adjustment of the values around the desired point.

The process of upsampling results in a discrete signal that is approximately the one that would have been produced by sampling the original continuous signal received in the hydrophone with a higher sampling frequency. In this case the upsampling factor has been chosen to be 10, to have a sufficient number of samples to finely select the zero-crossing points. This choice results in a discrete signal of 18880 samples per array element in every measurement.

A window of analysis is established around each of the points that were estimated to be the sample delay of each element in the first approach. Then, the nearest zero crossing (from positive to negative values of the signal) to this point is selected as the new time of flight. Results for this approach are shown in Figure 3.17.

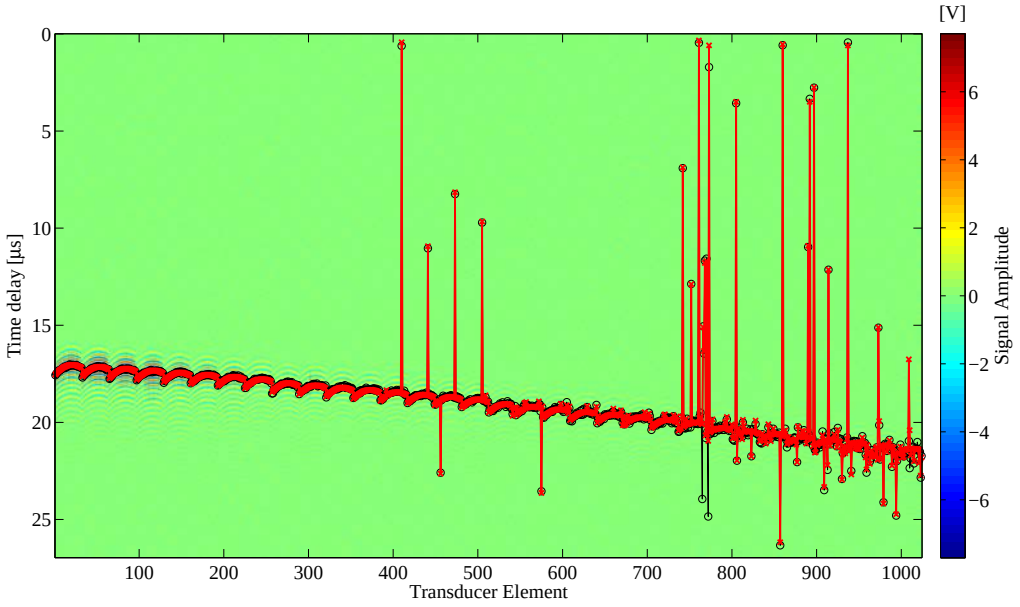

Figure 3.17 – Received signals, calculated time of flight (black) and fitted time of flight (red) for measurement 250

In this case it can be observed that in terms of the most relevant phenomena, shown in close ups in Figure 3.18, the behaviour of the zero-crossing approach is different than the one of the polynomial approximation:

Good Fit Region of the samples where the zero crossing approximation of the time of flight is in accordance with the first estimation of the time of flight, one of such regions is presented in Figure 3.18a.

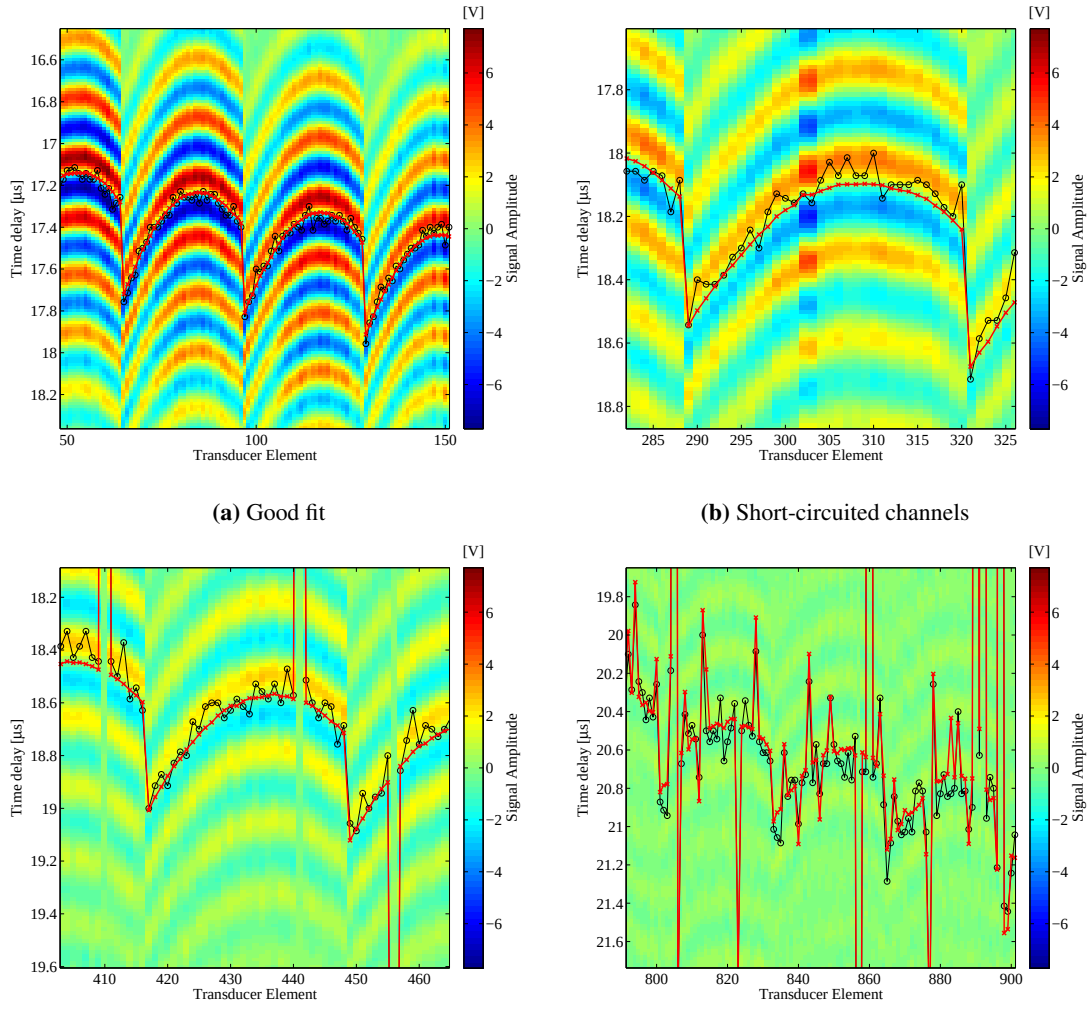

(a) Good fit

(b) Short-circuited channels

(c) Dead channels

(d) Wrong fit

Figure 3.18 – Close-ups of different phenomena in time of flight calculation with zero crossing for measurement position 250

Short-circuited elements When two adjacent elements are short-circuited, and thus emit the same signal, they are both assigned the same time of flight value, as shown in Figure 3.18b.

Dead Elements Elements of the transducer array that are not emitting any signal, as shown in Figure 3.18c, are not corrected, since the closest zero crossing to the originally estimated valued is still an incorrect value, mostly influenced by random noise.

Wrong fit elements where the signal is weaker and thus the SNR makes the original time values incorrect and so the zero crossing approach also fails to accurately reflect the behaviour of the arriving signal. This can be observed in 3.18d.

3.4 Dead Elements Detection

In both of the estimations of the time of flight explained before, dead elements, i. e. elements of the transducer array that do not produce any emission, represent a challenge in terms of detection and estimation. For that reason it was decided to do a separate analysis of the data in terms of emitted energy in order to

detect those elements. In this way, once the dead elements have been detected they can be excluded from the time of flight calculations and other processing.

The energy of the received signal can be expressed as:

$$E_x = \sum_{n=1}^{N} |x[n]|^2 \tag{3.9}$$

Where N indicates the number of samples of the signal. A sweep over all the measurements and all elements is carried out, and the energy for each of the elements of the transducer array is calculated, obtaining a total of 1024 energy levels for each of the 643 measurements.

Once this is done, the average energy received in the hydrophone in each measurement position is calculated. For each position the elements that have energy levels under 20% of the mean of their measurement are marked as possible dead elements. If an element is marked as possibly dead in more than 50% of the measurements then it is considered as dead, i.e. not emitting.

In the 2012 data set under analysis 14 elements were found not to be emitting. A sample of the appearance of the signals received in the hydrophone when these elements are considered to be emitting is shown in Figure 3.19.

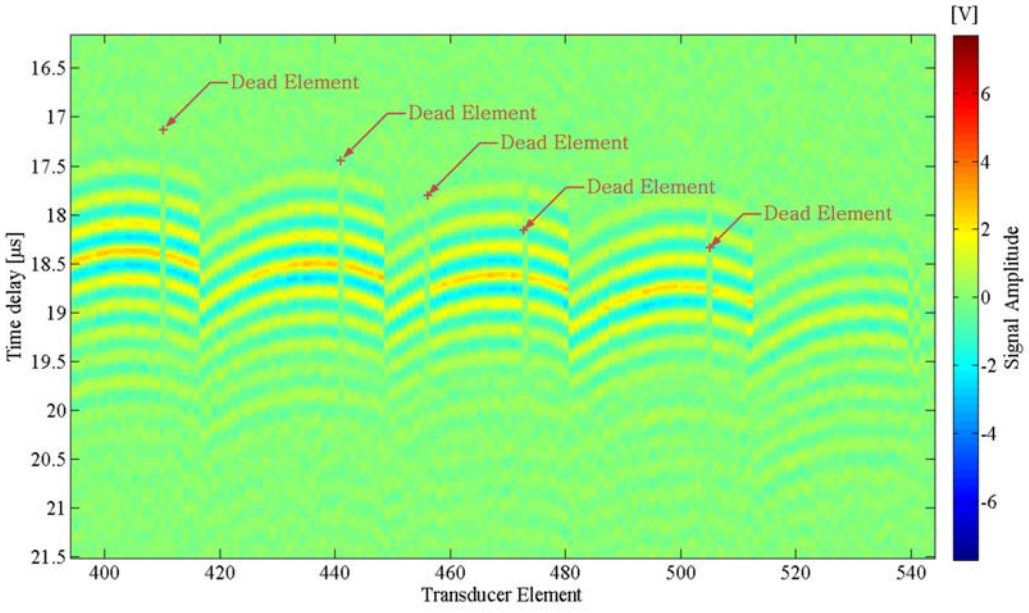

Figure 3.19 – Close-up of received signal, for measurement 250

Here reference is made to the performance data sheet provided for the array that has been included in Appendix A. In it, it was indicated that 12 elements were missing in the array. Using the method explained above it was possible to detect that 2 more elements had been damaged. Furthermore, the data sheet does not indicate which elements are the missing ones, so the methodology described in this section allows the identification of these elements within the array.

3.5 Noisy Measurements

During the first investigations and analysis of the data set it was detected that some measurements had recorded a weak signal or just noise.

This was a problem when detecting the time of flight,with erroneous results that could not be neutralized by applying any of the methods explained before. An example of such a measurement is shown in 3.20.

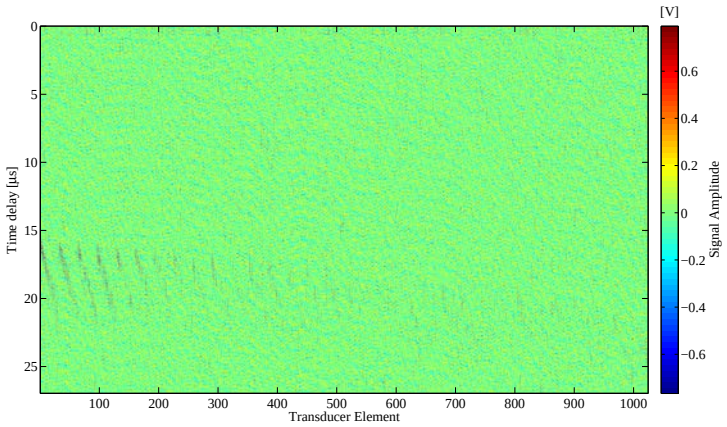

(a) Measured samples

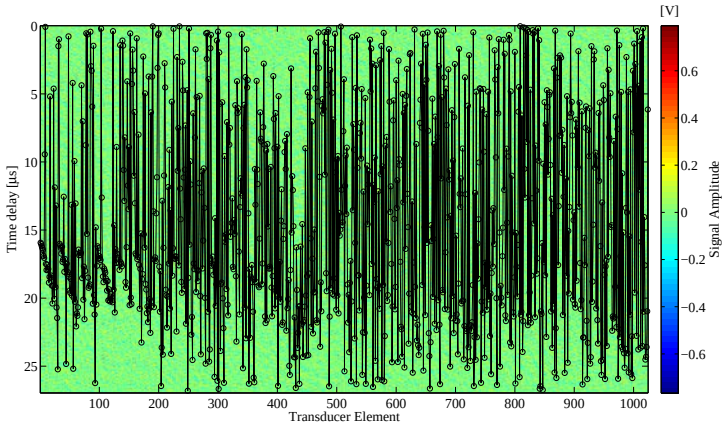

(b) Samples with calculated time of flight

Figure 3.20 – Results of measurement number 301 with coordinates [-16.6; -19.1; 10] mm

It must be observed that these measurements - in Figure 3.20 measurement number 301 corresponding to the hydrophone position [-16.6, -19.1, 10.0] mm is shown as an example -, were too noisy to yield meaningful values for the time of flight with any of the two methods, since the results of the first rough estimation described in section 3.3.2 were already erratic.

These measurements present, in general, low energy values as was made clear by the energy sweep performed originally to detected dead elements. Taking this into account an energy criterion was chosen to determine which measurements would be considered to determine the positions of the elements of the array.

The mean energy across elements for each measurement was calculated after the energy of each element

was found according to equation 3.9. These values where compared to the average energy across all measurements, and those with energy below 15% of the average energy of all the measurements were considered as noisy.

With the purpose of illustrating these findings, in Figure 3.21 the mean energy received at every position of the hydrophone is plotted.

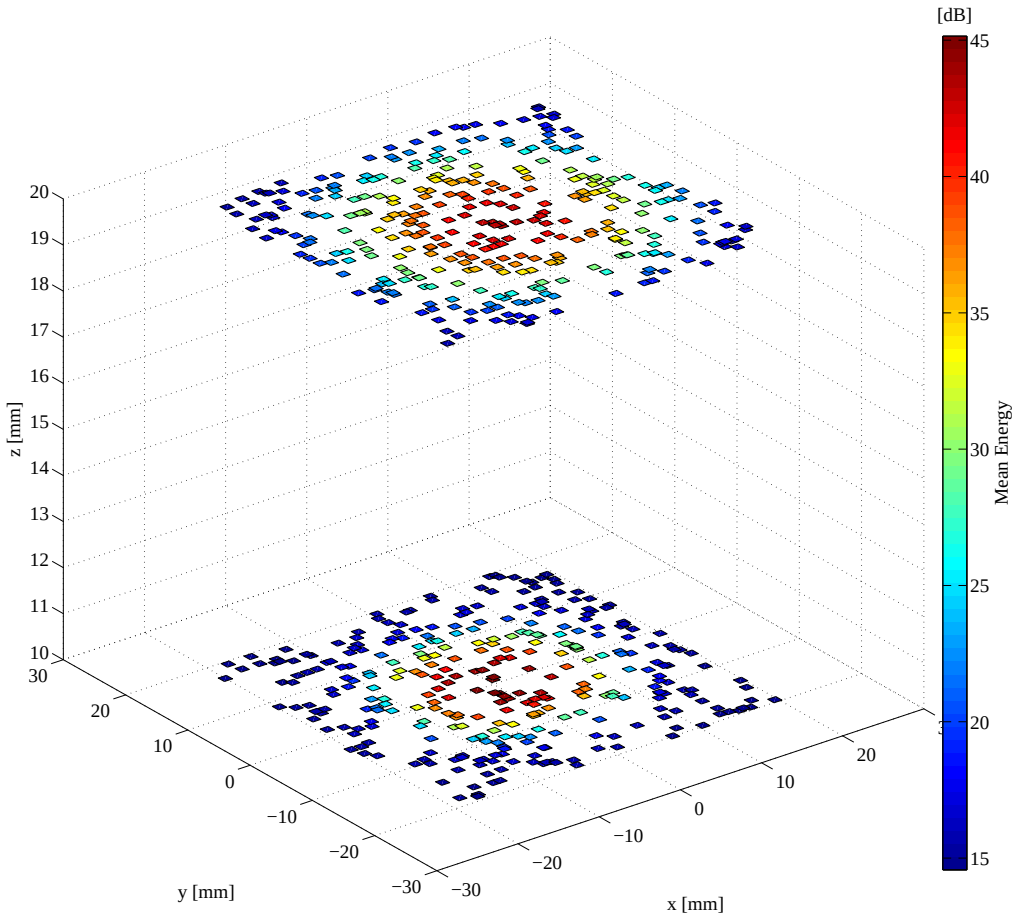

Figure 3.21 – Mean energy received at every position of the hydrophone

It can be observed in the figure that the elements with lower energy values, and thus the noisier ones, are the ones placed further away from the center of the measurement planes, indicating that they are the measurements with bigger distance to the array and with wider angles to the normal vector of the array.

3.6 Position Estimation

This section is concerned with the determination of the exact spatial localization of each array element within the coordinate system established by the hydrophone positions, the coordinates for these positions were assigned during the experiment considering the center of the transducer array to be the center of

coordinates [0, 0, 0].

Once the time of flight of the signals from each emitting element to the hydrophone for all of the recorded positions of the latter device are calculated, they can be used to infer the coordinates of the transducer array elements through an optimization process. In the following sections each step of the process will be described and the corresponding results and findings presented.

3.6.1 Time of Flight Model

After the time of flight is calculated this information can be used to determine the distance between the hydrophone and the emitting element using the simple relation shown in equation 3.2. However, this distance does not provide a unique coordinate for the transducer array element.

To accurately determine the spatial location of each element of the array it is necessary to develop a model for the time of flight that is dependent of the coordinates of the emitting transducer elements. Minimizing the difference between the time obtained from such a model and from the calculations explained in section 3.3, will allow to establish the coordinates of the elements.

This model for a theoretical time of flight that makes use of the element's spatial coordinates can be seen in Figure 3.22.

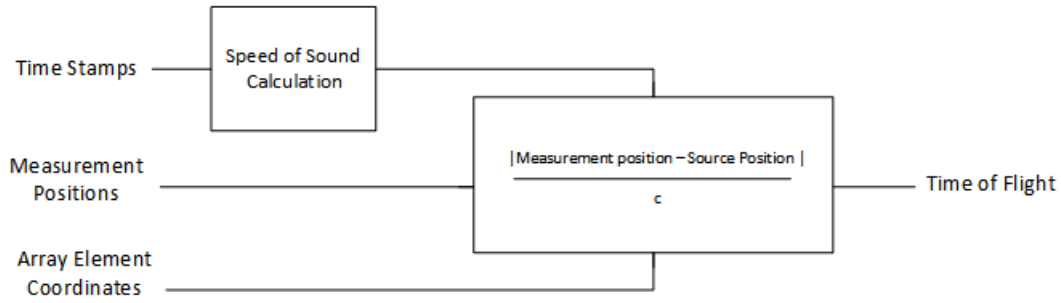

Figure 3.22 – Block diagram of the model for calculating the time of flight

It works by calculating the distance between a proposed array element position (also referred to as source position) and the coordinates of the hydrophone for a given measurement. To do this, equation 3.2 is used, rearranging it to obtain a time value, i.e. $t = {}^{d}/_{c}$. The speed of sound for each position of the hydrophone is calculated as explained in section 3.2.

3.6.2 First Optimization

The idea behind the first optimization is to minimize the difference between the modelled time of flight and the time of flight calculated from the measured data.

For each of the 1024 elements in the array, 643 different times of flight have been calculated with the model, to match the 643 hydrophone positions during the experiment. Thus generating 643 error values

when comparing modelled and measured time delays. The error is simply defined as:

$$error[m] = \text{modelled ToF}[m] - \text{measured ToF}[m] \tag{3.10}$$

Where ToF indicates the time of flight and m denotes the measurement number. The coordinate value assigned to each element would be the one that generates values for the times of flight that minimize the least-squares problem generated by the m errors. The least-squares problem is defined as:

$$\begin{aligned} min||e(s)||^2 &= min(e_1(s)^2 + e_2(s)^2 + \ldots + e_m(s)^2) \\ &= min(\sum_{m=1}^{M} e_m(s)^2) \end{aligned} \tag{3.11}$$

Where s is the array element under study, M the total number of measurements used to determine the spatial position of the element and e_m each of their corresponding errors. The method explained above was tested with the rough times of flight calculated in section 3.3.2 and then with the times of flight estimated using the two approaches described in section 3.3, i.e. the polynomial approximation and the zero-crossing approach.

Position estimation based on rough values of time of flight

The first attempt to determine the positions of the elements in the array was made using the first rough values of the times of flight. The results are shown in Figure 3.23

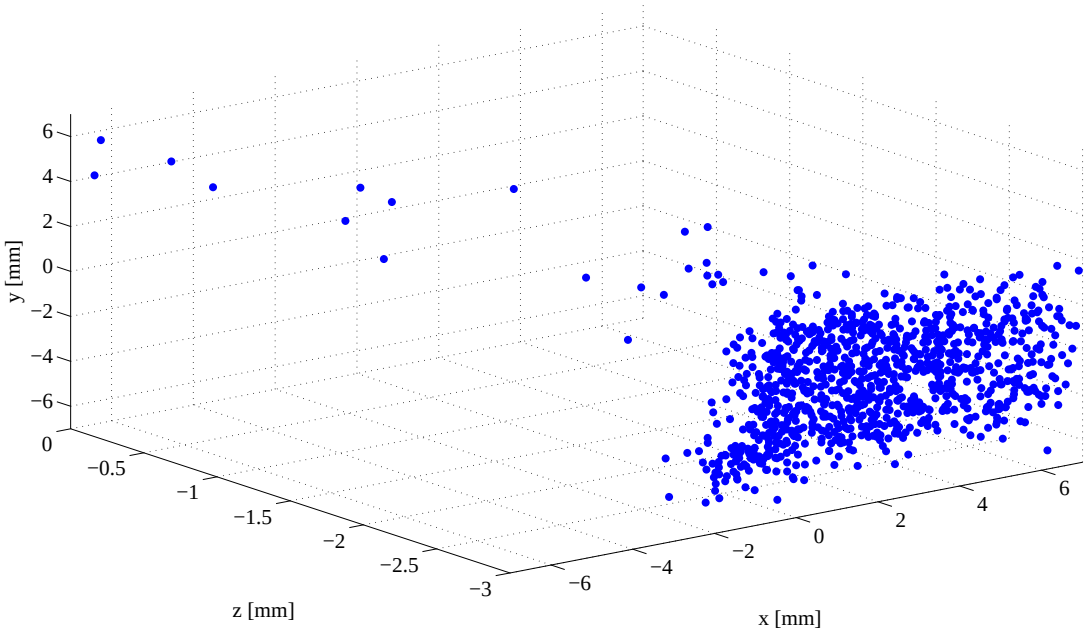

Figure 3.23 – 3D distribution of the array elements using time of flight data obtained from rough calculations

It is clear that these values of the time of flight were not accurate enough to obtain precise results, since the distribution of the coordinates does not resemble that of the array.

To improve the obtained results, it was decided that the values for the times of flight found through the zero crossing approach and the polynomial fit should be used to solve the least-squares problem. In addition another measure was taken: to discard the low energy measurements found in section 3.5. This was done in order to avoid including measurements that only added noise to the model and could lead to a faulty determination of the coordinates of the array's elements.

Position estimation based on polynomial fitting approach

The resulting element positions obtained from the times of flight calculated using the polynomial fit approach can be seen in Figures 3.24 to 3.26.

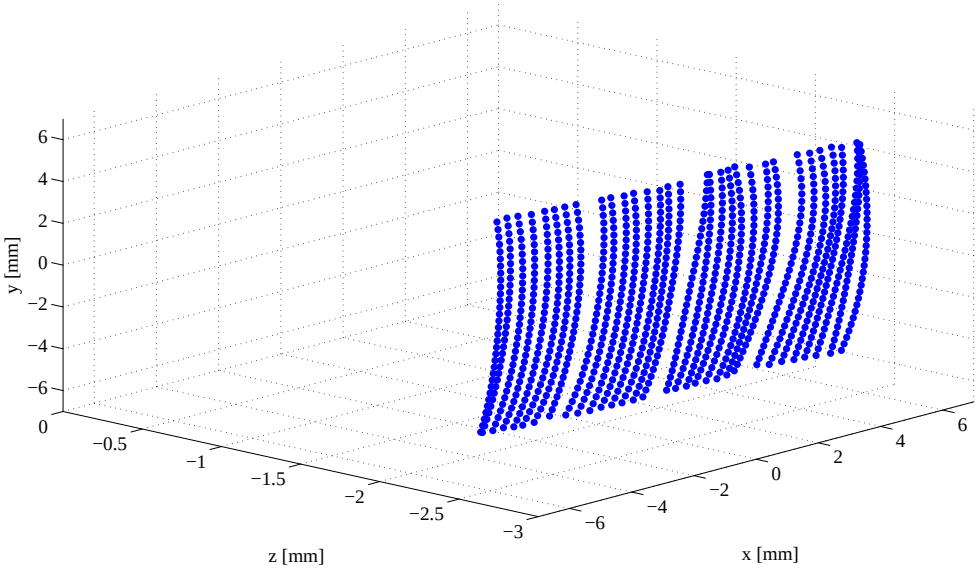

Figure 3.24 – 3D distribution of the array elements using a simple fit. Time of flight data obtained using polynomial fitting

As it can be observed in the figures, the improvement from the rough estimation is obvious, with the obtained coordinates resembling what could be the layout of the elements in an array. There is some dispersion in the distribution: In terms of the z-direction a curvature of ± 0.2 mm appears, as it can be seen in Figure 3.26. The worst estimations seem to take place on the sides of the array, specially in the right hand side (positive x coordinates).

The polynomial fitting leads to some forced patterns when the position is estimated, this can be observed in, for example, the column formed from elements 513 to 545.

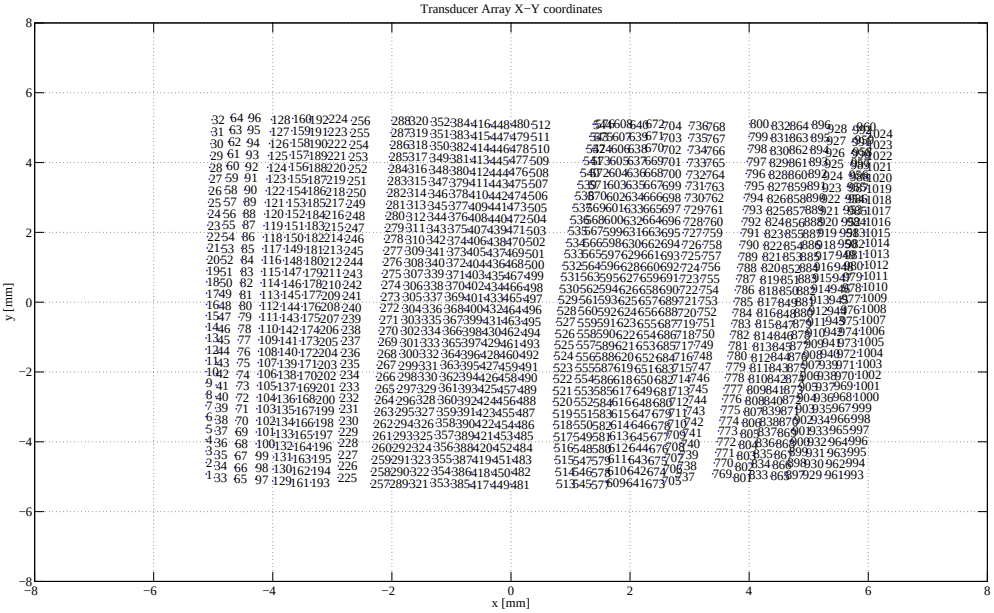

Figure 3.25 – xy-plane distribution of the array elements using a simple fit. Time of flight data obtained using polynomial fitting

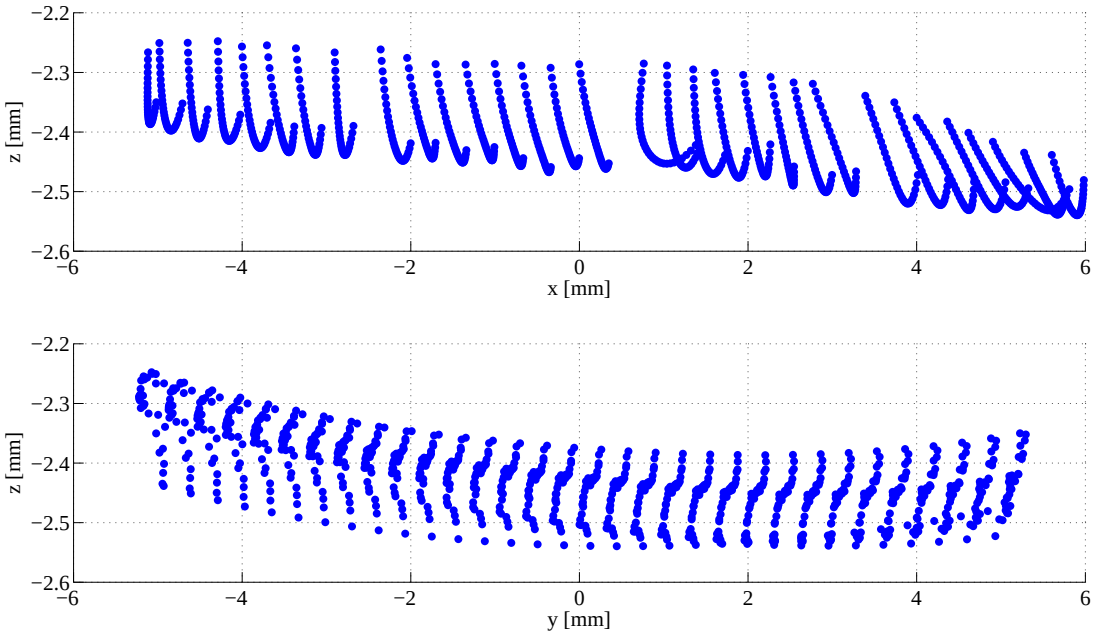

Figure 3.26 – xz and yz distribution of the array elements using a simple fit. Time of flight data obtained using polynomial fitting

Position estimation based on zero crossing approach

In an alternative approach, the times of flight calculated using the zero crossing approach are used to solve the optimization problem. The resulting elements' positions obtained from these times of flight can be seen in Figures 3.28 to 3.27.

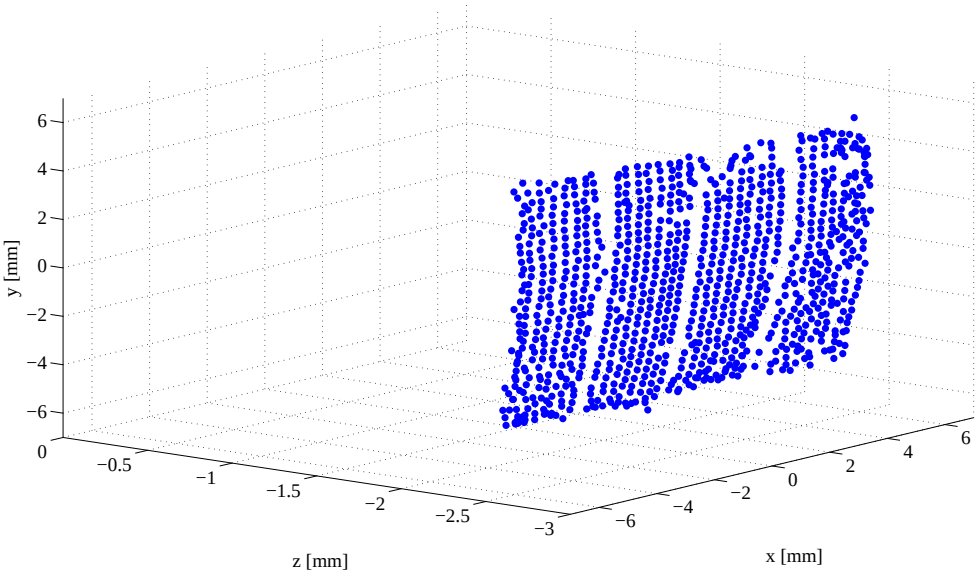

Figure 3.27 – 3D distribution of the array elements using a simple fit. Time of flight data obtained using zero crossing

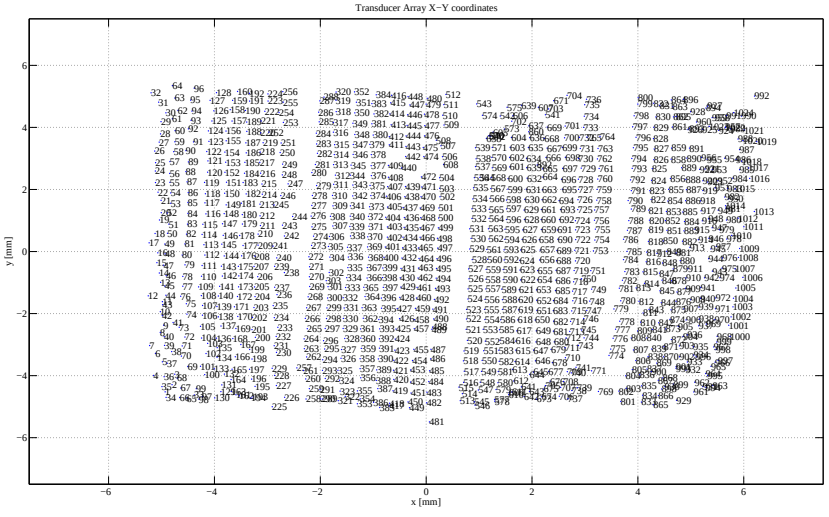

Figure 3.28 – xy-plane distribution of the array elements using a simple fit. Time of flight data obtained using zero crossing

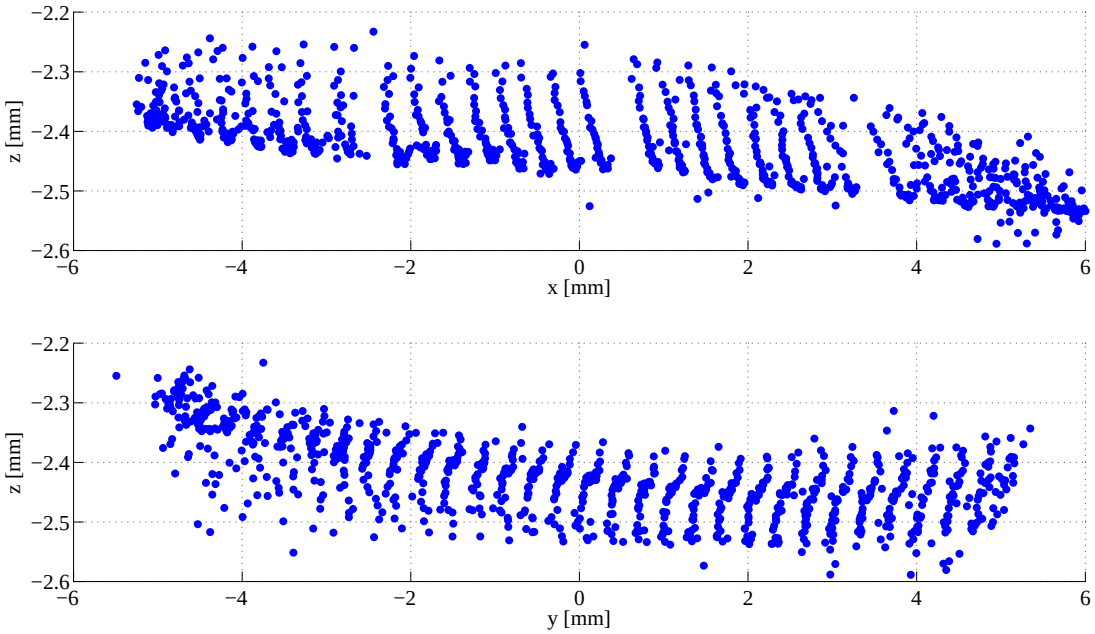

Figure 3.29 – xz and yz distribution of the array elements using a simple fit. Time of flight data obtained using zero crossing

Although the estimation is still fairly rough, it is an improvement from the original estimation. Central elements of the array seem to be better aligned, but there is a lot of dispersion of the exterior ones. This can be clearly seen in the x- distribution of Figure 3.29. In the z-drection it can be observed that there is a ± 0.2 mm distribution around -2.4 mm. It is also perceivable in Figure 3.29 that the array seems to be somewhat curved, especially on its sides.

If these results are compared to the ones obtained by means of the polynomially-fitted times of flight, it must be noted that both methods yield similar results. Some patterns are repeated, like the curvature in some rows and the lack of accuracy on the sides of the array. Although the zero crossing approach seems to produce less aligned elements, it does not reproduce any forced fitting that might end up causing incorrect estimations due to the fact that the polynomial fitting uses a modelized time of flight.

The conflictive areas, i.e. the outer parts of the array, appear to be the same no matter the methodology used, but in the zero crossing faulty results arise as heavily dispersed elements whereas in the polynomial fitting the results appear as curved columns or diagonally spread elements.

In both cases some of the error values taken into the least square problem were very small for certain measurement positions, but this error was quite big for others, meaning some of this measurements were actually outliers and could account for some of the dispersion in the data. It became apparent that a single straight-forward optimization of the least-squares problem would not be sufficient to solve the problem, and a more powerful optimization algorithm, that could take into account the presence of these outliers should be used.

An algorithm that can deal with the presence of outliers in data is the Random Sample Consensus

algorithm that will be discussed in the following section.

3.6.3 RANSAC Algorithm

The *RANdom SAmple Consensus* algorithm was proposed by Fischler and Boyer in 1981, [15], it is a model fitting algorithm designed to deal with a large number of outliers in the input data. It works by proposing minimum sets of data to be used to fit the model and by adding points to the proposed set if their deviation from the model is less than a pre-defined error threshold.

When applied to the particular problem of the data investigated for this project, the data points to be fitted correspond to the positions of the hydrophone, and the model to be fitted is the estimation of the elements' positions. The RANSAC algorithm is applied individually for each element of the array.

On each iteration of RANSAC a number of random hydrophone positions is selected to solve the least-squares problem, that is the initial consensus set, the rest of the points are then studied and included in this consensus set if the deviation between the measured time of flight and the time of flight they generate with the model is smaller than a threshold value.

Once the consensus set is sufficiently big, the least-squares problem is re-calculated and a new coordinate value is generated. The value of the newly found coordinate, as well as the consensus set is saved and an error value is assigned for this iteration. To calculate this error value firstly a new set of theoretical times of flight is calculated following equation 3.2, from the element to each of the measurement positions as:

$$t = \frac{|\text{Measurement coordinates} - \text{Element coordinates}|}{c} \tag{3.12}$$

The error is then calculated as the mean of the difference between each new calculated time of flight and the measured time of flight.

For each iteration, the error is compared with the previous iterations' error, and if is smaller the coordinate found is saved as the best guess for the element's position, the error as the best error, and the consensus set as the best consensus set.

In order to define the parameters of the algorithm, that is number of iterations, error thresholds and so on, the deviation between the modelled time of flight and the time of flight obtained from the measurement was investigated for each element.

This first estimation of the error is calculated following equation 3.12, and using the values for the coordinates obtained in the first optimization, described in the previous section. Figure 3.30 shows these errors for element 512 and all the measurement positions.

Analysing these error plots for different channels it could be observed that a good threshold value for accepting a measure into the consensus set will be a deviation of 5 µs difference between times of flight.

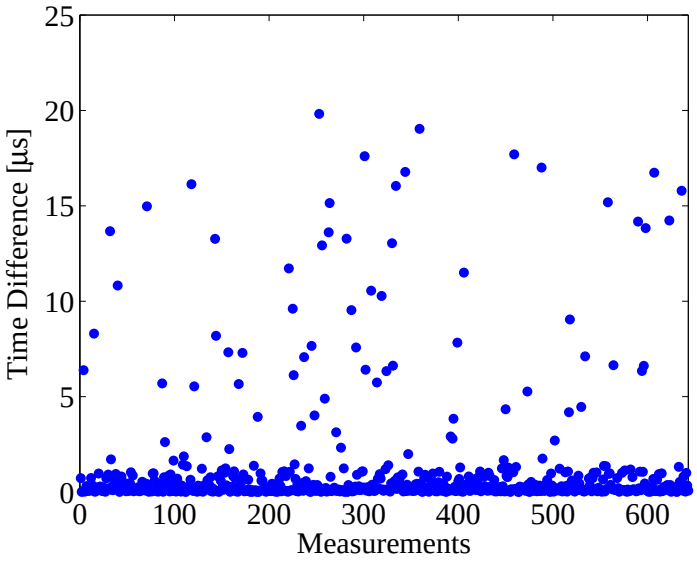

Figure 3.30 – Error plot for channel 512

Also a big number of outliers was detected, suggesting that a small initial set should be chosen and that the number of iterations of RANSAC should be quite large. These values are defined in order to assure that at least one of the proposed sets will not include any outliers. Let p be the probability of a measurement being an outlier:

$$p = \frac{\text{Number of outliers}}{\text{Number of measurements}} \tag{3.13}$$

Then, the probability of an initial consensus set that has no outliers will be the probability that none of its elements are above the error threshold:

$$\mathrm{P}_{proposed\ set\ not\ contaminated} = q = (1-p)^n \tag{3.14}$$

Where n is the number of elements of the initial consensus set. Equation 3.14 shows that as the size of the initial consensus set increases so do the chances of it being contaminated by outliers.

Accordingly, the probability that all the proposed consensus sets are contaminated will be dependent on the number of sets proposed, that is, the number of iterations of the algorithm, d, with the following relation:

$$\mathrm{P}_{all\ proposed\ sets\ not\ contaminated} = \varepsilon = (1-q)^d \tag{3.15}$$

Then the number of iterations can be found as:

$$d = \frac{\log(\varepsilon)}{\log(1-q)} \tag{3.16}$$

The quality of the RANSAC implementation will depend on the parameter ε, the number of iterations and the

number of elements in the proposed consensus set. The choice of these values should be a balance between accuracy and computational time and resources.

In the empirical assessment of the quality of the datasets, the number of possible outliers was determined to be around 150 out of 643, which lead to values of around $p = 0.23$. The quality was set to $\varepsilon = 0.001$, meaning that that the probability of all the proposed consensus sets being contaminated by outliers was of 0.1% . Based on these parameters the rest of the algorithm's inputs were chosen by means of the previously stated calculations. A summary of the input parameters can be found in Table 3.1.

Table 3.1 – RANSAC Input Parameters

Parameter	**Chosen value**
Set of observations	643 measurements
Model to be fitted	Coordinate of the element
Size of the first proposed set	25
Number of iterations	1500
Threshold error value	5 µs
Number of data points required to fit from the data set	250

To check the validity of these parameters, error plots are rechecked for the best consensus set found through RANSAC after all its iterations have been completed. In Figure 3.31 the error distribution for the measurements included in the consensus set is plotted. As it can be seen the presence of measurements above the desired threshold, i. e. outliers, have not been included, reducing the number of measurements used to minimize the least-squares problem.

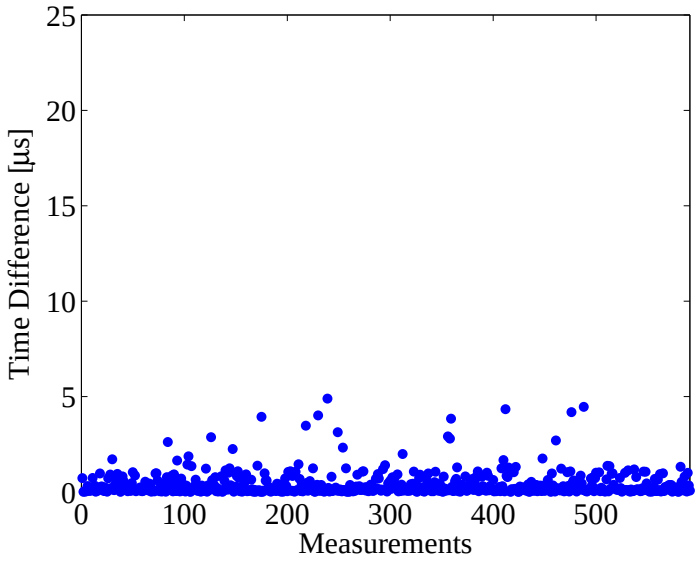

Figure 3.31 – Error Plot for channel 512, after applying RANSAC Algorithm

The process of applying the RANSAC algorithm was time and resource consuming, since it had to be done for each of the 1010 active elements - it was decided not to include the dead elements found as explained in section 3.4 -. Then 1500 iterations where specified for each element and lastly the optimization

algorithm of the least-squares problem also required a significant number of iterations to find the minimizing coordinate value.

Figures 3.33 to 3.32 show the results obtained after running the RANSAC algorithm over the data set.

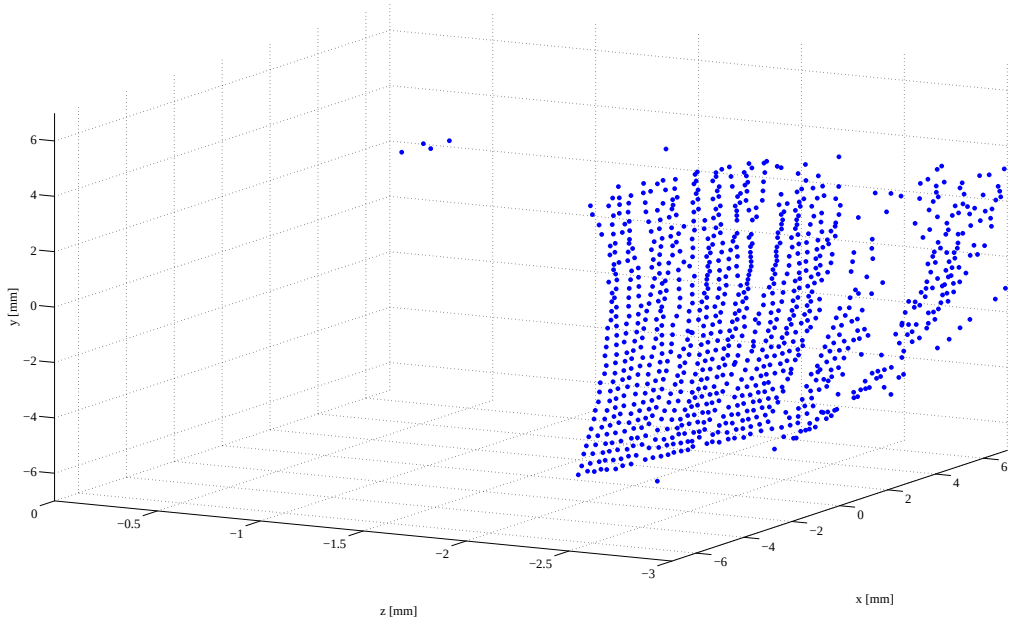

Figure 3.32 – 3D distribution of the array elements after RANSAC

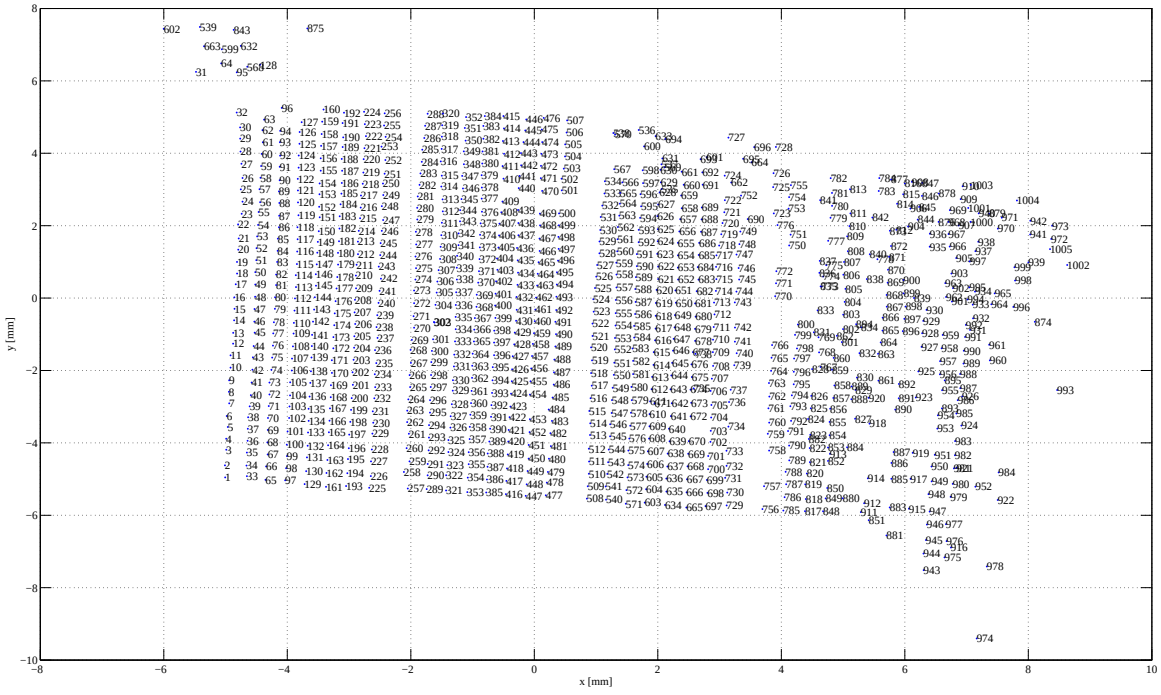

Figure 3.33 – Distribution of the array elements in the xy-plane after RANSAC

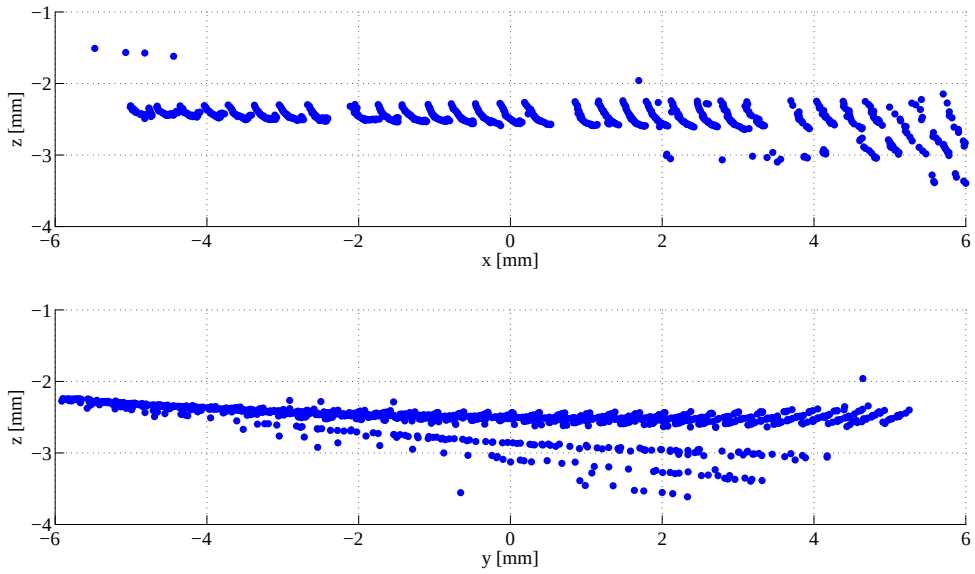

Figure 3.34 – xz and yz distribution of the array elements after RANSAC

Observing the figures it can be seen that the results of applying the algorithm are not consistent trough the whole array. Improvement is clear in some areas, specially in the left hand side of the array (positive values of x) as well as in the central areas of the transducer array. The improvement is mostly shown in the xy-plane, where elements seem to be better aligned, as can be seen in Figure 3.33. However, the right side of the array presents a significant dispersion in the layout of the elements.

In the z-direction, improvement seems to be focused on the left side of the array while, again, the values on the right side are completely disperse. Still after having applied the algorithm, the dispersion of the data has not been overcome and in some cases it even appears to have been worsened, for when deviations appear, they are much pronounced than when the algorithm was not used.

A possible explanation for this is that not enough measurements were taken or that their spatial distribution was not optimal. Moreover, other sources of error could come from the definition of the RANSAC parameters: not enough iterations or a too low/high error threshold can have a direct influence in the results.

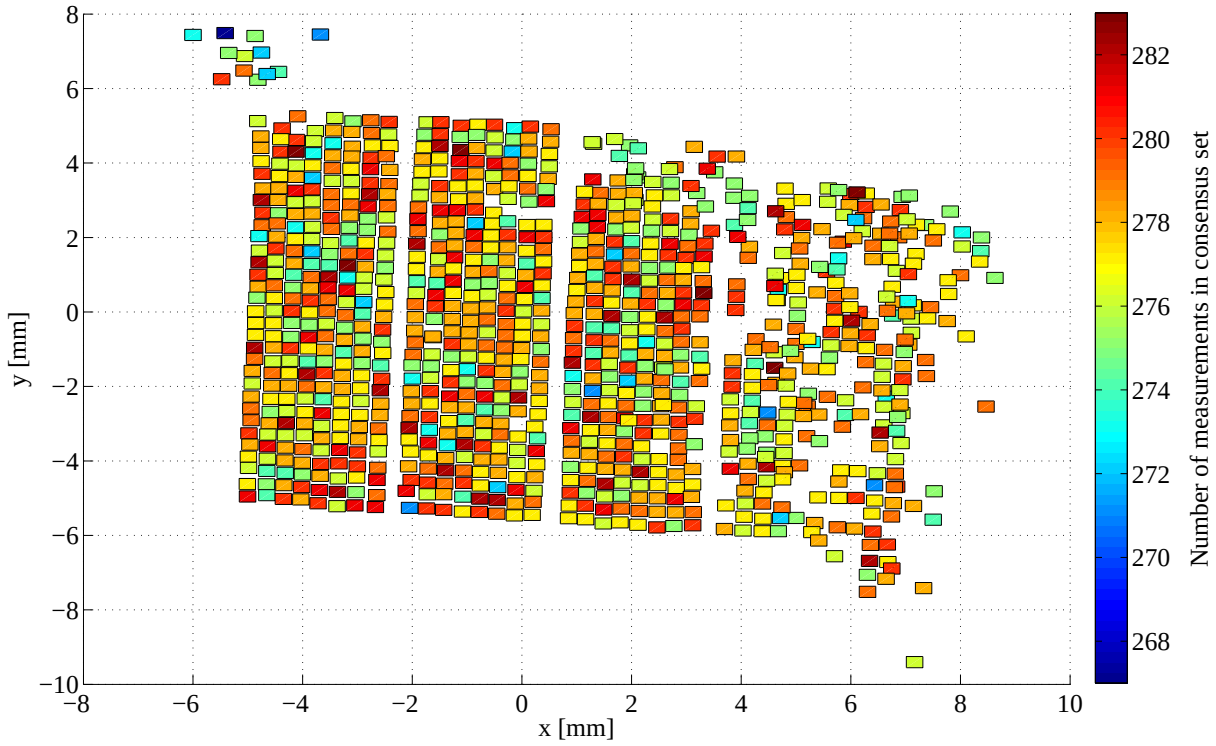

Figure 3.35 – Distribution of outliers in the estimated values

Figure 3.35 shows for each element the number of measurements included in the consensus set used to generate the coordinate value or, in other words, the number of measurements used to optimize the least-squares problem.

The first thing that can be read from this plot is the fact that there is not a large difference between the sizes of the consensus sets across elements of the array and that the more disperse coordinates on the right side of the array do not present extremely small consensus sets. This is the case only for the completely misplaced elements in the second quadrant (negative x and positive y values), where most of the elements seem to be in the lower half of the scale.

The small consensus sets are a result of a strict error threshold and a small accepted size of the consensus set. It is clear from these results that a balance must be kept between this value to keep a meaningful dataset and to avoid the inclusion of outliers in these datasets.

In this case applying the RANSAC algorithm has not meant an overall improvement of the estimations, although a large part of the coordinates have been corrected from their previously found values. In the future, to fully profit the potency of the RANSAC algorithm, it is recommended to set a looser value for threshold error, while increasing the minimum size of accepted consensus sets. However, this must be done without overlooking the fact that it could lead to a higher presence of outliers.

3.7 Directivity and Acceptance Angle

Once the positions of the transducer array elements have been determined this information can be used to study the directivity of each array element and their angle of acceptance. In order to do that is necessary to calculate the energy received in the hydrophone at each measurement point for each transducer element and to calculate the angle between the array element and the measurement position. This process is explained in detail throughout this section.

3.7.1 Energy Calculation

The energy of the received signal is calculated in the same manner as in section 3.4 to detect dead elements and noisy measurements. For reference the energy equation is repeated here:

$$E_x = \sum_{n=1}^{N} |x[n]|^2 \tag{3.17}$$

Where N is the number of samples of the signal, n is the sample received, and $x(n)$ the value of the measured signal. Using this method, an energy value will be generated for each of the positions of the hydrophone.

Instead of measuring the energy received in the hydrophone during the whole measuring time, a region of interest is defined to avoid the influence of noise. The region of interest is reduced and centred around the estimated time of flight. The time of flight values used are the ones obtained in the zero-crossing approach and the chosen window size is the equivalent in samples to three periods of the emitted signal, after and before the time of flight value.

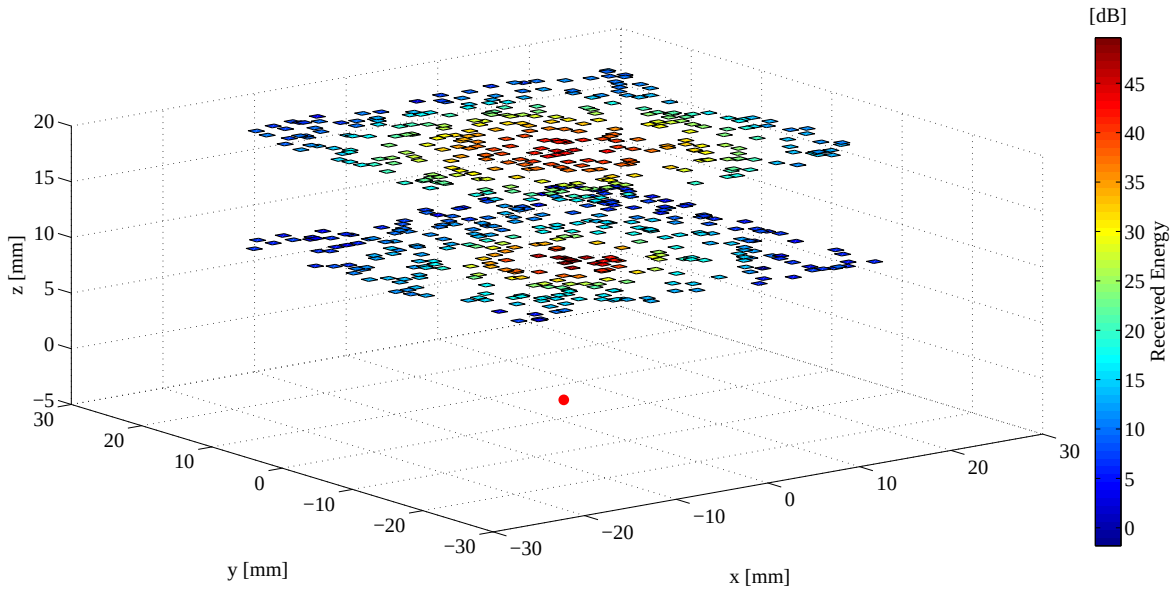

Figure 3.36 – Energy distribution for the 643 measurements for emitting element number 295. Red dot indicates the estimated position of the transducer element

Figure 3.36 shows the energy distribution for the transducer element 295. The energy is expressed in decibels (dB). In the graph, it can be seen that there are two separate depths of measurement in the data set, one at a depth of measurement of 1 cm composed of 319 measurements and the other at a depth of measurement of 2 cm with 324 measurements performed on it. In order to analyse the distribution and directivity they will be dealt with separately. It is expected that the behaviour would be analogous in both planes, even when the exact values vary.

3.7.2 Angle Calculation

In order to understand how the energy is emitted from the transducer element, the idea of directivity has to be introduced. This is one of the parameters that serves to characterize the transducer element and it is defined as the energy distribution in terms of the angle between the vector normal to the transducer array and the vector that links the array element and the position of the hydrophone. This vector is defined as:

$$\vec{u} = \frac{\text{Hydrophone Coordinates} - \text{Element Coordinates}}{\| \text{ Hydrophone Coordinates} - \text{Element Coordinates } \|} \tag{3.18}$$

Where $\vec{u}$ is a unit vector with direction from the array element towards the hydrophone position. The angle θ between this vector and the normal vector $\vec{n}$ is defined as:

$$\cos(\theta) = \frac{\vec{u} \cdot \vec{n}}{|\vec{u}||\vec{n}|} \tag{3.19}$$

In the researched literature ([6], [8], [16]) directivity and acceptance angle are measured as a 2D problem (as shown in Figure 3.37), and thus the directivity is expressed between -90 and 90 degrees. In the approach taken for this investigation it would not make sense to have the second angle quadrant, because θ indicates the rotation of $\vec{u}$ around the normal vector, where both $\vec{u}$ and $\vec{n}$ are 3D vectors, and consequently θ only varies between 0 and 90 degrees, as shown in Figure 3.38.

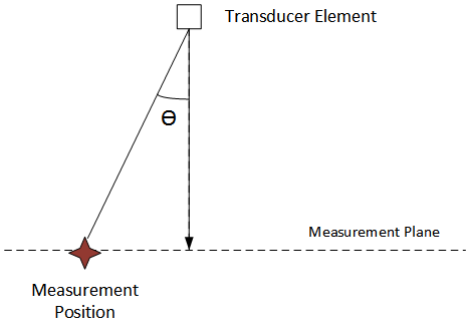

Figure 3.37 – 2D diagram of the angle calculation

In the previous section the energy was calculated, showing that distribution of energy is symmetrically spread (see Figure 3.36), and thus, ideally, for the same value of θ the energy values should be the same or at least similar, no matter the orientation of the aperture angle. This is illustrated in Figure 3.38, where the angles between an array element and one of the measurement planes are represented. The energy is equally distributed in circles corresponding to the same angle, even when the measurements (and thus the vectors) are spread in different directions.

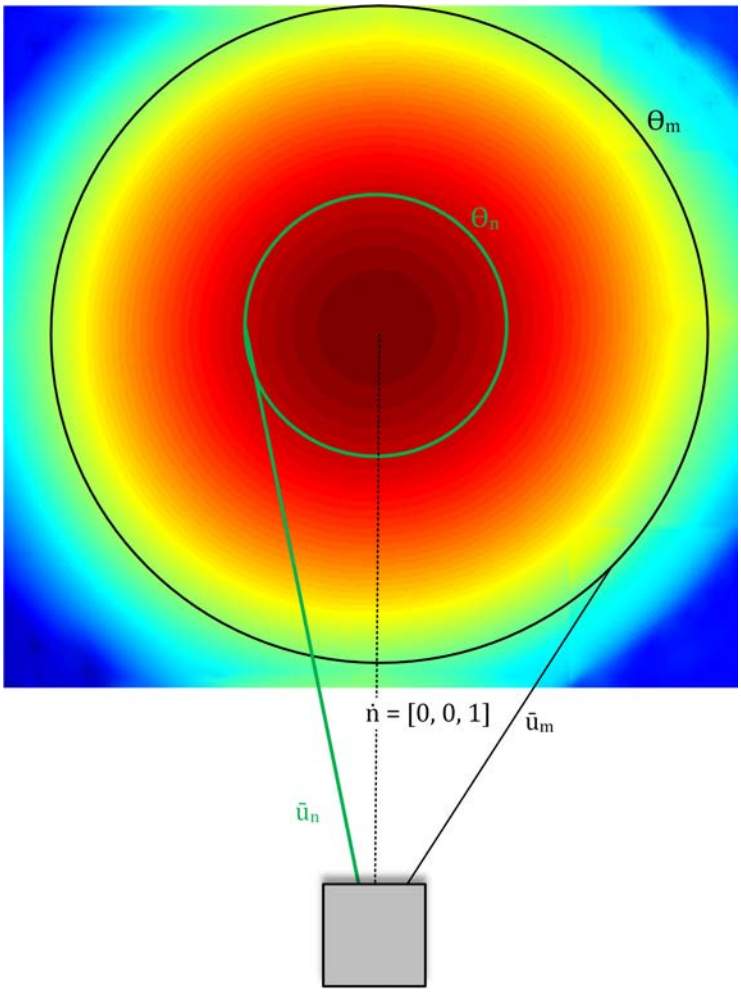

Figure 3.38 – 3D diagram of the angle calculation

In the figure, the energy levels on the measuring plane are represented with different colors and angles θ_n and θ_m are sample sample angles aiming to illustrate how energy and angles are expected to be related, showing how for different measurements that share the same angle to the array normal should, in principle, have the same energy values.

To analyse the effect of the angle, the measurements have been divided in two groups according to their depth of measurement: 1 and 2 cm far from the transducer array and so, they have been dealt with separately. It is expected that the behaviour of the energy distribution across planes has the same appearance, meaning that it behaves in the same manner, but the energy values, and consequently the angle of acceptance will change between measuring planes.

Results for both planes are shown in Figure 3.39 for element number 295 and in Figure 3.40 for element 400. Both figures display the energy value in decibels as a function of the angle θ and to find the values of this angle the normal vector from the array has been assumed to be [0, 0, 1]. The results are presented for all the 643 measurements, and the outliers detected when using the RANSAC algorithm are indicated in red.

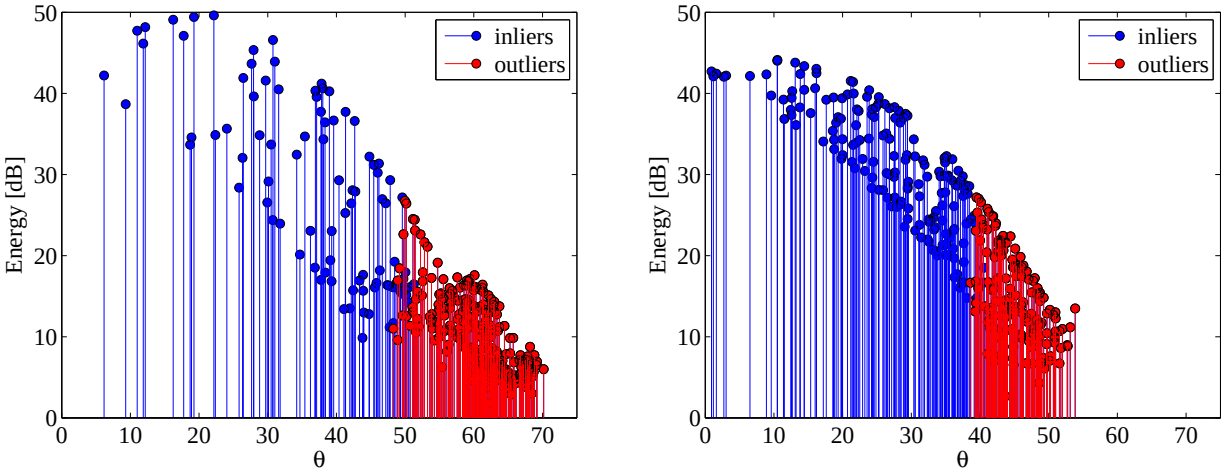

(a) Measurement depth 1 cm **(b)** Measurement depth 2 cm

Figure 3.39 – Energy distribution in terms of the angle between normal vector to the array and the measurement position. Element 295

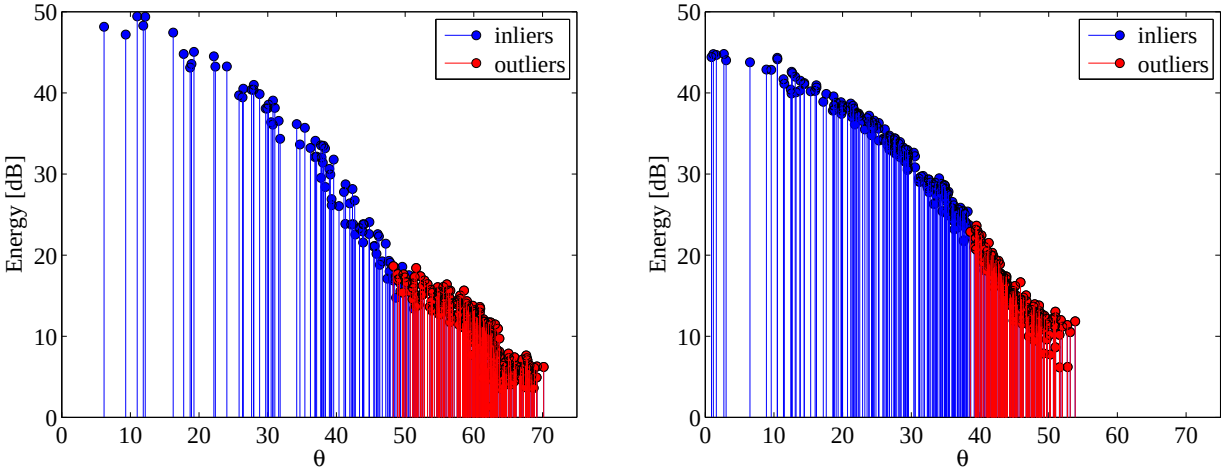

(a) Measurement depth 1 cm **(b)** Measurement depth 2 cm

Figure 3.40 – Energy distribution in terms of the angle between normal vector to the array and the measurement position. Element 400

These two elements have been subjectively assessed by the author as a *"bad"* estimation (element 295) and a *"good"* estimation (element 400). It was estimated that for the analysed data, out of the 1024 array elements this directivity calculation yielded correct results for only 30% of the elements. This judgement was taken based on the spreading of the data points and whether a discernible directivity curve could be read from the generated plots or not. The correct values were obtained mainly for the central elements of the array.

When the directivity plots are accurate, the values for the acceptance angle can easily be read from them. In Table 3.2 average values for the -3 dB, -6 dB and -12 dB are presented.

Table 3.2 – Angle of acceptance values

Measurement depth	Level	Acceptance angle
1 cm	-3 dB	$18.30° \pm 2.09°$
	-6 dB	$25.09° \pm 1.19°$
	-12 dB	$31.93° \pm 1.22°$
2 cm	-3 dB	$13.83° \pm 0.97°$
	-6 dB	$19.09° \pm 1.06°$
	-12 dB	$28.78° \pm 0.47°$

The results presented show a decrease of the energy values as the angle θ increases, this is in accordance to theory and also agrees with results shown in literature [16]. For example, findings by Felix et al. in [20] pointed to angels of $25°$ and $36°$ for -3 dB and -12 dB acoustic levels when testing an emitting element of a 4MHz array with 500 µm pitch at a 70 mm depth of measurement.

However, when the analysed elements do not present a simple curve, meaning that the values of energy present a higher dispersion, it is harder to produce estimations on the angle of acceptance. The decay of energy with an increasing angle is still present but this is not a consistent pattern through all measurements and a clear spread in the data can be observed in both measuring planes.

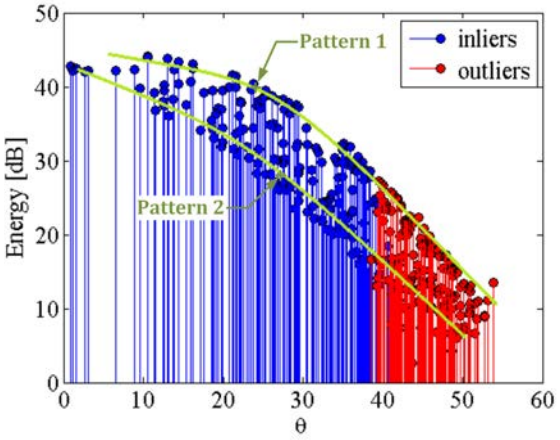

Figure 3.41 – Directivity plot for element 295 with depth of measurement 1 cm

It appears that two different patterns are present in the values - for sake of clearness they are indicated in Figure 3.41-. Both patterns follow a similar decay function, but have different energy values. This dual performance was not expected, since the energy roll-off was seen as a symmetrical phenomenon and, as seen in the 3D schematic (Figure 3.38) the envisioned results should have presented a smoother curve.

An explanation for this behaviour of the results, could be that for this calculation the normal vector from the array was assumed to be [0, 0, 1], however, observing the results obtained, it seems that this might have been a wrong approach since it does not take into account the possibility of the array not being aligned with the measurement planes. Such a case, in which the array and the measuring planes are misaligned is illustrated in Figure 3.42.

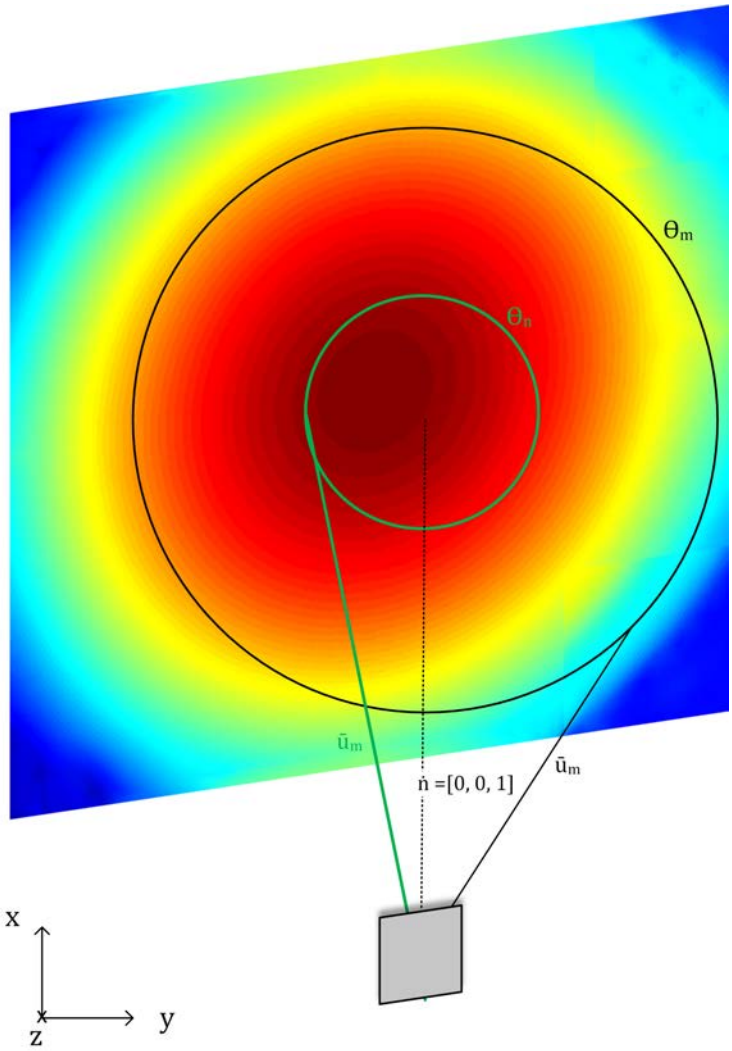

Figure 3.42 – 2D diagram showing the effect of a tilted array on the normal vector for the angle calculation

As the diagram shows, when the array element is not exactly parallel to the measurements' planes, by keeping the value of the normal vector as $\vec{n} = [0,\ 0,\ 1]$ an error is introduced because the angle values are no longer related to the behaviour of the energy distribution. If this is indeed the case, it would mean that for different measuring points that yield the same angle with the array's normal vector, the energy values might not be necessarily similar.

Different approaches can be taken in order to improve the angle calculation by means of refining the values for the normal vector. They are described in the following sections.

3.7.2.1 Array Fitting

The first strategy used to find an accurate value for the normal vector to the transducer array was the estimation of the plane in which the array elements are placed and consequently, the calculation of the value for the normal vector to that plane.

The main difficulty laid in the fact that the estimated positions were also subject to an estimation error and, as it was shown in previous sections, not all elements where estimated with the same level of accuracy. For that reason only the points that seemed to be better estimated were used to fit this plane to the array and, on the other hand, the most disperse values were not taken into account when modelling the planar surface to predict the value of the normal vector.

A plane is defined in the three dimensional space by the general plane equation:

$$a \cdot \mathrm{x} + b \cdot \mathrm{y} + c \cdot \mathrm{z} + d = 0 \tag{3.20}$$

The vector $\vec{n} = [a,\ b,\ c]$ defines the normal vector to the plane. Values for the parameters a, b, c and d are calculated so that the resulting plane adjusts as much as possible to the values of x, y and z defined by the estimated coordinates of the chosen array elements.

The plane fitted to the positions is depicted in Figure 3.43:

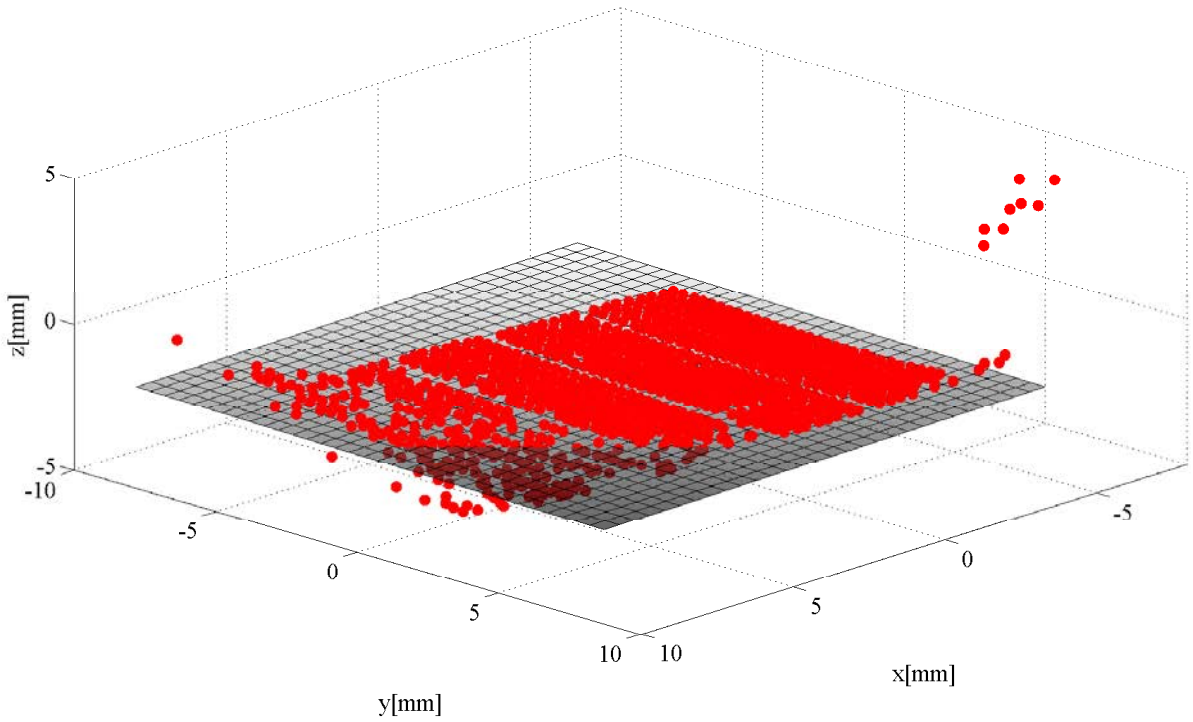

Figure 3.43 – Estimated array positions and fitted plane

The value for the normal vector obtained is: $\vec{n} = [0.0148,\ 0.0160,\ 0.9998]$. The results for the energy distribution along the angle values when using this new normal vector in the angle calculation explained in the previous reason, are shown in Figure 3.44.

It can be seen from Figure 3.44, that the improvement in the results using this method is not significant. There are slight variations in the values, but the difference between the normal vector and the ideal normal [0, 0, 1] is not big enough as to yield notable changes.

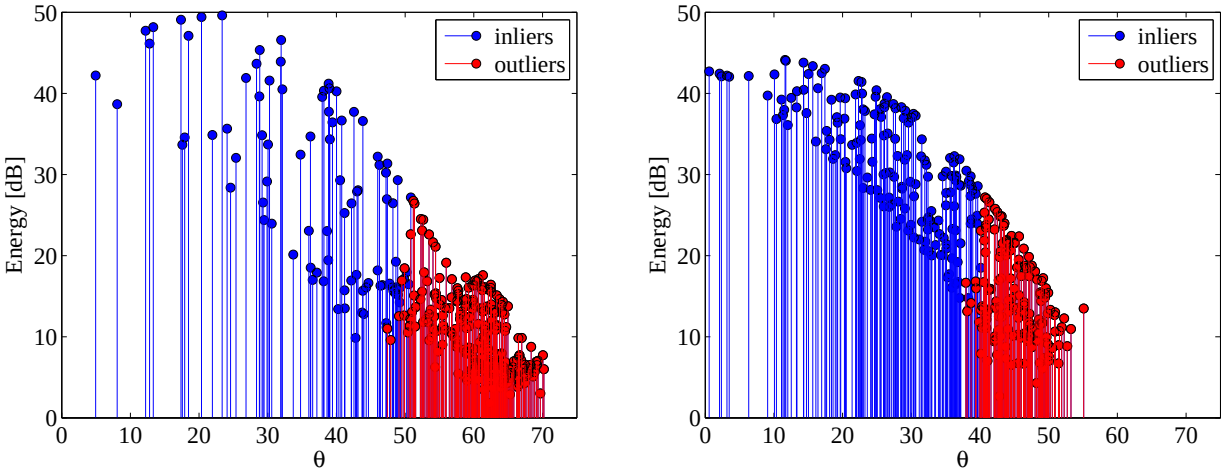

(a) Measurement depth 1 cm

(b) Measurement depth 2 cm

Figure 3.44 – Directivity plot for element 295

Furthermore, if we compare Figures 3.44 and 3.39 it can be observed that the two patterns are, to some extent, more present when using the normal value calculated through plane-fitting the array. This is probably due to the fact that the estimation of the positions of the array elements is not accurate enough and thus, the modelled plane cannot model the inclination of the array.

3.7.2.2 Energy Fitting

Other approach investigated to determine the value of the normal vector was to fit the distribution of the energy to a model in order to calculate the exact coordinates were the energy maximum was achieved. Assuming the maximum energy is obtained in the normal trajectory from the array, a value for the normal vector could be obtained using the energy maximum in the two planes (see Figure 3.45).

The process followed to find these energy distributions and their maximums consisted on the subsequent steps:

1. The measuring planes are sampled as a grid with coordinates ranging between -20 mm and +20 mm for both x and y with a pitch of 50 µm, thus generating a fine set of coordinate values to describe the plane.

2. A model to relate coordinate values with energy values is found using the coordinates of the measurement positions and their corresponding energy values.

3. The new found coordinates are inputed into the model, thus obtaining the energy pattern along the planes, as shown in Figure 3.46.

4. One maximum value is found for each plane, consequently attaining their coordinate value.

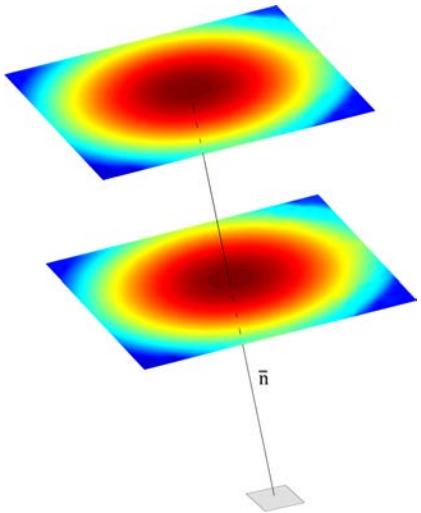

Figure 3.45 – Energy fitting schematic

5. The normal vector is defined as the vector that links the two energy maximums.

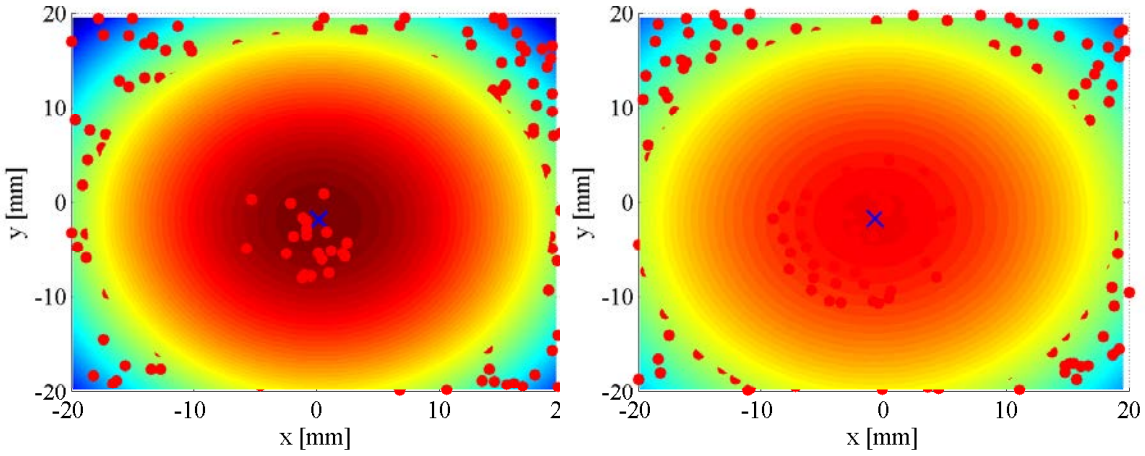

(a) Measurement depth 1 cm **(b)** Measurement depth 2 cm

Figure 3.46 – Energy distribution model. Red dots indicate measurement coordinates. Blue cross indicates the maximum energy point of the model

The value for the normal vector calculated using this method was $\vec{n} = [-0.0847,\ 0.0100,\ 0.9964]$, and the directivity patterns obtained using this normal vector for the calculation of the angle θ are displayed in Figure 3.47:

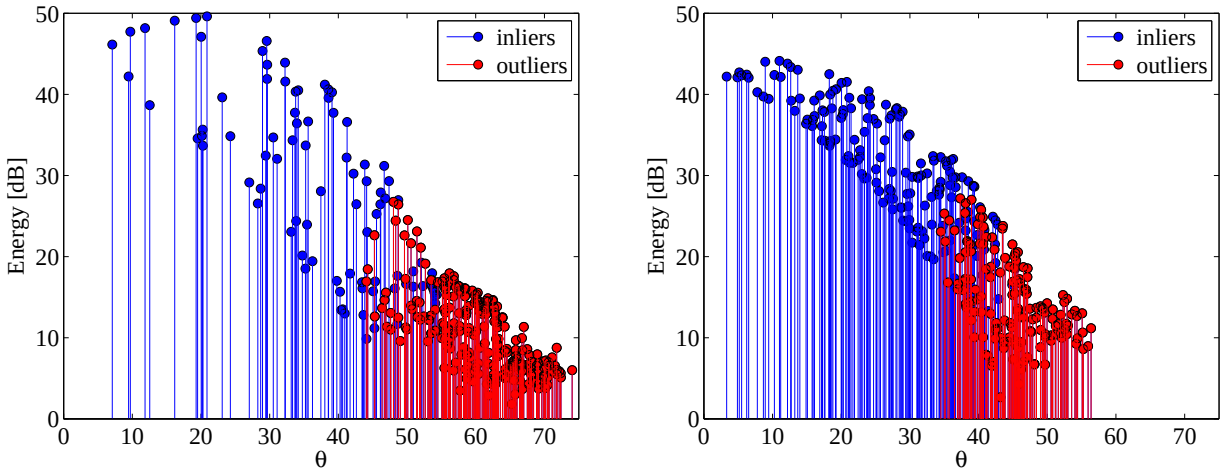

(a) Close measurement plane **(b)** Far measurement plane

Figure 3.47 – Energy distribution in terms of the angle between normal vector calculated by energy fitting and the measurement position. Element 295

At first glance the main difference with the results for the unfitted normal vector is that a shift has occurred in the angle values: for the same measurement positions the angles to the normal vector are wider. In terms of the directivity pattern this method does not compensate the two emerging patterns in the data, although the spread of the data-points seems to be less regular and the patterns appear less clearly.

Comparing this results with the ones obtained with the array fitting approach in terms of the distribution of the energy, the energy fitting method seems to work better. However, the introduction of the angle shift was not present in the array fitting approach. In terms of efficiency, the array fitting has to be performed once for all elements, while the energy fitting varies for different elements.

3.7.2.3 Center of Mass Fitting

After seeing the slight improvement that the energy fitting had achieved, the idea of the center of mass of the energy and the measurement positions was investigated to observe whether the energy models accurately depicted the energy distribution of the measurements. The center of mass in terms of the energy was found following the equation:

$$R = \frac{1}{M}\sum_{i=1}^{n} r_i m_i \tag{3.21}$$

Where R are the coordinates of the center of mass, M is the total energy, m_i each measurement's energy and r_i the coordinates for each measurement.

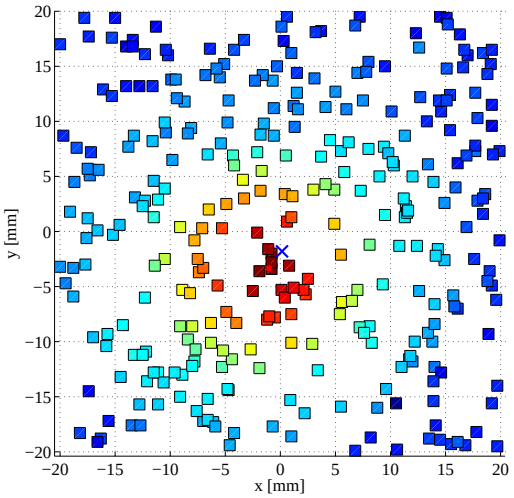

Figure 3.48 – Mass center (red) and modelled energy maximum (blue) over the measurement close plane

After calculating the coordinates for this point it is interesting to see how it differs from the maximum energy point found in the energy modelling. In order to illustrate this fact both points have been plotted in Figure 3.48. It seems as if the energy maximum is a bit displaced from the value that could be expected from the energies measured. This suggests that the energy model was too coarse and did not approximate the energy distribution in the measurement plane accurately enough.

However, the energy model was used in the same way in the far and close plane, and as the normal vector of the array element is calculated as the vector that connects the maximums of the two planes, the deviation between model and reality could be the same and the direction of the vector could actually be quite similar to the one obtained with the center of mass approach. This would account for the fact that the results for both methods are not that different, as can be seen when comparing Figures 3.49 and 3.47 .

The value obtained for the normal vector using this method is $\vec{n} = [-0.0791,\ 0.0440,\ 0.9959]$, which is quite similar to the one obtained through the energy fitting approach. The results obtained using this normal vector do not show an improvement from the unfitted results, since the data points appear more scattered than in the original case. They also show slightly worse results than the energy fitting ones, with presence of the angle shift, and less defined patterns than in the array fitting results.

3.7.2.4 Optimization of the Normal Vector

Lastly, and given the inconclusive results that the previously described methods obtained, a more mathematical approach to the problem was taken. The driving idea was to find an optimized value for the

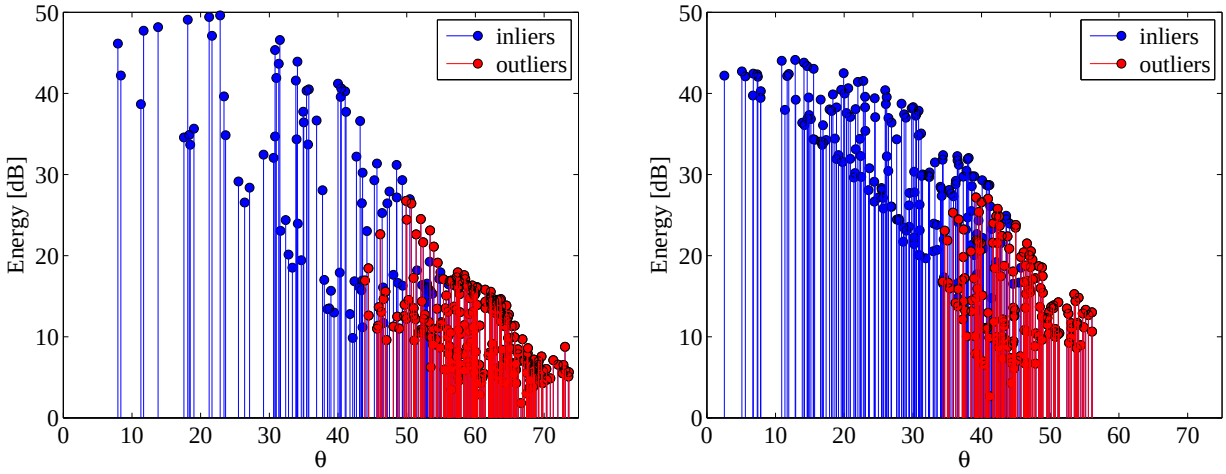

(a) Measurement depth 1 cm

(b) Measurement depth 2 cm

Figure 3.49 – Energy distribution in terms of the angle between normal vector calculated with the mass center approach and the measurement position. Element 295.

normal vector that could reduce the dispersion of the data.

The optimized normal vector is found by choosing the coordinate values that smooth the energy curve the most. The norm chosen to characterize the smoothness of the curve is the cross-correlation of the curve with a version of itself delayed one sample:

$$C_{xx} = \sum_{n=-\infty}^{\infty} x[n] \cdot x[(n+1) - l] \tag{3.22}$$

This value is normalized, so that when the two signals are equal, the output of the cross correlation will be 1. The optimization problem consists in finding the normal vector that generates the curve with a cross-correlation closest to one.

The results obtained using this method are shown in Figure 3.50:

It can be seen that there is a clear improvement in the curves, specially in the plane 2 cm away from the transducer. The optimal normal vector has been found to be $\vec{n} = [-0.065,\ -0.118,\ 0.9905]$. This results must be treated with caution, since the normal vector has been calculated in order to obtain desired values, meaning that, in principle, there was no physical explanation behind these results. However, the fact that adjusting the normal vector according to physical estimates did not yield such good results leads to believe that by choosing an optimized normal vector, a compensation is being introduced to another problem.

The fact that the elements that were estimated to have *"good"* directivity curves were the central ones of the transducer array is not without importance, since they were also the ones whose coordinates were more accurately estimated. The angle calculation is very much dependent on this coordinate value because it defines the vector that would rotate around the normal and thus generate the angle values. This lead to the conclusion that in this optimizing process, when the normal vector is changed to adjust the angle values, what is actually being done is compensating for a faulty estimation of the coordinate position.

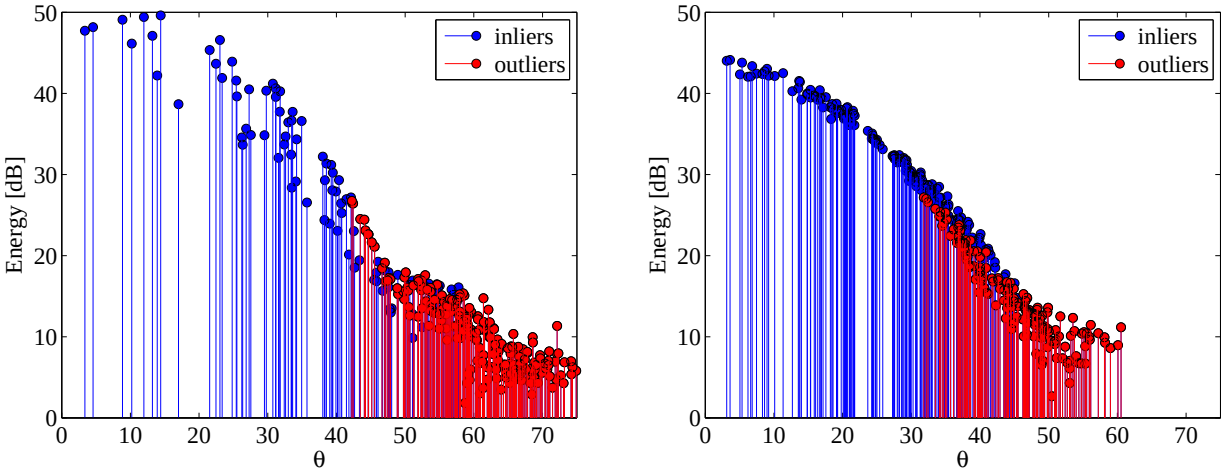

(a) Measurement depth 1 cm

(b) Measurement depth 2 cm

Figure 3.50 – Energy distribution in terms of the angle between the optimized normal vector and the measurement position. Element 295

After using this approach over the elements that were judged to have *"bad"* directivity curves, values for the acceptance angles could be calculated. They are shown in Table 3.3.

Table 3.3 – Angle of acceptance values after optimization

Measurement depth	Level	Acceptance angle
1 cm	-3 dB	$18.14° \pm 2.04°$
	-6 dB	$24.09° \pm 1.59°$
	-12 dB	$32.99° \pm 1.59°$
2 cm	-3 dB	$13.57° \pm 1.10°$
	-6 dB	$18.96° \pm 1.02°$
	-12 dB	$27.18° \pm 0.92°$

These values are quite similar to the ones estimated for the *"good"* elements, showing that this method is useful to overcome the problems of non-accurately defined coordinates for the elements and thus permits to estimate the angles of acceptance precisely.

3.7.3 Hydrophone Influence

In the previous sections, the directivity curves and acceptance angles of the elements of the transducer array were investigated. Up to this point the influence that the measuring device, i.e. the hydrophone, had over the measured signals was not taken into account. This means that the hydrophone's own directivity pattern was neglected. In this section the extent to which this assumption holds true will be investigated.

The measurements were performed with a Onda HGL-0400 Hydrophone.(Its data sheet is included in Appendix B). This hydrophone has its own directivity pattern which influences the data measured by the device, meaning that the recorded signal will vary depending on the angle of incidence of the travelling wave.

In order to remove the effect of the hydrophone's directivity from the measurements the first step should be finding the directivity function of the hydrophone. The technical information provided for the device includes a directivity curve for a resonance frequency of 5 MHz and, since this information is given from an empirical measurement, a function that models this curve must be found.

In order to calculate the directivity function of the hydrophone the method indicated in [19] will be used, and a continuous wave field will be assumed. This assumption is made due to the fact that, even though the field generated by the ultrasound probe is a pulsed field, derivation of the directivity function in such fields is not trivial, as it is disscussed in [17], and neither is measuring it in an experimental set-up, [18]. Since the measurements were produced in a mono-frequency field, it will be assumed that the approximation of a continuous field holds.

The directivity function expected for a piston transducer is defined as:

$$D(\theta) = \frac{2J_1(ka_e \sin\theta)}{ka_e \sin\theta} \tag{3.23}$$

Where θ is the aperture angle to the normal of the hydrophone, a_e is the effective radio of the hydrophone's surface and k is the wave number. A complete derivation of this equation can be found in [28].

The effective hydrophone radius can be obtained following the IEC standard 62127-3, [29]. The angles corresponding to -3 dB and -6 dB must be read from the directivity plot in order to obtain a_{e3} and a_{e6}, as follows:

$$a_{e3} = \frac{1.62c}{2\pi f \sin\theta_3} \tag{3.24}$$

$$a_{e6} = \frac{2.22c}{2\pi f \sin\theta_6} \tag{3.25}$$

The effective radius should be taken as the average of the two values. Consulting the data sheet, the values found for the angles are $\theta_3 = 22.5°$ and $\theta_3 = 32.5°$. Taking the average of equations 3.24 and 3.25 the value for the effective radius of the active element of the hydrophone is found to be: $a_e \approx 0.29$ mm.

The calculated directivity function found applying this method is plotted against the empirical one found in the data sheet in Figure 3.51.

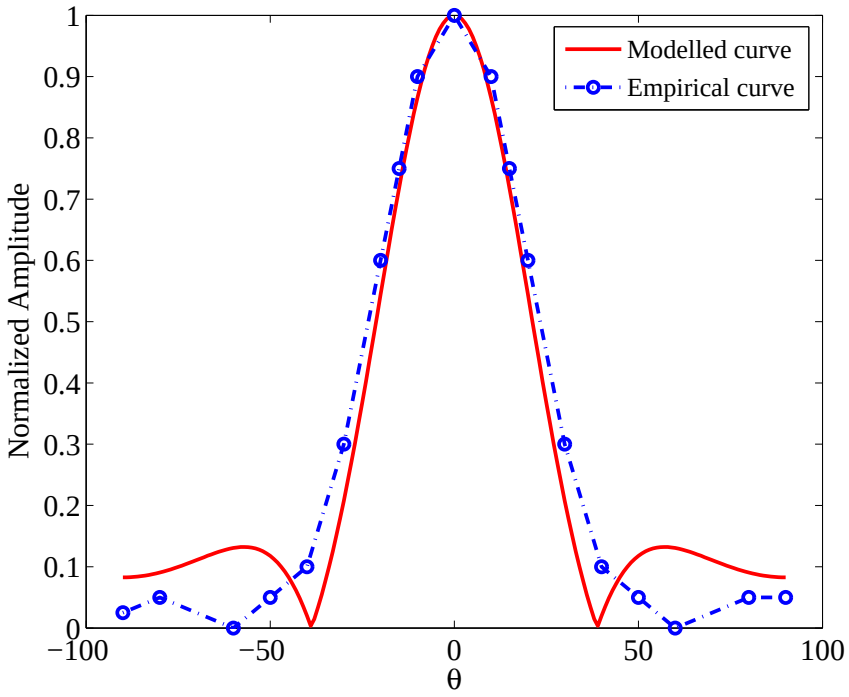

Figure 3.51 – Hydrophone directivity. Frequency 5 MHz

The modelled curve is a fairly accurate approximation for angles below $40°$. However, a problem arose at this point of the investigation due to the fact that the effective radius used to develop the function is dependent on the frequency and thus, the empirical and modelled curves might not hold true for the experiment under study, where the resonance frequency was 3.5 MHz.

For the sake of studying how to remove the hydrophone's influence from the measured data the values from the 5 MHz curve were used here, although it must be kept in mind that this is not strictly correct. When performing this task in an experimental set-up, the adequate values for the hydrophone's directivity should be used.

The hydrophone's directivity is given in terms of its normalized amplitude, thus the effect of the hydrophone in the energy values can be compensated by dividing the measured values with the normalized directivity in the angle of incidence.

Results for element 492 are shown in Figure 3.52, where the energy values are presented before and after applying the compensation for the energy and are expressed in a logarithmic scale:

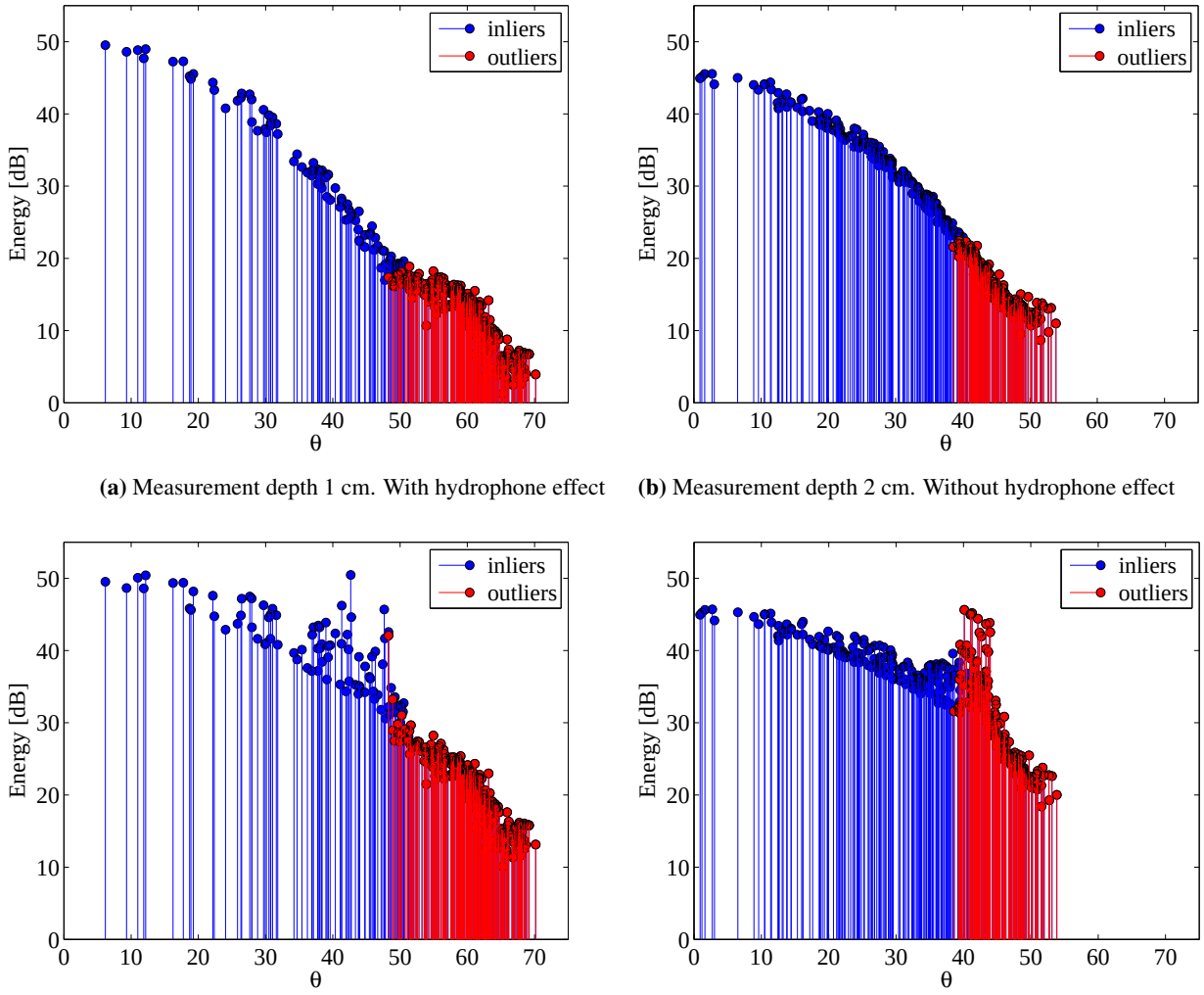

(a) Measurement depth 1 cm. With hydrophone effect

(b) Measurement depth 2 cm. Without hydrophone effect

(c) Measurement depth 1 cm. With hydrophone effect

(d) Measurement depth 2 cm. With hydrophone effect

Figure 3.52 – Energy distribution in terms of the angle for element 492 with and witouth hydrophone correction

The effect shown in the results is a decrease in the steep of the directivity curve, that also leads to wider acceptance angles. Problems appear around the points where the directivity function of the hydrophone presents values close to zero. This denotes the fact that a mathematical function was used to model the hydrophone's directivity, where in reality there are not zeros in the directivity function of the hydrophone, as it is shown on its data sheet (Appendx B).

The process of removing the effects of the hydrophone's directivity which has been described in this section is potentially useful, but depends (as it was to be expected) highly in the characterization of the

hydrophone's directivity pattern. In this case a number of assumptions have been made, like using a continuous field approximation as well as accepting that the curves for a 5 MHz emission could be used with 3.5 MHz data. These are not small assumptions, and thus the results presented in Figure 3.52 must not be regarded as the actual directivity functions of the transducer array element.

However if the hydrophone's directivity was measured in the frequency of interest, it would be possible to apply the models described in the IEC standard 62127-3 to obtain a normalized directivity function that could be suppressed from the measured data. In that scenario the results would more accurately describe the directivity of the transducer array elements.

Another option would be to use a hydrophone with a wider directivity pattern, i.e. wider acceptance angle, in the experiment, so that the influence of the hydrophone's directivity would be considerably reduced. Such hydrophone's are, for example, Onda HGL-0200 or Onda HGL-0085, as it can be consulted in Appendix B.

3.8 Radiation Pattern

Another way of characterising the emission of a transducer is that of its radiation pattern, that is the time-space representation of the pressure emitted by the element.

These radiation patterns for elements 25 and 306 are shown in figures 3.53 and 3.54, respectively. They have been estimated using the envelope of the recorded signal in logarithmic scale at the two depths of measurement performed in the experiment, 1 and 2 cm away from the transducer.

The main difficulty when obtaining this information from the recorded data laid in the fact that the positions of the hydrophone were spread randomly through the measuring planes, resulting in an uneven distribution on the xy-plane. As shown in literature, references [4] or [20] describe such experiments, ideally the hydrophone is placed in a fixed x-axis, while moved around in the y axis to record the spatial distribution of the emitted ultrasound field.

However, in the experiment realized to obtain the data under study this procedure was not followed. It is possible, nonetheless, to approximate the radiation pattern by making the assumption that the field across the x-direction is kept constant. In that sense, the results shown here correspond to fixed values of the z-coordinate but for varying values of the x coordinate. Another problem that arose due to the spatial distribution of the measurement positions is that, for the same values of the analysed y-axis, different waves were recorded (for different x coordinates). The approach used to overcome this issue was to plot the envelope of the mean value of the recorded waves in the repeated positions.

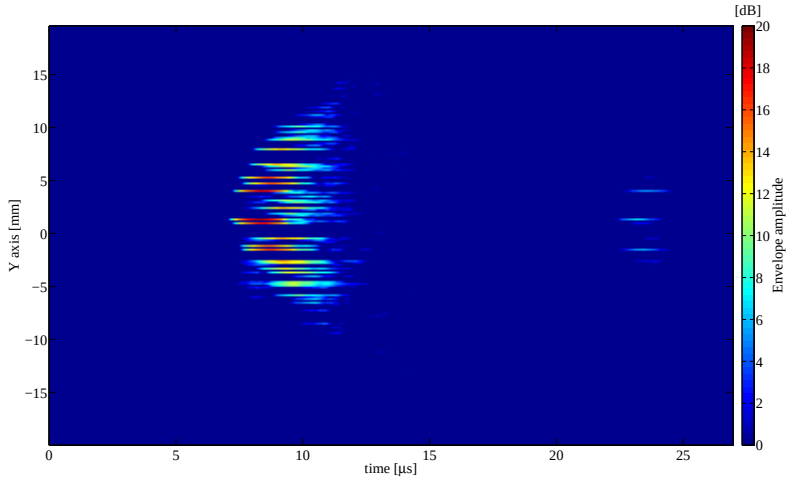

(a) Measurement depth 1 cm

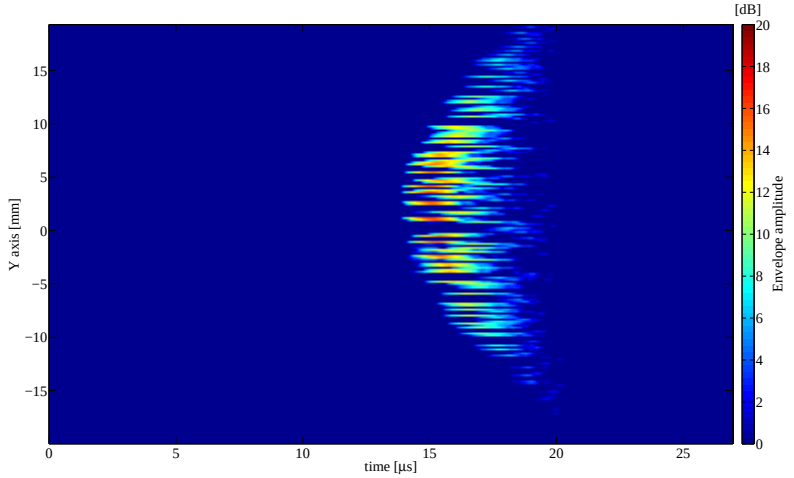

(b) Measurement depth 2 cm

Figure 3.53 – Radiation Pattern Element 25.

Lastly, a lack of resolution was found in the obtained images, this is a result of the number of measurements along the y-axis not being enough to produce a smooth image. However, an outline of the pressure field produced by the transducer array element can be clearly observed.

The pressure distribution suffers a decay in the signal amplitude alongside the z-direction, this is noticeable in the lower amplitude values of the measuring plane further away from the transducer. The pressure fluctuations appear to be wider in the second plane, pointing to a widening beam of the transducer element.

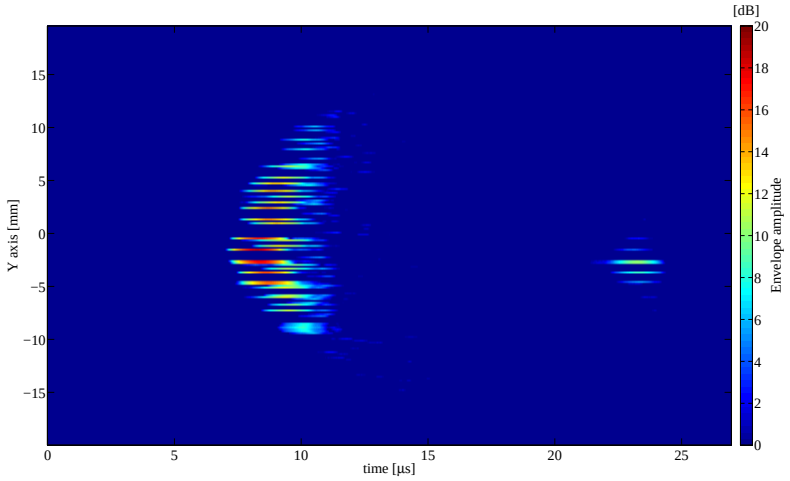

(a) Measurement depth 1 cm

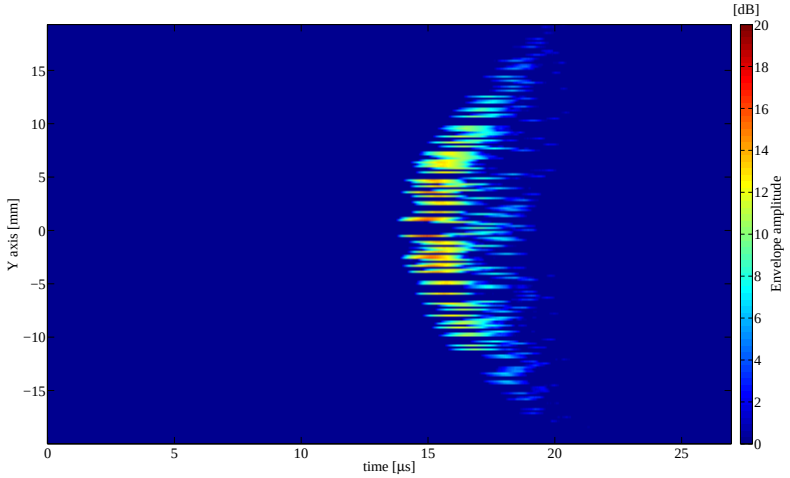

(b) Measurement depth 2 cm

Figure 3.54 – Radiation Pattern Element 306.

It is noticeable the presence of echoes in the radiation patterns with depth of 1 cm from the transducer. These echoes are believed to be produced by the surface of the hydrophone (see Figure 3.4) and then reflected again by the transducer element thus, being recorded in the hydrophone as a delayed and attenuated version of the received signal.

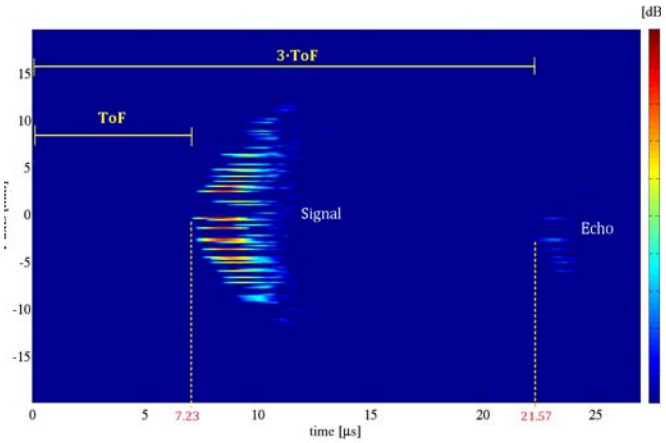

Figure 3.55 – Presence of Echoes for element 457

This is in accordance with the time where these signal are recorded. As it can be seen in Figure 3.55, the time of arrival of the first signal, that is the Time of Flight (ToF), is a third of the time of arrival of the echoed signal, which makes for the time to travel

from the hydrophone back to the transducer and then back again to the hydrophone. In the case of the measurements performed 2 cm from the array, the echoes do not appear in the radiation plots since the time needed for the pressure wave to travel back and forth from the hydrophone is longer than the measuring time.

In terms of variation throughout elements, all patterns have the same shape and similar amplitude values across elements. Some variations appear in the amplitudes of the different elements that can be linked to the fact that these elements don't have the same sensitivities, as described in the data sheet of the array (Appendix A).

The appearance of the field does not suffer significant variations. There are small changes in terms of the arrival time, -that depends on the relative positions of hydrophone and emitting element-. Changes can also be perceived in terms of the spatial distribution of the pressure, with small shifts over the y-axis taking place between elements, presumably due to the spatial location of the element. This can be seen by comparing Figures 3.53 and 3.54, the first one corresponds to element 25 with an xy coordinate of [5, 2.9] mm, whereas the second one corresponds to element 306, with coordinates [-1.8, 0.4] mm and this difference in the element position translates into a spatial shift in the pressure field shape.

There is a group of elements that generate a complete different looking pressure field, and those are the elements that were detected as not emitting, or dead, in section 3.4. As it could be expected they do not produce any disturbance in the form of pressure variations. As an example, "radiation" patterns for element 410 in Figure 3.56.

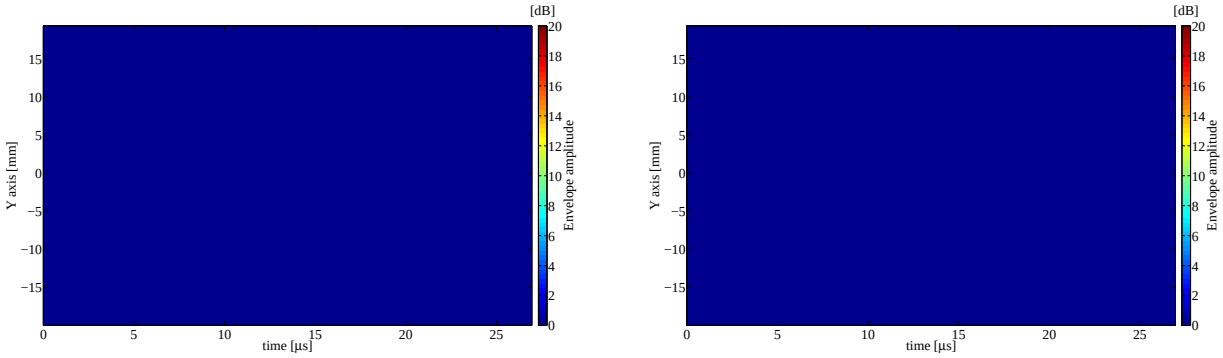

(a) Measurement depth 1 cm **(b)** Measurement depth 2 cm

Figure 3.56 – Radiation Pattern Element 410.

It has been shown in this section that is possible to estimate the radiation patterns of the array elements from the studied experiment. The main drawbacks are the lack of resolution due to a small number of measurements with different y-coordinates and the fact that it was not possible to fix the value of the x-coordinate, thus having to accept some uncertainties in the results, as opposed to results obtained from experiments specifically designed to determine radiation patterns.

Nonetheless the process to obtain this time-space representations is relatively straight forward and the results allow to ha a clear idea of the pressure field generated by the tranducer's elements.

CHAPTER 4

Measurement Models

Once the data has been analysed, it has been shown that having a meaningful data set, composed of an optimal number of measurements and taken in relevant positions, is determinant to obtain the parameters chosen to characterize a transducer array.

In order to design an optimal experimental set-up that would allow to gather such a dataset, a model of the experiment is generated and tested. First, a simple model is developed generating times of flight for each element of the array. Once this model has been tested, a more complex model is implemented by constructing modelled signals in image of the ones recorded in the empirical experiment .

These models and the different tests they were subjected to are explained in more detail in this chapter.

4.1 Simple Model

The model searched for has to reproduce the experimental set-up that was used to generate the data analysed throughout this project and that was described in section 3.1.

The first approach to implement such a model is a simple design that can be explained in the following steps:

1. Generate a set of coordinates for the different transducer array elements (see Figure 4.1).
2. Generate sets of coordinates for possible measurement positions of the hydrophone.
3. Using equation 3.2, calcuate time of flight values for the coordinates generated in steps 1 and 2. The value of the speed of sound in water has been assumed to be 1490 $\mathrm{m\,s^{-1}}$.
4. Apply the optimization algorithm detailed in 3.3.2 to the generated times of flight in order to find the coordinates for the transducer array elements.

To asses the quality of the model, the deviation between the defined array positions and the ones obtained after applying the optimization through the model will be calculated.

This model has been tested with and without the presence of noise and different parameters have been analysed such a the impact of the number of hydrophone positions, the magnitude of the noise or the

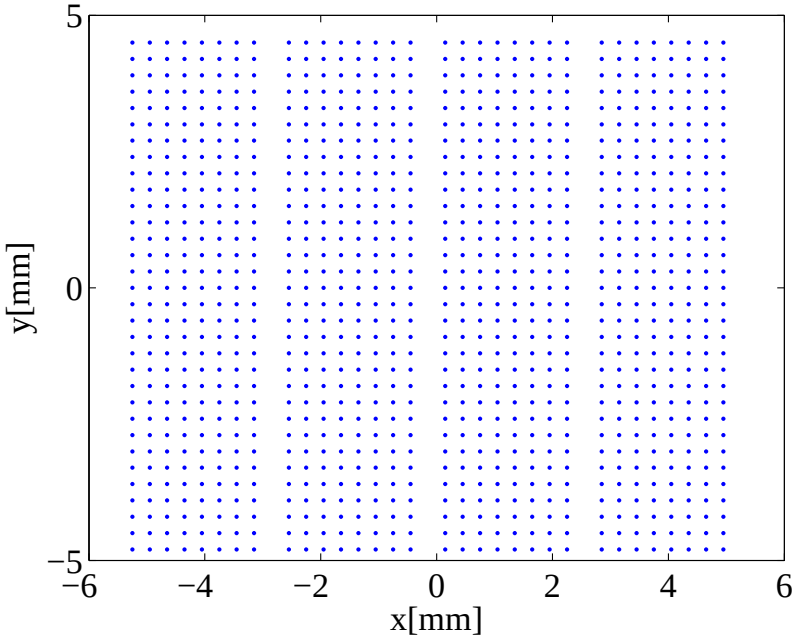

Figure 4.1 – Coordinates of the array elements in the XY plane

distribution of the hydrophone positions. The obtained results are shown and discussed below.

4.1.1 Noiseless Simulation

First, the model has been tried considering an ideal scenario where the times of flight are not subject to the effect of any external modification. The effect on the accuracy of the model of the number of measurements performed and how they are distributed has been studied.

The accuracy of the model is measured in terms of the mean deviation between the coordinates obtained by the model and the ones manually generated to calculate the times of flight.

Distribution of measurement positions

This part of the investigation aims to determine whether the distribution of the positions of the hydrophone measuring has an effect in the accuracy of the model. Different set ups for a fixed number of measurements have been tried: randomly in two planes, randomly also around the axial direction and equally distributed along one and two planes, among others. The results obtained are shown in Table 4.1.

Table 4.1 – Error values for different measurement set-ups

Distribution	**Mean deviation** [mm]
Equally distributed in one plane	5.63×10^{-15}
Equally distributed in two planes	8.11×10^{-15}
Equally distributed in three planes	1.04×10^{-14}
Randomly distributed in one plane	5.73×10^{-15}
Randomly distributed in two planes	6.45×10^{-16}
Randomly distributed in three planes	7.50×10^{-16}
Randomly distributed in 3D	1.34×10^{-14}

Number of measurements

To study the effect that the number of hydrophone positions, and thus the number of measurements inputed in the model, has on the results obtained when applying the model, a single plane 10 cm away from the transducer is chosen to contain all measurements. The distribution of the coordinates around the xy-plane will be done randomly in the range of -1 cm to 1cm in both x and y directions (where the origin [x, y] corresponds to the center of the transducer array). An example of such a set up is shown in Figure 4.2.

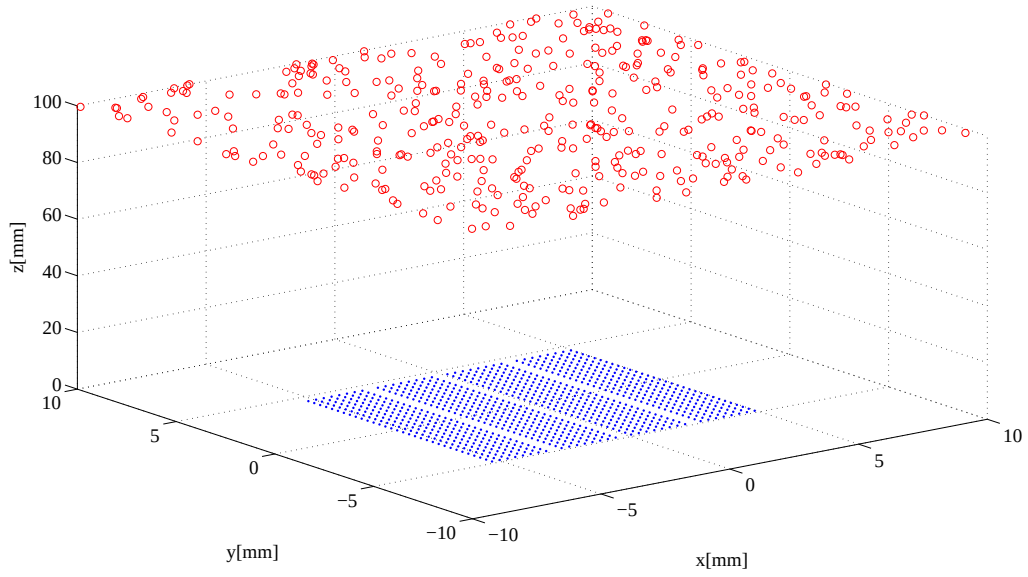

Figure 4.2 – Example configuration for 200 measurements. The array coordinates are shown in blue while the red dots indicate measurement coordinates

Error values for different number of hydrophone positions are shown in Table 4.2.

Table 4.2 – Error values for different number of measurement

Number of measurements	**Mean deviation** [mm]
100	1.23×10^{-14}
250	6.3×10^{-15}
500	4.56×10^{-15}
750	4.23×10^{-15}
1000	3.85×10^{-15}

It is difficult to draw conclusions from these results, since they all indicate a good agreement between the modelled and the original positions, as indicated by the small error values. Tables 4.2 and 4.1 show that the model works perfect when there is no noise present.

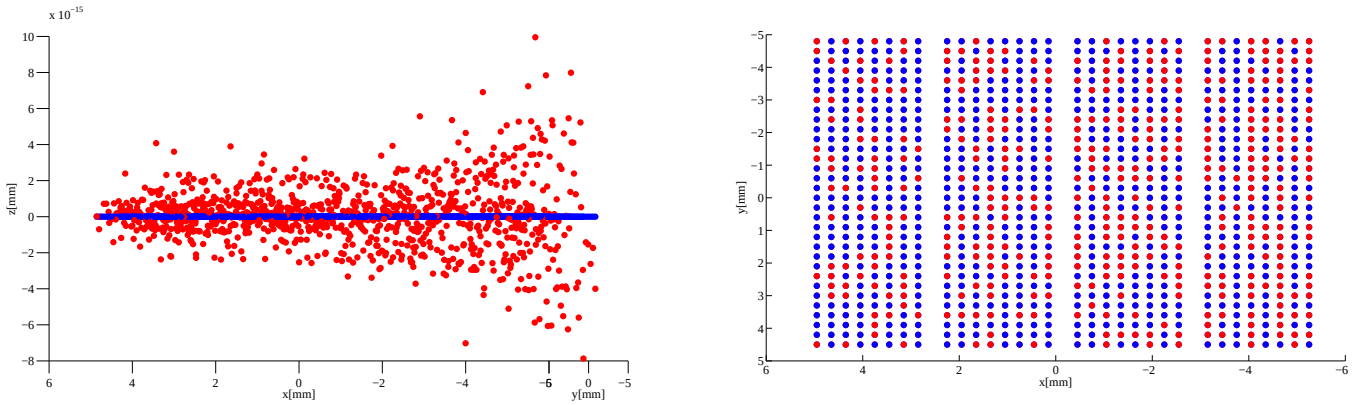

(a) XZ plane. **(b)** XY plane.

Figure 4.3 – Original (blue) and modelled (red)array positions

As it is shown in Figure 4.3, the deviations are really small (in the order of 10^{-14} mm), and mainly in the axial plane. That is why the real potency of this model should be assessed in the presence of noise.

4.1.2 Effects of Noise

In order to be able to draw conclusions from the model it is necessary to include the effects of noise. As explained previously, this is a simple model based on calculating the times of flight directly from the coordinates of the array elements and the hydrophone positions. In that sense the included noise cannot be regarded as measurement noise, that is, it does not correspond directly with the electronic noise that could be recorded by the hydrophone in a real experiment.

It is possible, nonetheless, to model some of this effects even with this simple model, assuming that noise in the measurement would create deviations in the detected time of flight. Such deviations can be, indeed, included in the model.

Another effect that can be included in the model is the time of flight bias. This is a unique value for each transducer element and introduces a delay in the time of arrival to the hydrophone, it can be due to different length of the cables from the signal generator to the transducer element, which will cause a delay in the emission of the signal.

Both effects have been tested and the results are discussed below.

4.1.2.1 Random Noise

As stated before, the effects of additive random noise are modelled as random variations in the time of flight values. The model has been tried with different distributions of hydrophone positions, number of measurements and magnitudes of noise.

Distribution of measurements

To determine whether the distribution of the positions of the hydrophone has an effect in the accuracy of the model, different set-ups for a fixed number of measurements have been tested: randomly in two planes, randomly also around the axial direction, equally distributed along one and two planes, among others.

The number of hydrophone positions has been set to 400, and the order of magnitude of the time deviations to 1 µs. When dividing the measurement positions into planes in the z-direction, the chosen depths of measurement have been 2, 4, and 6 cm. The xy-plane is defined between +1 cm and -1 cm of the origin, where the origin [x, y] corresponds to the center of the transducer array.

The error norm chosen is the mean deviation of the coordinates obtained for the array elements by the model and the original ones. Since the time deviation is random, the model is tried 5 times in order to find the mean error and the standard deviation across trials.

Table 4.3 – Error values for different distributions of the measurements in noisy model

Number of measurements	Mean Error [mm]	Standard Deviation [mm]
Equally distributed in one plane	0.21	1.60×10^{-3}
Equally distributed in two planes	0.25	4.60×10^{-3}
Equally distributed in three planes	0.30	5.88×10^{-3}
Randomly distributed in one plane	0.22	4.71×10^{-3}
Randomly distributed in two planes	0.27	6.88×10^{-3}
Randomly distributed in three planes	0.31	8.23×10^{-3}
Randomly distributed in 3D	0.34	8.55×10^{-3}

Table 4.3 shows the results of this modelling, they show better results when the hydrophone positions are localized within one plane. This could be explained by the fact that as the number of planes increases while keeping constant the number of positions, what is happening is that we are placing the hypothetical hydrophone further away from the array, and thus making the results worse. The effect of the distance between hydrophone and array has also been investigated in order to prove this, and the results are shown in the next sections.

Number of measurements

The effect that the number of measurements, that is the number of hydrophone positions, has over the results of the model has been studied. Also, the effect of the distance from these measuring positions to the array has been investigated by means of placing the same number of measurements at different distances. Results are shown in Table 4.4.

Two parallel models have been run, the time deviations for both of them have been set to be randomly generated with an order of magnitude of 1 μm. The positions of the hydrophone have been chosen randomly in all three dimensions. In the xy-plane they are distributed between -10 and 10 mm in both the x-direction and in the y-direction. In the z-direction, that is the depth of the measurements, the distribution is different for the two models, one having a distribution between 2 and 6 cm of distance from the array and the other between 10 and 30 cm away from the array.

Table 4.4 – Error values for different number of measurement in noisy model

Number of measurements	Mean Error [mm]	Standard Deviation [mm]
100	0.69	43.30×10^{-3}
250	0.44	15.60×10^{-3}
500	0.31	2.90×10^{-3}
750	0.25	2.80×10^{-3}
1000	0.22	5.20×10^{-3}

(a) Measuring positions distributed between 2-6 cm

Number of measurements	Mean Error [mm]	Standard Deviation [mm]
100	3.18	9.67×10^{-2}
250	2.04	5.49×10^{-2}
500	1.45	6.33×10^{-2}
750	1.17	0.68×10^{-2}
1000	1.03	1.84×10^{-2}

(b) Measuring positions distributed between 10-30 cm

The simulations have been run five times for each case in order to find mean values of the error, this is done to minimize possible discrepancies due to the random nature of the coordinates of the positions. Values of the mean errors and the standard deviations of these error have been plotted in Figure 4.4.

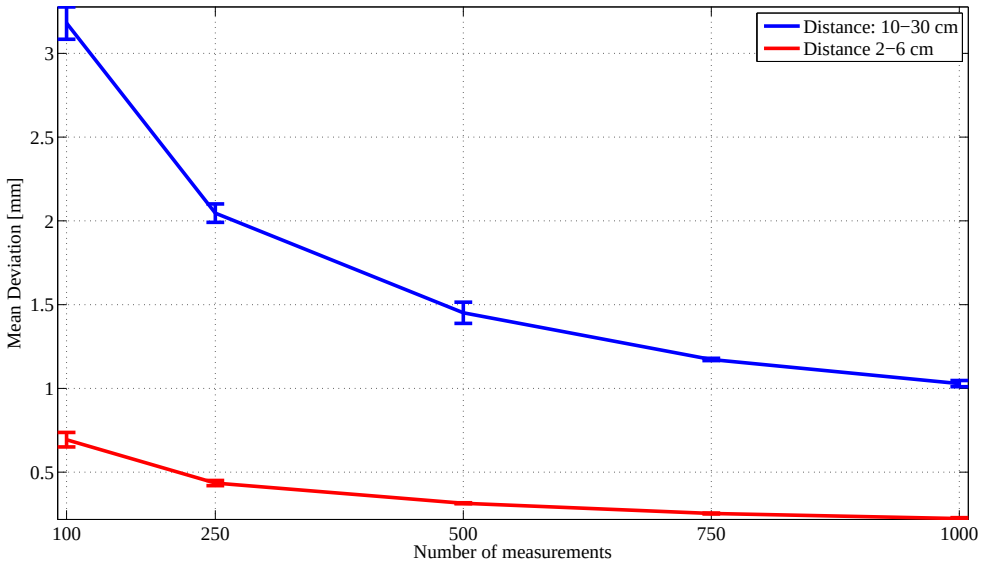

Figure 4.4 – Estimation error as a function of number of measurements for different distances

It is clear from both Table 4.4 and Figure 4.4 that increasing the number of measurements leads to better results of the model, although this pattern tends to stabilize as the numbers increase. The results also pointed out to the phenomenon addressed earlier, when the depth of measurement was considered a determinant factor to precisely find the correct array coordinates, because the model performs visibly better when the hydrophone is placed closer to the array.

Magnitude of the deviations

It is also important to test the extent of the model's resistance to the time deviations by subjecting it to variations of different magnitudes.

It is not possible to talk of signal to noise ratio (SNR) since the model deals only with times of flight and does not model the sent and received signals. However, it must be taken into account that the ideal times of flight (i.e. with no deviations) are in the order of magnitude of 10 µs. The order of the deviation should be studied according to this value, since it is the ratio between the ideal time of flight and the size of the noise-induced deviations what determines the effect that these deviations have in the model.

The number of hydrophone measurement positions was set to 400, distributed randomly in the three dimensions, the z-dimension varies between 2 and 6 cm far away from the array, and the x and y dimensions vary between -1 cm an +1 cm from the center of coordinates, where the origin [x, y] corresponds to the center of the transducer array.

The results presented in Table 4.5 show how the model is not able to support time deviations that are bigger than the order of magnitude of the time of flight -10 µs-, but that is strongly protected against them when the deviations are smaller.

Table 4.5 – Error values for different magnitudes of the time deviation

Order of magnitude of time deviation [s]	**Mean error** [mm]	**Standard deviation of error** [mm]
10^{-2}	217.07	6.43
10^{-4}	23.46	0.19
10^{-6}	0.35	7.21×10^{-3}
10^{-8}	3.53×10^{-3}	1.07×10^{-4}
10^{-10}	3.54×10^{-5}	9.25×10^{7}
10^{-12}	3.50×10^{-9}	8.44×10^{-9}

These results are shown in Figure 4.5 having chosen a logarithmic scale in order to precisely depict the behaviour of the model for the smallest time deviations.

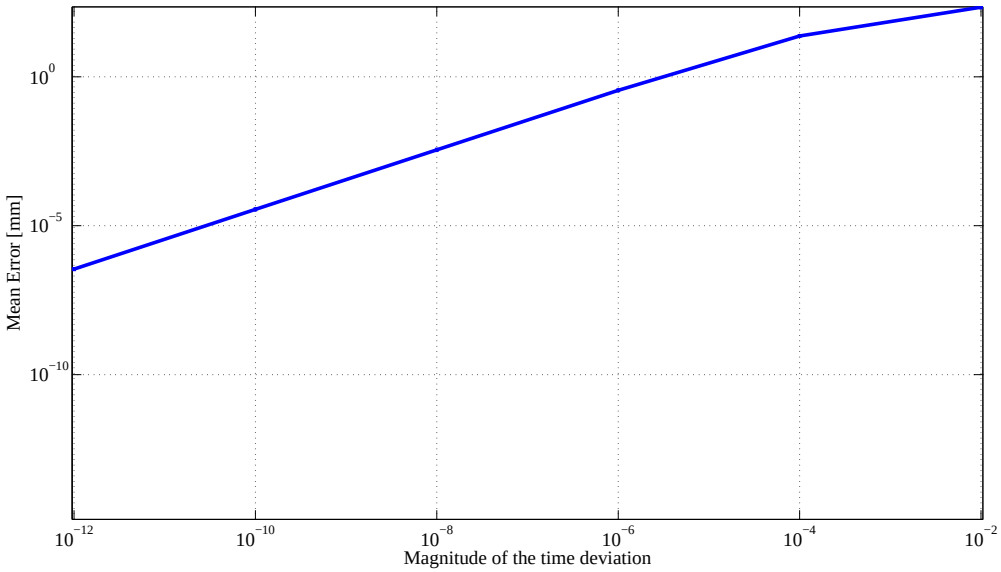

Figure 4.5 – Estimation error as a function of the magnitude of the time deviations

4.1.2.2 Bias from Array Elements

The time of flight values could be affected by other phenomena other than random noise. It is interesting to study the was bias affect the performance of the model, the term bias is used here to define a time delay that is constant throughout measurements.

In this section the effect of bias in the times of flights is analysed in terms of the magnitude of this bias, the number of elements affected by it and the number of measuring positions f the hydrophone.

The nature of this bias comes from the idea that all elements might not emit equally. This could be due to, as stated before, different lengths of the cable that connects the source of excitation with the transducer element, or other factors like different connectors or mismatches in the set up of the elements.

The bias is constant through all measurements, it is a value associated with each element, since is dependent of the physical characteristics of the array and of the element. This bias is randomly generated for each of the 1024 array elements.

In order to account for the time bias, the model must be slightly modified to include a new parameter that accounts for this time deviation. The equation that now defines the model is:

$$t = \frac{d}{c} + \tau = \frac{|\text{Measurement coordinates} - \text{Element coordinates}|}{c} + \tau \tag{4.1}$$

That is, ecuation 3.2 has been modified to include a time bias parameter τ. The value for the speed of sound in water, c, has been assumed to be 1490 $\mathrm{m\,s^{-1}}$. The optimization process that was described in section 3.6, is also applied in this case. The aim is still to minimize the error between the time of flight calculated and the measured time of flight for all measurements, but the parameters on which this optimization is based now include the time bias, τ , as well as the element's coordinates.

Number of measurements

It is also useful to study how the number of measurements positions affects the biased model. In this case, the hydrophone positions have been distributed randomly in the three dimensions, the z-dimension varies between 2 and 6 cm far away from the array, and the x and y dimensions vary between -1 cm and +1 cm from the center of coordinates, where the origin [x, y] corresponds to the center of the transducer array. the bias magnitude has been set to 1 µs and the number of elements that are affected by this bias has been set to 75% of the total.

Table 4.6 – Error values for different number of measurements in biased model

Number of measurements	**Mean error** [mm]	**Standard deviation of error** [mm]
100	2.62×10^{-14}	3.01×10^{-15}
250	2.42×10^{-14}	2.14×10^{-15}
500	1.99×10^{-14}	1.49×10^{-15}
750	2.04×10^{-14}	0.35×10^{-15}
1000	1.97×10^{-14}	1.15×10^{-15}

Table 4.6 shows the values obtained for the mean error and the standard deviation of the error after five runs of the model have been carried out. This was done to account for the fact that the time bias is generated randomly. It should be highlighted that the error values are really small, in the order of 10^{-14} mm, indicating that the model, with the modifications explained above, is strong enough to support time biases.

Figure 4.6 shows graphically the same results, showing that the error decreases with the number of measurements. However, if the scale of he error is noted, the improvement or lack of thereof does not seem so significant in absolute terms.

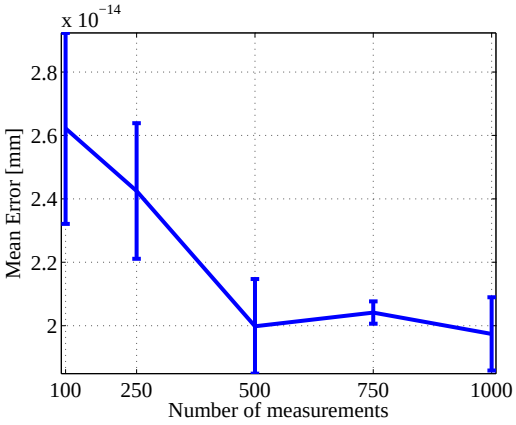

Figure 4.6 – Estimation error as a function of number of measurements in biased model

Magnitude of the bias

Just as the effect of the magnitude of the random noise was tested, so should the magnitude of the bias be, in order to asses how this variable affects the estimation of the positions of the array's elements.

In this case the number of measurement positions has been set to 400, distributed randomly along the three dimensions, and the number of elements affected has been set to 75%. Different orders of magnitude have been chosen to generate the random bias. The results are summed up in Table 4.7. They show small errors and deviations, indicating the strength of the model when dealing with this external bias, no matter its magnitude.

Table 4.7 – Error values for different magnitudes of the bias

Magnitud of the time bias	**Mean error** [mm]	**Standard deviation of error** [mm]
10^{-2}	31.93×10^{-14}	51.42×10^{-15}
10^{-4}	2.06×10^{-14}	1.01×10^{-15}
10^{-6}	2.33×10^{-14}	1.21×10^{-15}
10^{-8}	2.29×10^{-14}	1.75×10^{-15}
10^{-10}	2.26×10^{-14}	1.63×10^{-15}
10^{-12}	2.22×10^{-14}	1.57×10^{-15}
0 (i.e. no deviation)	1.10×10^{-14}	0

Number of elements affected

Lastly, the influence on the accuracy of the model according to the number of elements biased has been tried. The bias magnitude has been set to 1 µs for 400 measurement positions distributed randomly in the three dimensions.

Table 4.8, shows mean errors and the standard deviations of the errors for different percentages of the number of elements affected by the bias. The values are in the range of 10^{-14} mm, which means that the

Table 4.8 – Error values for different percentage of elements biased

Percentage of biased elements	**Mean error** [mm]	**Standard deviation of error** [mm]
10%	2.68×10^{-14}	2.74×10^{-15}
25%	2.48×10^{-14}	1.07×10^{-15}
50%	2.29×10^{-14}	0.76×10^{-15}
75%	2.22×10^{-14}	1.08×10^{-15}
100%	2.03×10^{-14}	1.09×10^{-15}

model is fairly accurate.

Again, the modified model appears to be able to cope satisfactorily with the bias values, no matter how many elements are affected by this phenomenon.

4.1.2.3 Random Noise and Bias

Finally the two sources of time deviations are added together to the model. Both the bias of each element and the random time deviations are inputed in the model. In order to account for the bias, the modified model presented in equation 4.1 is used in this section.

Based on the previous tests, the number of measurements is set to be 500, distributed randomly: in the z-direction coordinates vary between 2 cm and 6 cm, in the x direction between -1 cm and +1 cm and in the y direction between -1 cm and +1 cm, where the coordinate [0, 0, 0] is defined by the center of the transducer array.

The model with these parameters has been run ten times to account for the random nature of the data and the accuracy is measured as the mean deviation between the designed array coordinates and the ones obtained after the optimization model has been run.

In this simulation 75% of the elements presented a time bias, randomly defined in the order of magnitude of µs. The effect of random noise is modelled as time deviations randomly distributed across measurements and elements in the order of microseconds.

The results, shown in Figure 4.7, present deviations between the original and the inferred coordinates of the elements of the array, both in the distribution of the elements in the xy-plane and the z-direction. However, the estimations are still close to the original values. The average error obtained for this set-up is 0.01 mm with a standard deviation of $\pm 1.4 \times 10^{-3}$, which shows that noise and bias have an effect in terms of the accuracy of the model, but that even for deviations close to the value of the time of flight the deviations can be rather overcome by the model.

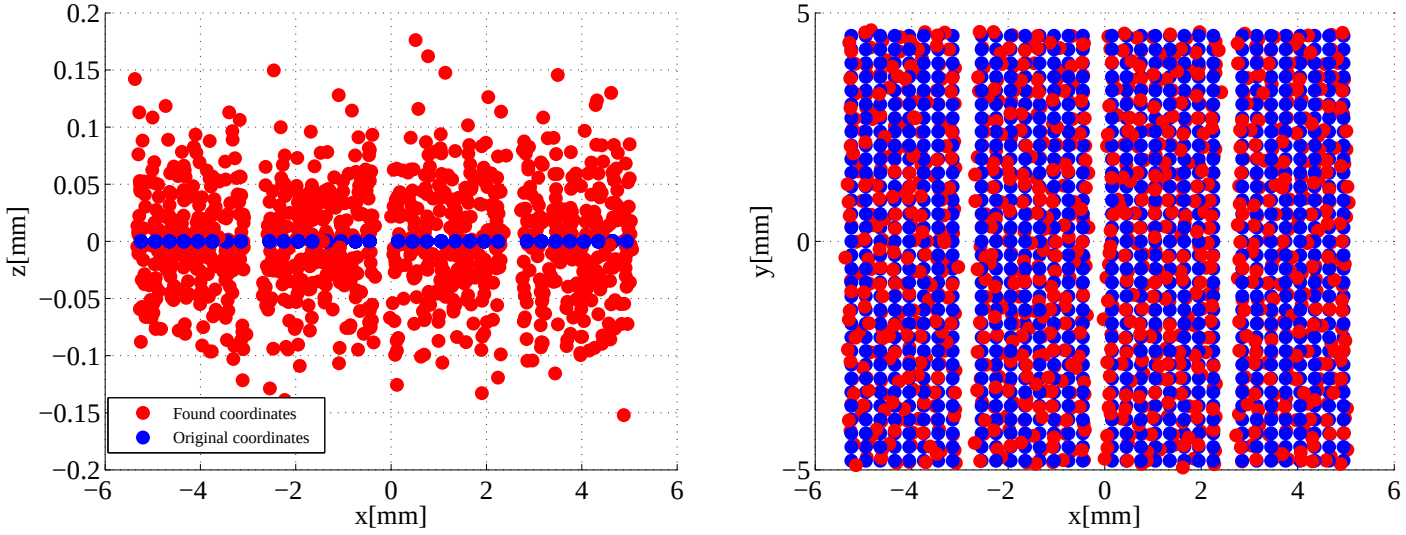

(a) xz-plane. **(b)** xy-plane.

Figure 4.7 – Model results with noise and bias

4.1.3 Model Results versus Experimental Results

A final test was performed in the model with the aim of comparing the results of this model with the real life experiment analysed in Chapter 3. For that purpose the hydrophone measurement positions are distributed in the model following the positions used in the empirical set-up. The array has been placed so that its center is corresponds to the center of coordinates [0, 0, 0]. The model positions for both the array and the hydrophone positions are shown in Figure 4.8.

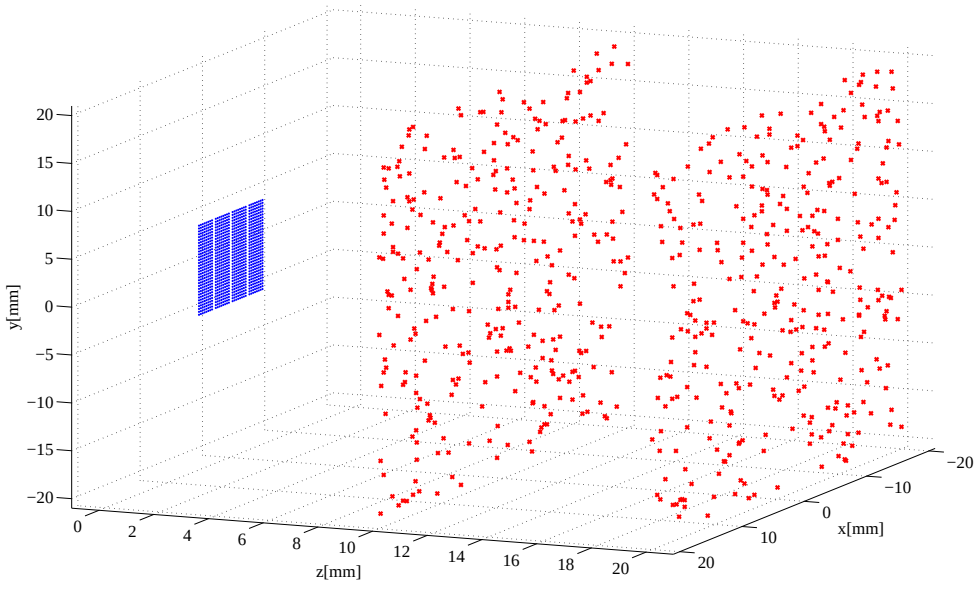

Figure 4.8 – Model set-up based on real life measurements

To simulate the effects of noise time variations are randomly generated for all elements and measurement positions in the order of 1 µs. That is, for each of the 643 hydrophone measuring positions, 1024 random deviations have been generated for each emitting element.

After the times of flight have been generated, the optimization process is applied ten times to account for the random nature of the introduced delays. The error values are generated as the mean of the deviations between the original array coordinates and the ones found by the optimization model.

The mean error across all optimizations is $0.01 \pm 1.76 \times 10^{-3}$ mm. A comparison between the original coordinates and the found ones after applying the model is shown in Figure 4.9.

The results are fairly accurate, although the presence of noise introduces some fluctuations in the them, both in the z-dimension and in the xy-plane. If compared with the results shown previously, it is clear that the fact that this measurements are performed closer to the array leads to smaller error values. This is in accordance to results shown in table 4.4. Also, the number of measurements is above 500, a number of measurements that showed good results in earlier runs of the simulation.

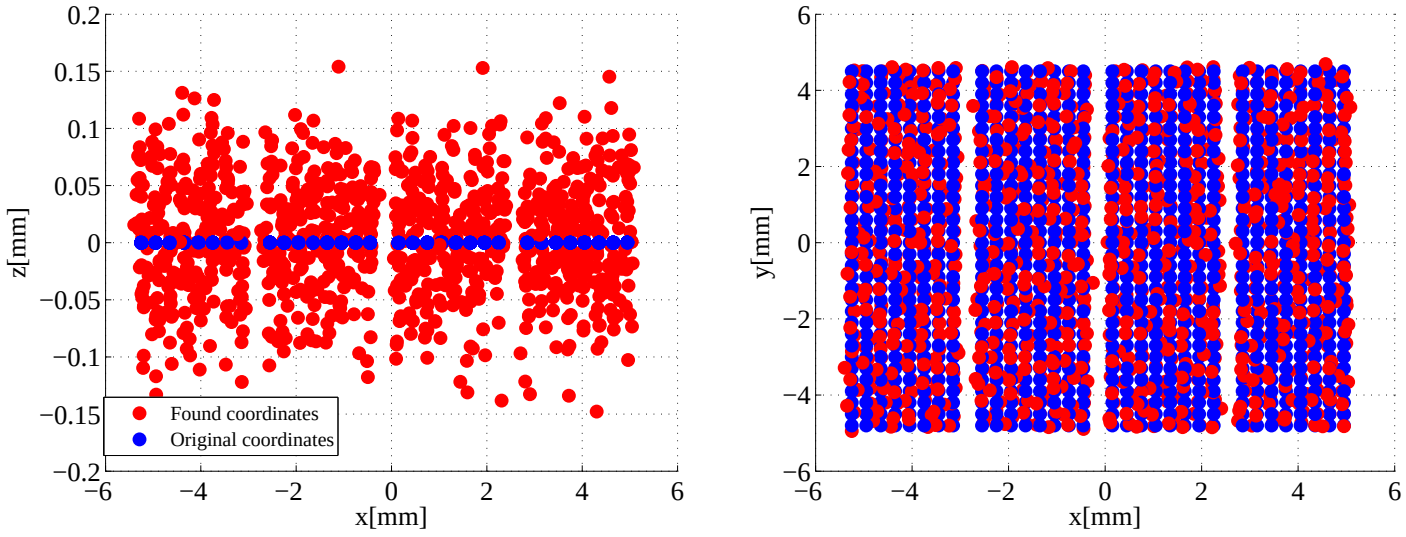

(a) 3D results

(b) xy-plane.

Figure 4.9 – Original (blue) and modelled (red) array positions

The trials for this model suggest that the proposed experiment could potentially gather meaningful results and provide a good estimation of the positions of the array. This, however, does not occur as accurately as predicted when dealing with real data, as was thoroughly explained in section 3.6.

This could be explained by the assumptions made to develop this model being too optimistic, for example the fact that the times of flight where calculated directly using equation 3.2 and did not go through the process of time of flight estimation used for the real data, or that the noise of the measurement was modelled as additive random time delay.

An extension of this model was developed in order to take into account this problems and it will be

explained in the following sections.

4.2 Complex Model

This model includes the generation of the signal received in the hydrophone, and thus covers not only the position estimation from the times of flight but also the calculation of the time of flight.

This model is a slight modification of the simple model and it can be explained in the following steps:

1. Generate a set of coordinates for the different transducer array elements (see Figure 4.1).
2. Generate sets of coordinates for possible measurement positions of the hydrophone.
3. Generate the emitted signal as four periods of a sinusoidal wave of frequency $f_0 = 3.5$MHz:

$$s(t) = \sin(2\pi f_0 t) \tag{4.2}$$

4. Using equation 3.2, calcuate times of flight values for the coordinates generated in steps 1 and 2. The value of the speed of sound in water has been assumed to be 1490 $\mathrm{m\,s^{-1}}$.
5. Calculate the corresponding sample value for the time of flight making use of a sampling frequency of $f_s = 70 \times 10^6$ samples/s.
6. Generate the samples of the model received signal, using the emitted signal and the value in samples of the time of flight.
7. Apply the time of flight estimation for the samples generated in the previous step using the zero crossing approach.
8. Apply the optimization algorithm detailed in 3.3.2 to the found times of flight in order to find the coordinates for the transducer array elements.

To assess the validity of this model, a set-up similar to the real life experiment analysed for this project has been used. The distribution of the coordinates is the same as was shown in figure 4.8. Both the ideal model and a model with the presence of noise have been tested.

4.2.1 Noiseless

A first simulation of the experimental model is done using as measuring coordinates the coordinates used in the real life measurement, see Figure 4.8.

The received signals are build applying a transformation to the emitted sinusoidal signal to mimic the impulse response of the transducer, by convolving it with a sinusoid and applying a Hanning window to the resulting signal. It must be noted that this is not - and does not intend to be - the real impulse response of the hydrophone, but it is a simplified model of the transformation the sent signal suffers when emitted from the transducer. To consult the real impulse response and transfer function of the transducer's elements reference is made to Appendix A.

The new signal is delayed a number of samples correspondent to the calculated time of flight of the element under study. In Figure 4.10 the real recorded signal and the modelled one are represented for element number 35 and measurement 512.

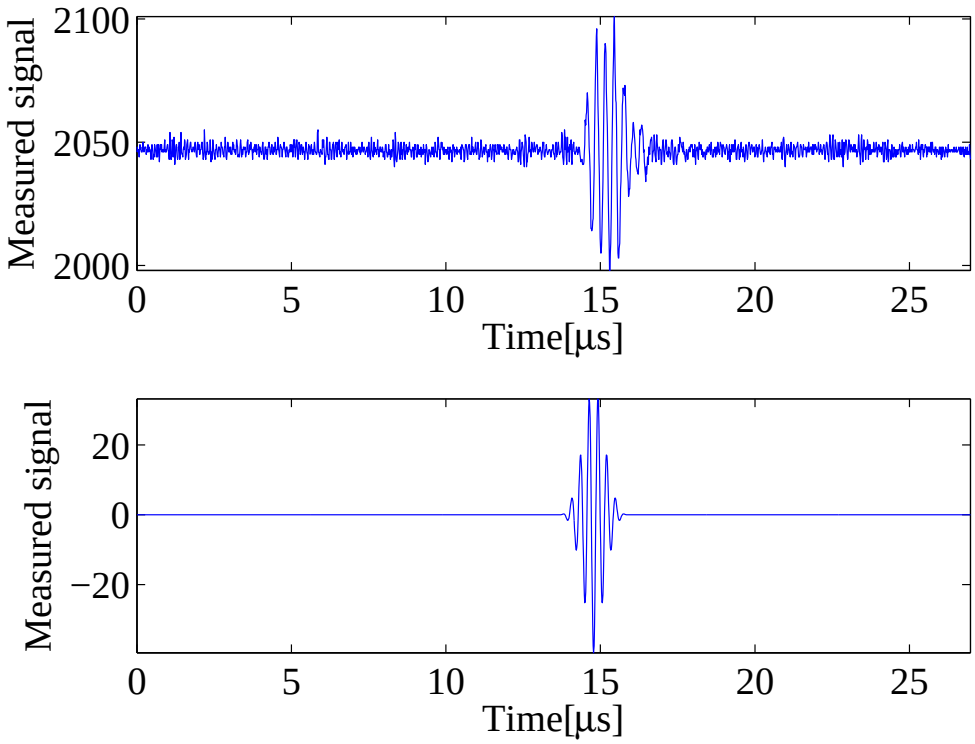

Figure 4.10 – Real and modelled recorded signals

A total of 1024 of these signals are generated, one for each of the elements, as it can be seen in Figure 4.11, and the process is repeated for the 643 measuring points.

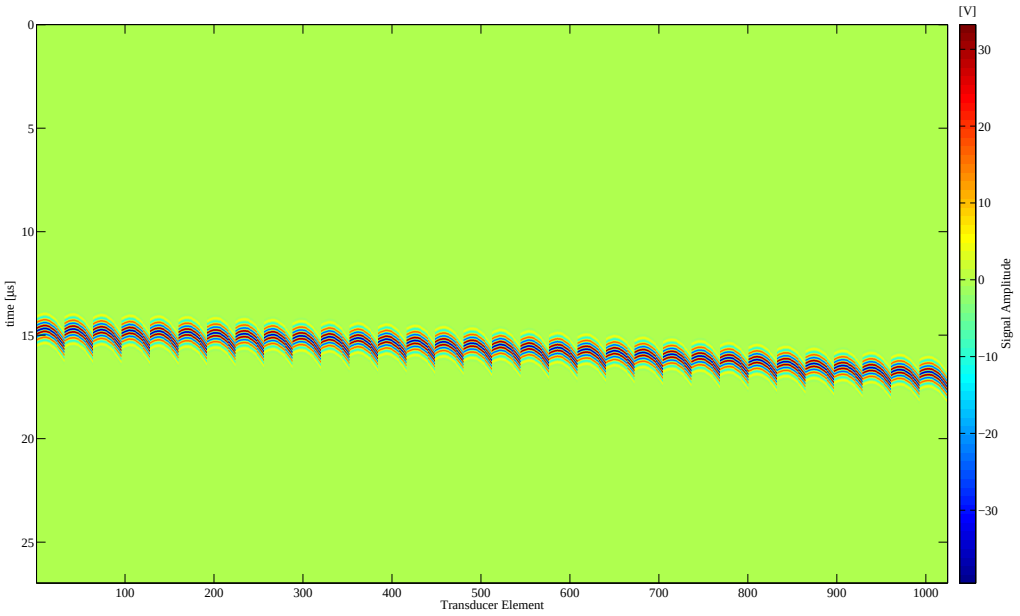

Figure 4.11 – Modelled samples for element 512

The resulting coordinates obtained from the optimization process are shown in Figure 4.12. The results show an obtained set of coordinates for the array elements centred in the z-direction around -2.3 mm. Obviously, this estimation is far from the originally defined array coordinates, and shows an average deviation of 2.4 mm. However it is observed that these results are actually in accordance with the results obtained in the real measurements, where the obtained coordinates were found to be placed around values of the z coordinate of -2.4 mm, as it was shown in section 3.6.2. A slight curvature in the estimated array can also be observed in the optimization results, just like it was observed in the estimation using the real data measured in the experiment.

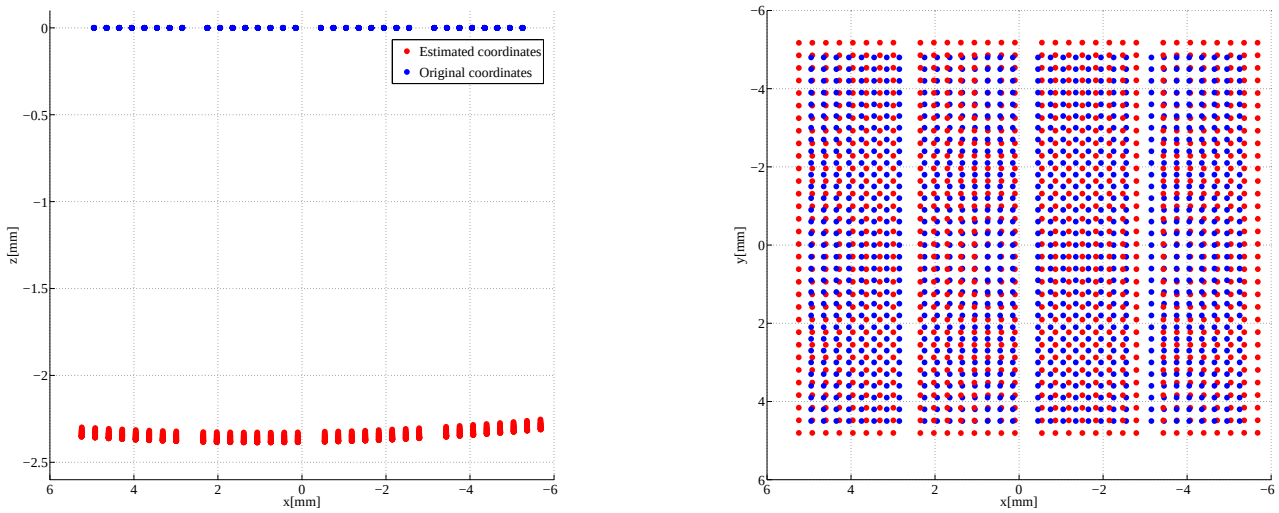

(a) xz-plane **(b)** xy-plane

Figure 4.12 – Original (blue) and modelled (red)array positions using complex model

An explanation for this behaviour can be found in the fact that the time of flight is being estimated as the maximum of the envelope of the correlation, as was explained in depth in section 3.3, while in this case to build the sent signal, that value of the time of flight is used to mark the moment when the sent signal is first detected.

To compensate for this discordance, the model is re-designed introducing a change in the generation of the received signal by aligning its central point to the found value of the time of flight. The results of this new modellization are shown in Figure 4.13.

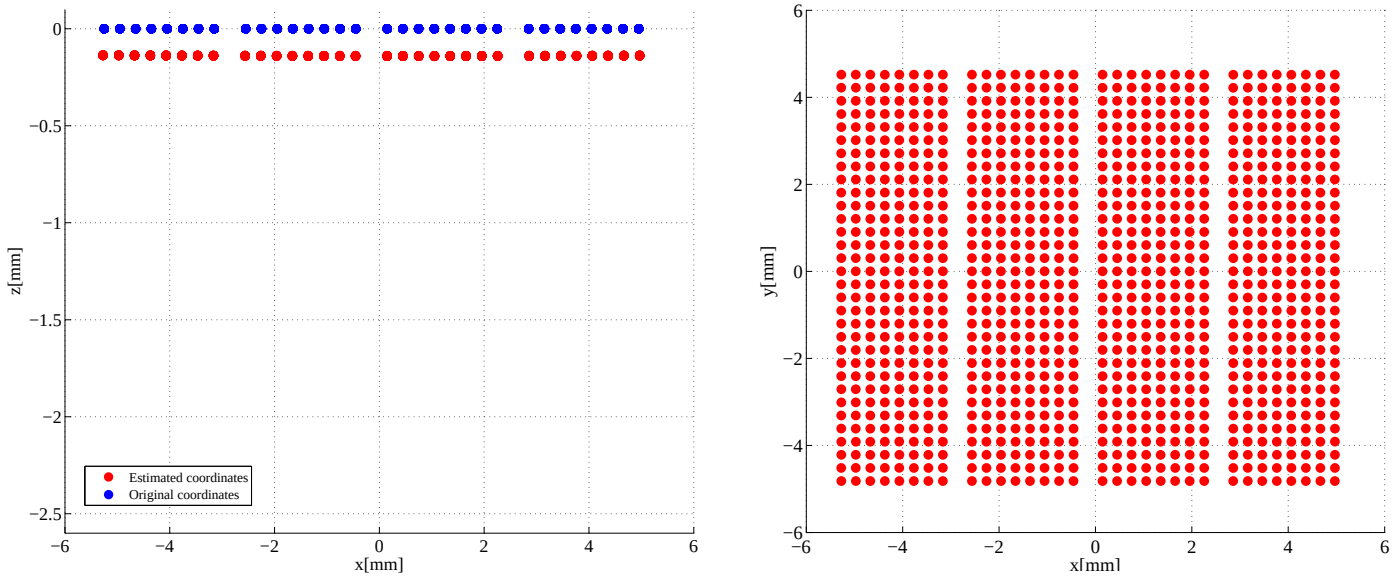

(a) xz-plane

(b) xy-plane.

Figure 4.13 – Original (blue) and modelled (red)array positions for modified complex model

Clear improvement has been achieved in the model's results by implementing this change, reducing the mean distance between original and estimated coordinates to 0.14 mm. The deviations in the xy-plane layout have been also drastically reduced. The remaining deviation could be explained by a lack of refinement in the estimation of the time of flight due to the discrete nature of the data and the assumptions taken in the zero-crossing estimation.

It is also investigated, in the case of the noiseless complex model, the importance of the number of measurements performed and the effect of this variable in the estimation of the array's coordinates. For that purpose trials with 250 and 450 measuring points have been performed.

These measuring coordinates are distributed randomly with z coordinates ranging between 1 cm and 2 cm far from the transducer array and x and y coordinates both distributed between -1 cm and +1 cm from he center of coordinates, where the center of coordinates has been assumed to be the central point of the transducer array.

The 250 and 450 measurement runs of the model produce results for the coordinates of the array elements that show maximum deviations from the original array coordinates of 0.13 mm and 0.11 mm, respectively.

For illustration, Figure 4.14 shows a comparison of the results obtained using 450 measuring positions and the 643 measurements results.

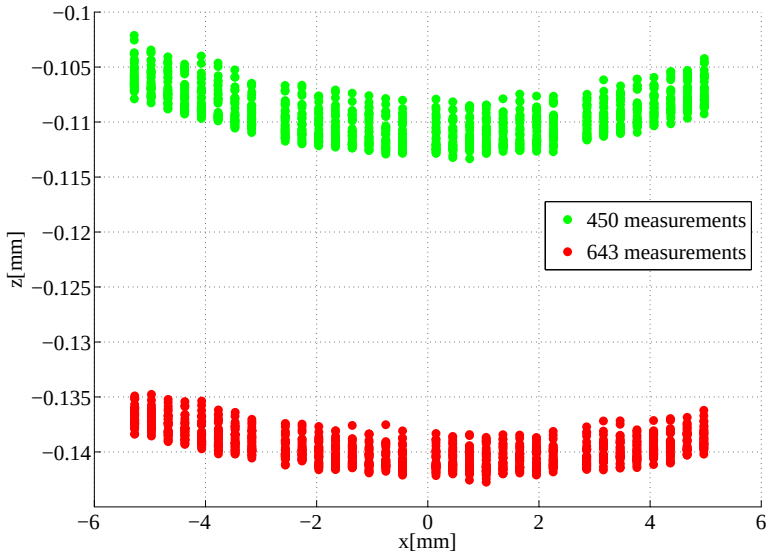

Figure 4.14 – Results of the modelling using 450 and 643 measurement positions

At first the results seemed somehow counter-intuitive, because a smaller number of measurements yielded closer results to the original array coordinates, contradicting the results obtained with the simple model. It was observed, however, that the distribution of the measuring positions differed in the two cases: The model designed according to the real life experiment had its measuring points distributed in both x and y directions in a range of -2 cm to 2 cm, versus the 450 measurements model where the points were distributed in a range varying from -1 cm to 1 cm. As it was shown with the simple model, the distance to the array played a key role in the accurate estimation of the elements' coordinates, a fact that could partially explain the obtained results.

It must also be noted that, even though the results from the 643 position measurement are further from the real ones, there is less variation among their z-coordinate values. That is, less curvature in the array's estimation appears with a higher number of measurements.

These results point to the fact that a high number of measurements is important, but that so it is the manner on which these measurements are distributed.

4.2.2 Effect of Noise

To study the strength of the model against noise, the original recorded data for the experiment is analysed in order to replicate reality as much as possible in the model.

The signal to noise ratio is calculated, as:

$$\mathrm{SNR} = \frac{P_{\mathrm{signal}}}{P_{\mathrm{noise}}} \tag{4.3}$$

To find a value for this parameter the noise's power was calculated from samples where the signal was not present. On the other hand the signal's power was calculated around the samples where the signal was present by subtracting the noise power from the power found in these samples were the signal was present, since in them contribution is made to the power by both noise and signal.

The main issue when calculating the SNR was that this parameter was highly dependent on the position of the hydrophone in the measurement, with very disperse values across measurements but also across elements, as shown throughout Chapter 3. Taking into consideration this fact, different levels of noise were considered. This noise was modelled as additive white gaussian noise and added to all measurements.

The model was designed with 643 measurement points in the same positions as in the real experiment. The time of flight was assumed to indicate the middle point of the sent signal, based on the conclusions reached using the noiseless model. An example of a sent noisy signal is plotted in Figure 4.15 for a noise power of 12 dB-Watts, where dB-Watt values are defined as the logarithmic values of the power with a reference to 1 Watt:

$$\text{dBW} = 10\log(\frac{\text{P}_{watts}}{1\text{W}}) \tag{4.4}$$

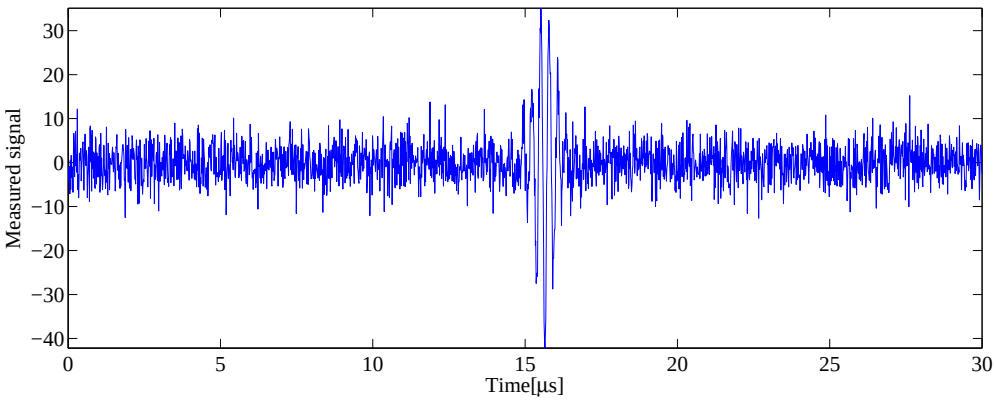

Figure 4.15 – Modelled recorded signal for measurement 27 and element 35

A complete noisy measurement is shown in Figure 4.16 for measurement number 27 when subject to noise of different levels:

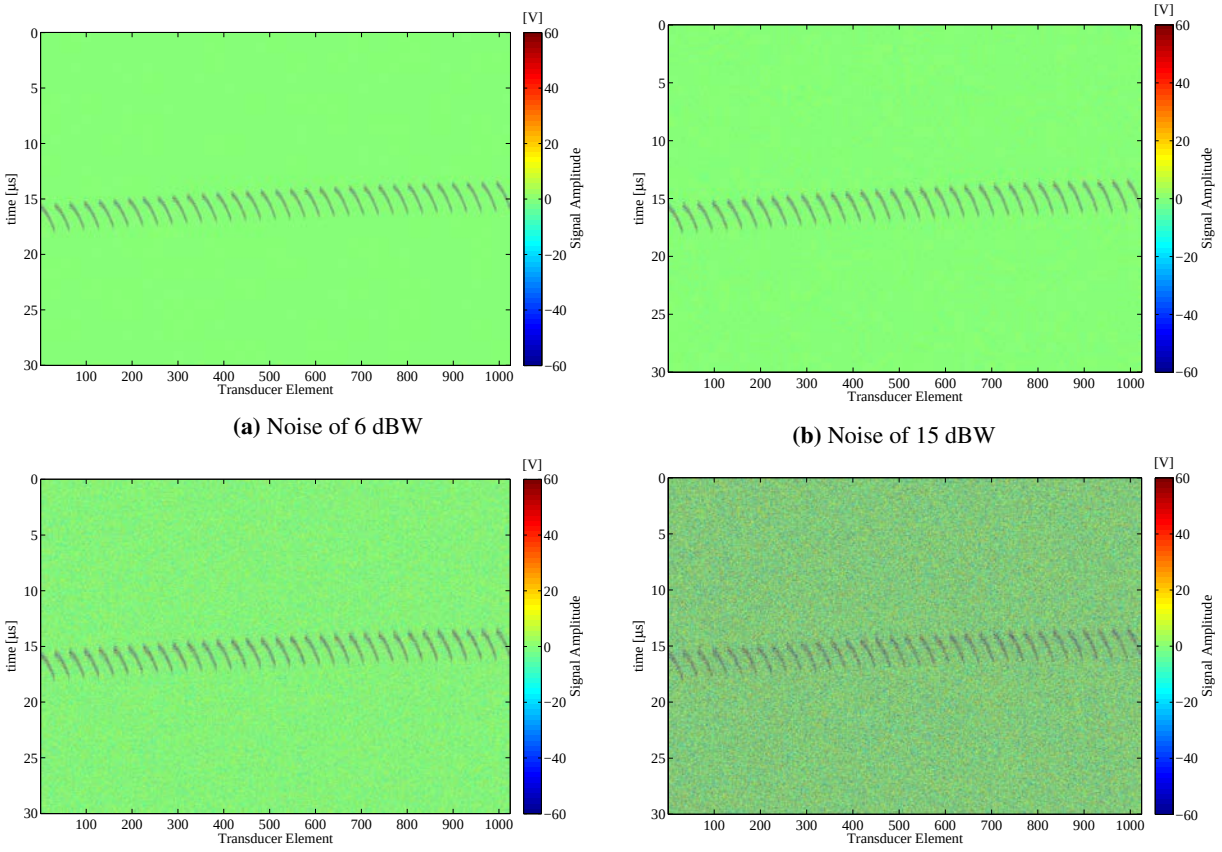

(a) Noise of 6 dBW

(b) Noise of 15 dBW

(c) Noise of 22 dBW

(d) Noise of 27 dBW

Figure 4.16 – Model of measurement number 27 with different noise levels

The results obtained for different values of noise power are shown in table 4.9:

Table 4.9 – Error values for different noise levels

Noise level	**Mean Error** [mm]	**Standard Deviation of the error** [mm]
12 dBW	0.13676	1.19×10^{-3}
15 dBW	0.13660	2.03×10^{-3}
18 dBW	0.13635	1.17×10^{-3}
22 dBW	0.16845	5.13×10^{-3}
27 dBW	0.05950	8.70×10^{-3}
35 dBW	0.12158	2.44×10^{-3}

These errors have been calculated as the mean distance to the original coordinates, and the table shows the mean error and its standard deviation after several runs of the model for each configuration.

It is hard to draw conclusions after the obtained results, since there is no clear pattern to connect noise power with error behaviour. An increase in the noise power does not translate into an increase of the error value as it could be expected. Furthermore, the mean distance, i.e. the estimation error, for the noiseless measurement was of 0.1406 mm, which would indicate that adding noise to the model yields in occasions

better results.

It must be concluded firstly, that the mean distance between estimated and original coordinates might not have been the best error criterion, and secondly that the addition of noise in some cases could add deviations that compensate for the original weaknesses of the noiseless model, that itself never yielded perfect results.

This can be seen in Figure 4.17, where the noiseless results and the ones with noise level of 27 dBW are plotted. Because the estimated values are closer in the z-direction to the original array, the error value is lower. However, the dispersion in the coordinates is clearly higher in the noisy model.

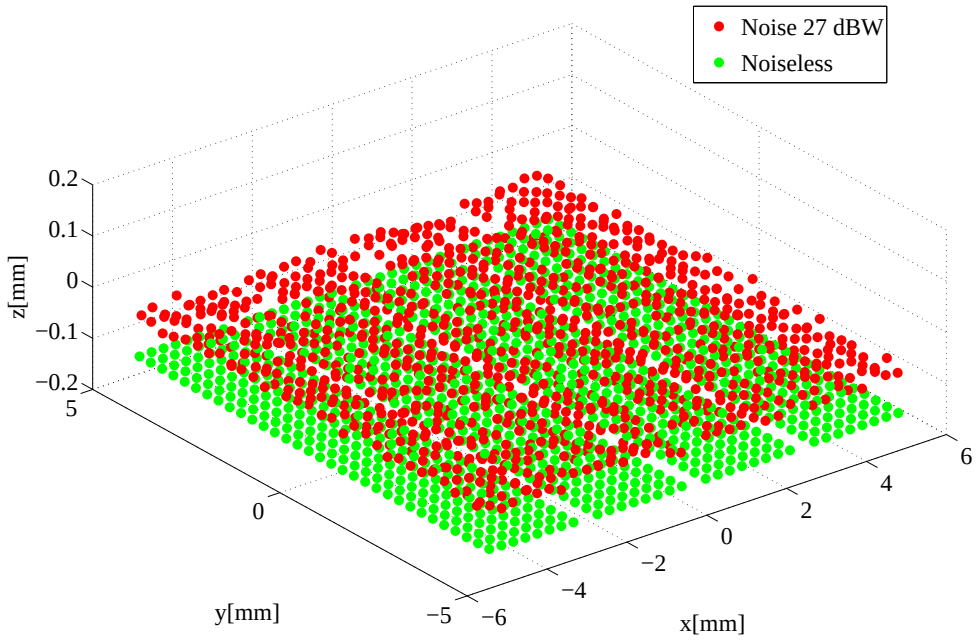

Figure 4.17 – Results of complex model without noise and with noise of 27 dBW

All in all, if compared with the real life measurements, there are many factors that this model is not able to simulate, specially significant are the fact that the SNR is not constant through measurements in reality as opposed to what was assumed for this model, and that aspects of wave propagation, like signal decay or attenuation have not been taken into account.

However, the model has been useful to detect faults in the time of flight estimation, and to prove the effect of noise in the measurements. Results for the highest studied noise - with power level 35 dBW- are shown to illustrate how, when the SNR is too low, the estimation of the array coordinates becomes a challenge for the developed method.

Both the simple and complex model could be useful in order to test and design experiment's set-ups under different noise conditions in order to obtain optimal results.

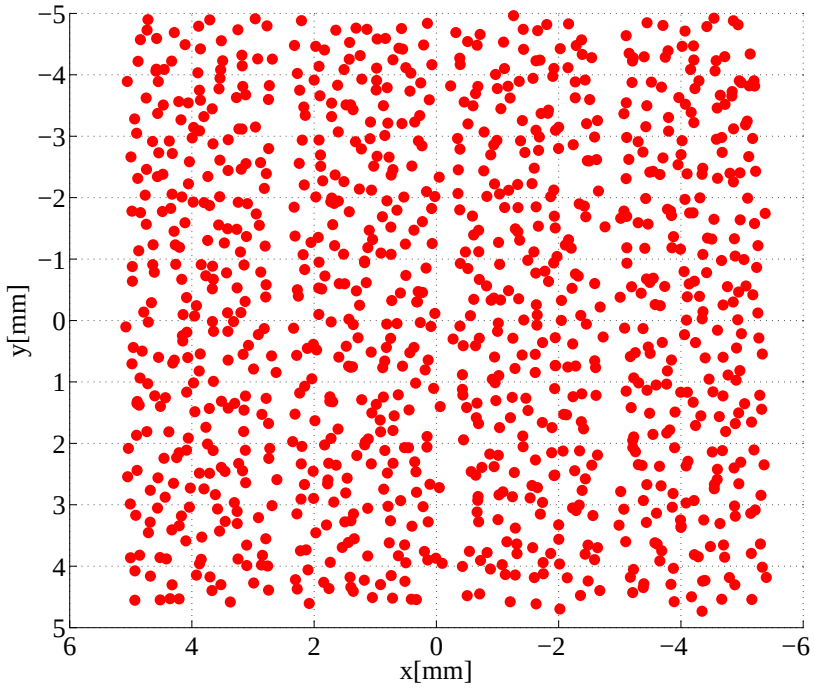

Figure 4.18 – Results of complex model with noise of 35 dBW

4.3 Ideal Measuring Set-up based on Model Findings

After the simple and complex model have been analysed a set of recommendations are made to perform an experimental measurement of the pressure field such as the one studied in this project. These guidelines have been outlined after studying the weaknesses of the dataset produced in the original experiment and the assessment of the potency and debilities of the method to obtain the researched characterization parameters .

Ideally, the experiment should be able to gather sufficient meaningful data to optimize the results while being simple enough not to generate a too large amount of data to process. For that reason it is recommended to keep the number of measuring positions of the hydrophone as low as possible while keeping the deviations minimum. It was shown by the models that this could be achieved with a number of measurements of around 400 measuring positions, higher number of measurements would allow better results and more resolution in the radiation pattern time-space representations, but also mean longer time spent in the measurement and in the processing of the data.

Also, to avoid irrelevant or noisy measurements, the distance to the array should be kept minimal in order to account for the signal's decay and to have finer estimations of the coordinates. The distribution of measurements that rendered smaller error values when assessing the model where: divided in two planes or randomly in the three dimensions, but the results of the different distributions are always relative to the chosen distances to the array, meaning that two planes too far away from the transducer would gather worse results than one single plane that was placed closer to the array. Good measuring distances were found to be between 1 cm and 4 cm away from the array.

The importance of aligning the array with the measuring planes has also been pointed out through this

study and it should be kept in mind when performing the experiment, specially to be able to accurately describe the directivity of the array's elements.

In terms of the angle between hydrophone and array, it was shown in this project that wider angles produced measurements with lower energy levels and thus, the recorded signals in those positions have higher signal to noise ratio and generate noisy data that should be avoided. In that sense narrower angles should be preferred. Furthermore, it was also pointed out that the hydrophone used to perform the measurements has an influence in the valid angles, making it recommendable to use hydrophones with wide acceptance angles or to be certain to keep the angles between the two devices as narrow as possible.

In short the ideal set-up should balance the time spent in performing the measurements and processing the results while still being able to produce a relevant dataset, this can be achieved by using an adequate number of measurements placed close enough to the array and by avoiding angles too wide to receive a sufficient amount of signal's energy.

CHAPTER 5

Conclusions

The importance of diagnostic ultrasound imaging in medicine, and in extension in society, is due to, among other factors, the fact that ultrasound systems are inexpensive compared to other techniques, and easy to use. The transducer used to emit and receive the ultrasonic signal is key in the development of such systems and thus, it is a field were research has been carried out steadily [4]-[13] in the past years and still is being carried out currently.

This project has focused on characterizing these ultrasound transducers, and in particular has aimed to study the feasibility of a simplified and condensed experimental procedure to characterize such devices. For this purpose a single experiment set up has been considered, consisting in pressure measurements of the field generated by a 32x32 transducer array, as it was described in Chapter 3.

Pressure field data recorded in June of 2012 has been analysed and from it methods to evaluate the directivity, angle of acceptance, radiation patterns and spatial location of each of the transducer array's elements have been developed. In this process the assessment of the location of the elements was proven to be pivotal to the characterization of the elements' properties, being specially significant when analysing directivity patterns.

Perfect estimation of the coordinates for the transducer elements has not been achieved, although different methods like the RANSAC algorithm have been investigated to improve it. Nonetheless, methods to overcome the problem of faulty localization were designed and proven to be efficient to permit estimation of the directivity patterns and acceptance angles of elements with flawed position coordinates.

Values for acceptance angles were obtained and shown to be in accordance with findings from other researchers, and the time-spatial behaviour of the pressure fields were also retrieved from the measurements. A methodology to remove the influence of the characteristics of the measuring device, i.e. the hydrophone, was also explained and a method for detecting dead elements of the array was developed. In summary, it was found that acoustic characteristics of the transducer elements could be inferred, or at least closely approximated, from the data of one single experiment.

The process, however, was not without complexity and drawbacks. Accurate estimations and a big computational power in order to optimize the results has been necessary, showing that operating with large amounts of data can be complicated and time consuming and thus, an effort should be put in minimizing the amount of data to handle.

Two models were produced to mimic the real life experiments in order to improve the quality of the data. The aim of doing so was to design an experimental set-up that could yield meaningful results and that would potentially allow researchers and developers to obtain sufficient information for characterizing ultrasound transducer arrays in an optimal way.

The effects of noise, of the number of measurements and the spatial placing of the experiment's devices were studied using a simple model based on modelled times of flight. The results of testing different set-ups and different experimental conditions - like noise and bias - allowed to outline a some of the guidelines for an optimal measurement.

A more complex model, that took into account the process of time of flight estimation, was developed and used to asses the methodology developed to calculate these time values as well as to study the performance of the model under noise in the measurements. The important number of assumptions that have been made when developing this model limited its results. However, it was useful to test how noise in the signal could affect the estimation of the array coordinates and to detect the limitations of the method used to estimate these positions from the real data.

The combination of studying both models and the problems and struggles observed in the process of obtaining characterization parameters from the data have allowed to define a set of recommendations for future experiments that, in general, should make sure to use an adequate number of measurements; to perform this measurements close to the array and to avoid, as much as possible, selecting measurement positions with wide angles to the normal of the array. An obvious follow up to the research conducted in this project would be to perform such an experiment and verify if following these recommendations the dataset obtained allows easier characterization of the ultrasound probe.

This project has put into the table the possibility of simplifying the process of ultrasound transducers' characterization, but it is far from being a closed research. New investigation lines have arisen during its development like optimization of the spatial estimation method, simplification and automation of the characterization routines or expansion of the number of parameters that could be obtained from the described experiment, among others.

If the definition of Characterization is revisited in these last lines of the project as *"the way in which something is described by stating its main qualities"*, [25]. It has become clear throughout this research that describing Ultrasound Transducers by their main qualities is a complex and difficult task on which many aspects and parameters must be taken into account, since mechanical, electrical and acoustical parameters are needed to describe these devices.

The acoustical characterization that has been taken upon in this project has aimed to simplify the the process used to gather knowledge about a transducer's parameters and has shown that it is indeed possible to retrieve the necessary information from a single experimental set up. Research lines are open to further improving the methods here explained and to broaden the number of characteristics that could be obtained from the researched pressure field experiment.

References

[1] Jørgen Arendt Jensen. *Estimation of Blood Velocities Using Ultrasound: A signal Processing Approach*. Technical University of Denmark, Department of Electrical Engineering. Denmark. 2008.

[2] Jerry L. Prince, Jonathan M. Links. *Medical Imaging. Signals and Systems*. Pearson Prentice Hall Bioengineering. 2006.

[3] Finn Jacobsen. *Duct Acoustics*. Technical University of Denmark. Acoustic Technology, Department of Electrical Engineering. Denmark. 2011.

[4] C. Meyner, Y. Yanamer, M. Canney, A. Nguyen-Dinh, A. Carpentier, J. Chapelon. *Performance Assesment Of CMUTs In Dual Modality imaging/HIFU Applications*. IEEE International Ultrasonics Symposium Proceedings. 2012.

[5] M. Ikhwan Hadi Yaacob, M. Rizal Arshad, A. Abd Manaf. *Theoretical Characterization of Square Piezoelectric Micro Ultrasonic Transducer for Underwater Applications*. 7th International Symposium of Mechatronics and its Applications, 2010.

[6] X. Jin, O. Oralkan, F. Levent Degertekin, B.T. Khuri-Yakub. *Characterization of One-Dimensional Capacitive Micromachined Ultrasonic Immersion Transducer Arrays*. IEEE Transactions on Ultrasonics, Ferroelectrics, and Frequency Control. Vol 48. No 3, May 2010.

[7] B. Bayram, M. Kupnik, G.G. Yaralioglu, O, Oralkan, A. Sanli Ergun, D. Lin, S.H. Wong, B.T. Khuri-Yakub. *Finite Element Modeling and Experimental Characterization of Crosstalk in 1-D CMUT Arrays*. IEEE Transactions on Ultrasonics, Ferroelectrics, and Frequency Control. Vol 54. No 2, February 2007.

[8] O. Oralkan, A. Sanli Ergun, J. A. Johnson, M. Karaman, U. Demirci, K. Kaviani, T. H. Lee, B. T. Khuri-Yakub. IEEE *Capacitive Micromachined Ultrasonic Transducers: Next-Generation Arrays for Acoustic Imaging?*. IEEE Transactions on Ultrasonics, Ferroelectrics, and Frequency cControl, vol. 49, no. 11, November 2002.

[9] M. Ho, M. Kupnik, K. Kyu Park, K. Eckhoff and B. T. Khuri-Yakub. *Wide pressure range operation of air-coupled CMUTs*. IEEE International Ultrasonics Symposium Proceedings. 2012.

[10] A. Savoia, G. Caliano and M. Pappalardo. *A CMUT Probe for Medical Ultrasonography: From Microfabrication to System Integration*. IEEE Transactions on Ultrasonics, Ferroelectrics, and Frequency Control, Vol. 59, No. 6, June 2012.

[11] X. Zhuang, I. O. Wygant, D. T. Yeh, A. Nikoozadeh, O. Oralkan, A. S. Ergun, C-H. Cheng, Y. Huang, G. G. Yaralioglu, and B. T. Khuri-Yakub. *Two-Dimensional Capacitive Micromachined Ultrasonic Transducer (CMUT) Arrays for a Miniature Integrated Volumetric Ultrasonic Imaging System*. Medical Imaging 2005: Ultrasonic Imaging and Signal Processing, edited by William F. Walker, Stanislav Y. Emelianov, Proc. of SPIE Vol. 5750.

[12] M.I. Haller and B.T. Khuri-Yakub. *A surface micromachined electrostatic ultrasonic air transducer*. Proceedings of IEEE Ultrasonics Symposium 1994, Vol 2, pp. 1241-1244.

[13] O. Oralkan, X.C. Jin, F.L. Degertekin, B.T. Khuri-Yakub. *Simulation and experimental characterization of a 2-D capacitive micromachined ultrasonic transducer array element*. IEEE Transactions on Ultrasonics, Ferroelectrics, and Frequency Control, vol. 46, no. 6, November 1999.

[14] J. Lubbers and R. Graaff. *A simple and accurate formula for the sound velocity in water*. Ultrasound Med. Biol. Vol 24, No 7, pp 1065-1068. 1998.

[15] M.A. Fischler and R.C. Bolles.*Random sample consensus: A paradigm for model fitting with applications to image analysis and automated cartography.*. Communications of the ACM, Vol. 24, No 6, pp 381-395, 1981.

[16] J. M. Cannata, J. A. Williams, Q. Zhou, T.A. Ritter and K. K. Shung. *Development of a 35-MHz Piezo-Composite Ultrasound Array for Medical Imaging*. IEEE Transactions on Ultrasonics, Ferroelectrics, and Frequency Control, Vol. 53, No. 1, January 2006.

[17] Jørgen Arendt Jensen. *Linear description of ultrasound imaging systems*. Notes for the International Summer School on Advanced Ultrasound Imaging. Technical University of Denmark.1999.

[18] S. Leeman, A,J. Healey, E.T. Costa, H. Nicacio, R.G. Dantas, et al. *Measurement of transducer directivity function*. Proc. SPIE 4325, Medical Imaging 2001: Ultrasonic Imaging and Signal Processing, 47. May 2001.

[19] C.I. Zanelli, S.M. Howard. *A Robust Hydrophone for HIFU Metrology*. AIP Conf. Proc. 829, 618. 2006.

[20] [20].N. Felix, D. Certon, L. Ratsimandresey, M. Lethiecq, and F. Patat. *1D ultrasound array: performance evaluation and characterization by laser interferometry*. IEEE Ultrasonics Symposium, 2, 1191-1194 vol.2. 2000.

[21] W.P. Mason. *Sonics and Ultrasonics - Early History and Applications*. IEEE Transactions on Sonics and Ultrasonics 23.4 : 224-232. 1976.

[22] K.R. Erikson, F.J. Fry, and J.P. Jones. *Ultrasound in Medicine - A Review*. IEEE Transactions on Sonics and Ultrasonics SU21.3. 144-170. 1974.

[23] J.F. Dias. *An Experimental Investigation of the Cross-Coupling between Elements of an Acoustic Imaging Array Transducer*. Ultrasonic Imaging 4.1. 44-55. 1982.

[24] N. Felix, D. Certon, E. Lacaze, M. Lethiecq and F. Patat. *Experimental investigation of cross-coupling and its influence on the elementary radiation pattern in 1D ultrasound arrays* Proceedings of the IEEE Ultrasonics Symposium. Volume 2, pp. 1053-1056. 1999.

[25] "Characterization." Def 2. *Cambridge Advanced Learner's Dictionary & Thesaurus*. Cambridge University Press, 2014. `http://dictionary.cambridge.org/dictionary/british/characterization_2`. Web accessed on February 5th, 2014.

[26] S. Berg and A. Rønnekleiv. *Backing Requirements For CMUT Arrays On Silicon*. Proceedings - IEEE Ultrasonics Symposium 4: 1952-1955. 2005.

[27] A.L. Lopez-Sanchez and L.W. Schmerr. *Determination of an Ultrasonic Transducer'S Sensitivity and Impedance In a Pulse-Echo Setup*. IEEE Transactions on Ultrasonics, Ferroelectrics, and Frequency Control, vol. 53, no. 11. 2101-2112. 2006.

[28] Nagy, Peter B. *Ultrasonic Nondestructive Evaluation*. Department of Engineering Mechanics. University of Cincinnati.2003.

[29] International Electrotechnical Commission. *Ultrasonics - Hydrophones - Part 3: Properties of hydrophones for ultrasonic fields up to 40 MHz*. IEC 62127-3:2007.

Appendices

Ultrasound Transducer Array's Datasheet

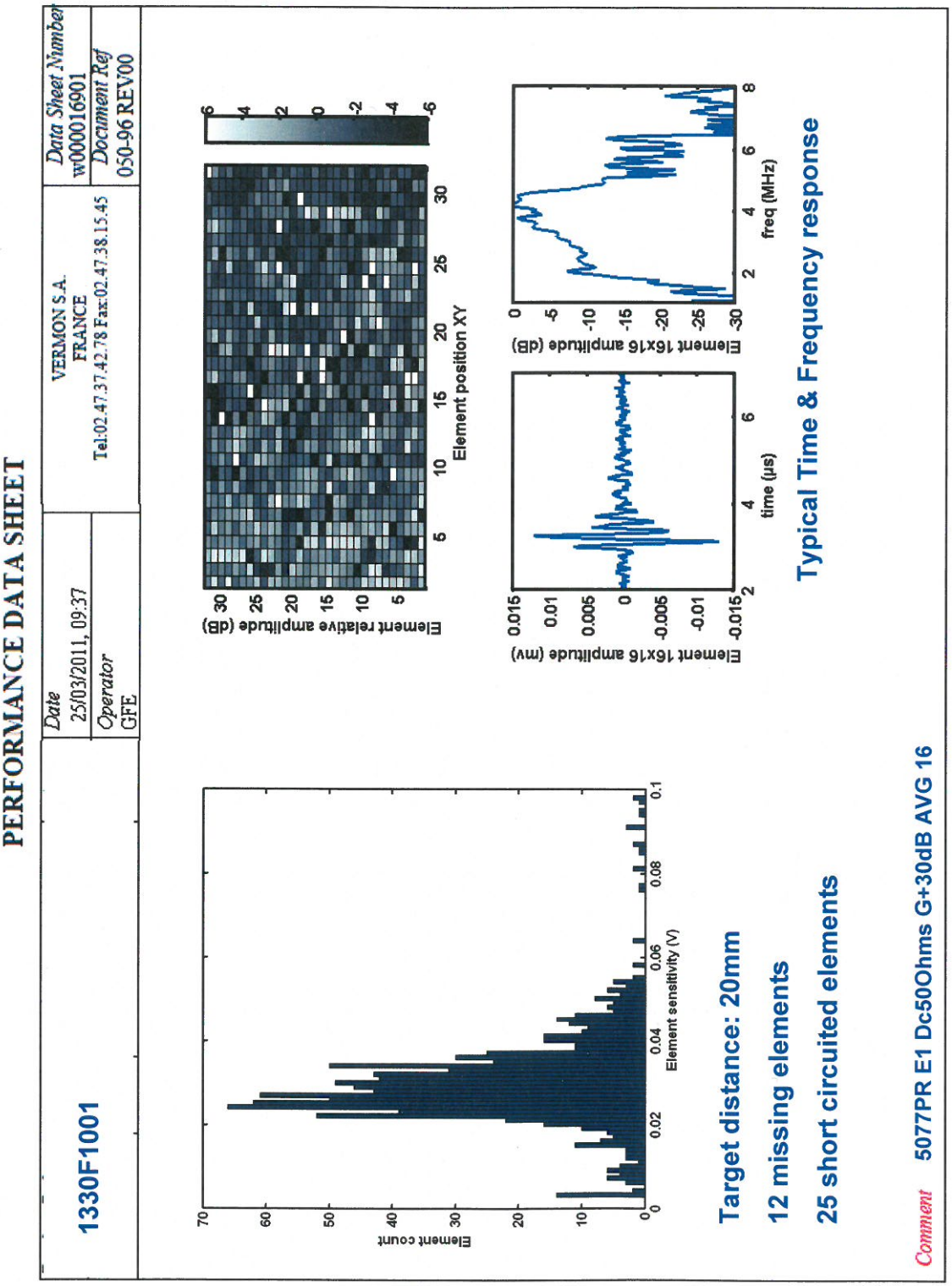

ONDA

APPENDIX **B**

Hydrophone's Datasheet

Putting Confidence in Ultrasound

HGL Hydrophones

The HGL Series hydrophones were designed to meet or exceed recommendations of section 3.3.2 of the AIUM Acoustic Output Measurement Standard (May 1998). They have an exceptionally flat sensitivity in a small and sturdy package. These hydrophones are excellent in-house standards for ultrasonic acoustic intensity measurements, and for general purpose field mapping.

HGL Hydrophone

Features

- High sensitivity
- Small effective aperture
- Broadband
- Solid construction
- Flawless integration with AH preamplifiers
- Flat (+/-3dB) 250 KHz to >> 20 MHz

Technical Specifications

	HGL-0085	HGL-0200	HGL-0400	HGL-1000
Frequency range (±3dB)	0.25 to 40 MHz		0.25 to 20 MHz	
Electrode aperture	85 mm	200 mm	0.4 mm	1.0 mm
*** EOC Nominal Sensitivity [nV/Pa]**	8	45	160	510
Acceptance angle (-6dB at 5 MHz)	>150º	100º	30º	20º
Capacitance	30 pF			
Max. Operating Temperature	50 ºC			

* EOC ("end of cable") is the open-circuit output sensitivity of the hydrophone. Calibration with an amplifier can be determined from the gain and input impedance of the amplifier.

Provided with traceable calibration 1-20 MHz at 50 KHz intervals. For other calibrations available visit our web site.

Specifications are subject to change without notice.

Typical Sensitivity Plot

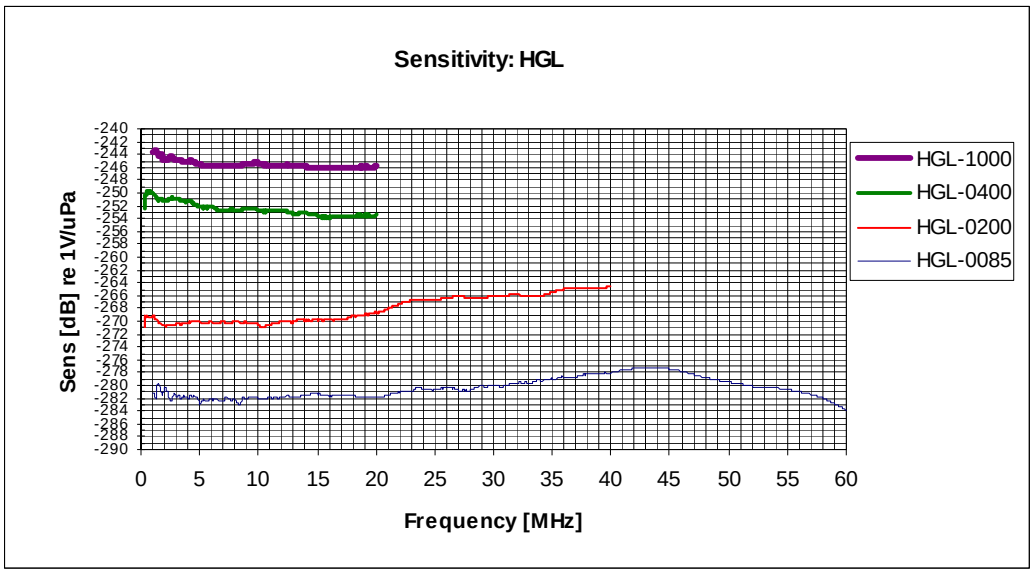

Typical Directivity Plots

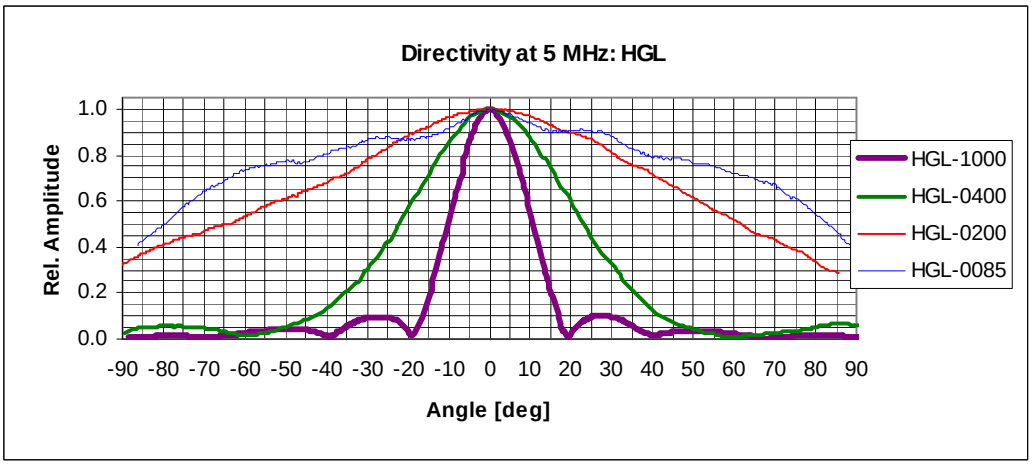

Mechanical Specifications

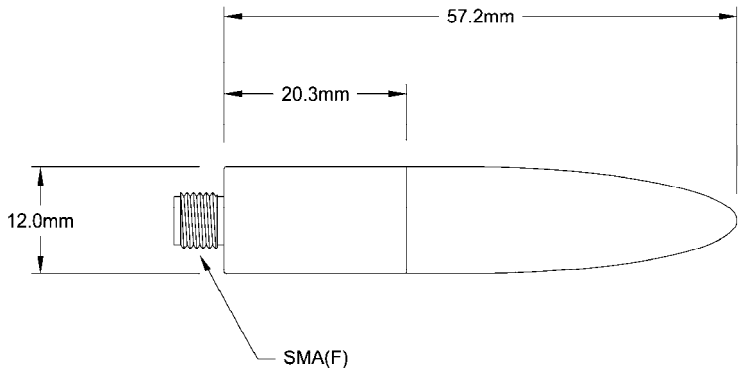

APPENDIX **C**

Introducción

El oído humano es capaz de percibir sonidos en el rango de frecuencias entre 20 y 20.000 Hz. Por encima de ese umbral los seres humanos no pueden detectar ondas acústicas y estas pasan a denominarse ultrasonidos. Las señales de ultrasonido tienen múltiples usos: desde el Sonar hasta sensores de movimiento, pasando por el análisis de materiales. Uno de los campos en los que mayor importancia tienen este tipo de señales es en el de generación de imágenes médicas.

Los sistemas de generación de imágenes a través de ultrasonidos (ecografías) son unos de los más utilizados hoy en día para el diagnóstico de patologías en medicina. El elemento principal de estos sistemas es la sonda de ultrasonidos que genera, y generalmente también recibe, la señal de ultrasonidos. Analizar y definir las propiedades de estas sondas de transductores es, pues, una parte clave del diseño y optimización de los sistemas médicos de ultrasonidos, y de ahí la importancia de ser capaces de caracterizar las mismas.

El objetivo principal del proceso de diseño de la sonda de ultrasonidos es el de obtener imágenes médicas de alta calidad. Sin embargo, los factores que afectan a la calidad de estas imágenes van más allá del mero diseño de la sonda. Este es el motivo por el cual las características de los transductores han de ser utilizadas a la hora de evaluar el comportamiento de estos dispositivos. El ancho de banda, el ángulo de aceptación o la respuesta en frecuencia han de ser definidos, no bastando utilizar tests basados en las imágenes que los sistemas son capaces de generar para evaluar las características de las sondas.

El proceso de caracterización de transductores de ultrasonidos no es trivial e involucra complejas mediciones. El presente proyecto tiene como objetivo evaluar el potencial de utilizar una única medición del campo de presión generado por un transductor para obtener la información relevante para caracterizar al mismo, centrándose en sus características acústicas. En concreto, en este estudio se investiga un método para caracterizar matrices de transductores de ultrasonidos basándose en mediciones del campo de ultrasonidos y en el desarrollo de modelos teóricos.

Con el propósito de contextualizar esta investigación, tanto en su marco histórico como dentro de las áreas de investigación actuales, este capítulo resume de forma concisa la historia y el estado del arte de la caracterización de transductores de ultrasonidos, para después abordar en profundidad la motivación, el ámbito y los objetivos del presente proyecto.

C.1 Perspectiva Histórica

El estudio de la transmisión de ondas de ultrasonidos se remonta a principios del siglo XX. En sus orígenes, su principal aplicación fue la de la transmisión a través del agua para la detección de submarinos, para lo que fueron utilizados ampliamente durante la Primera Guerra Mundial [21]. De forma paralela el efecto piezoeléctrico, es decir, la transformación electro-mecánica que se produce en materiales cristalinos, fue descubierto. Esto condujo al desarrollo del primer transductor de ultrasonidos por parte de Paul Langevin usando cristales de cuarzo, si bien estos primeros transductores no fueron utilizados hasta la Segunda Guerra Mundial.

Entre los años 1939 y 1945, se investigaron otros usos de los ultrasonidos. Una de las principales aplicaciones fue la detección de irregularidades y la medición del grosor de materiales. Así mismo se reforzó la investigación sobre elementos piezoeléctricos utilizando materiales ferroeléctricos (es decir con polarización eléctrica instantánea), que rápidamente se convirtieron en la elección más popular a la hora de fabricar transductores de ultrasonidos.

Tras la Segunda Guerra Mundial, los conocimientos adquiridos en el campo de investigación de los ultrasonidos fueron utilizados para estudiar fenómenos físicos tales como las oscilaciones magnetoacústicas en metales, el efecto de dislocaciones e impurezas en la transmisión de ondas de sonido así como las interacciones spin-fonón en solidos, entre otros. En [21] puede ser consultada una lista exhaustiva de las aplicaciones de los ultrasonidos en la física, así como explicaciones pertinentes de estos fenómenos.

Uno de los aspectos más importantes de los ultrasonidos es su uso en el campo de la medicina. Desde sus orígenes se investigaron dos usos principales de las ondas de ultrasonidos en esta área: Por un lado el estudio de los ultrasonidos de baja intensidad y de su capacidad para permitir la diferenciación entre distintos tipos de tejidos condujo al desarrollo de los sistemas acústicos de generación de imágenes médicas. Por otro, el potencial de los ultrasonidos de alta intensidad para intervenciones médicas también fue objeto de investigación.

Las primeras investigaciones sobre la interacción de los ultrasonidos con el tejido vivo se remontan a principios de los años veinte, [22], y desde entonces se la investigación en este campo se ha desarrollado de forma continuada. No fue hasta las décadas de los sesenta y setenta, sin embargo, cuando doctores y hospitales comenzaron a considerar los ultrasonidos como una herramienta de diagnóstico válida. Algunas de las áreas de investigación incluyeron el estudio de los efectos irreversibles de las ondas de ultrasonidos sobre diversos tejidos así como el estudio de los peligros de la radiación de ultrasonidos en humanos. Estos estudios condujeron a definir la técnica de generación de imágenes a través de ultrasonidos como no invasiva. En comparación con los Rayos-X o con los métodos nucleares de generación de imágenes médicas, la tecnología de ultrasonidos se basa únicamente en la naturaleza de los tejidos humanos y el cambio de impedancia que se produce entre distintos tipos de tejidos, sin influir en ellos de ninguna forma.

A lo largo de los años se han desarrollado técnicas para la aplicación de ultrasonidos en tejido aislado, *in vitro*, así como en tejidos vivos, i.e. *in vivo*, así como sistemas de ultrasonidos Doppler, que permiten registrar las velocidades de objetos en movimiento haciéndolos relevantes para la estimación del flujo de la sangre en el cuerpo humano. A mediados de la década de los ochenta se desarrollan las primeras imágenes a color y sistemas de representación del flujo, y ya en los años noventa la generación de imágenes en 3-D utilizando ultrasonidos se convirtió en una realidad. Algunas de las aplicaciones más conocidas de

estos sistemas de imágenes médicas son las ecografías de fetos dentro del vientre materno así como las ecocardiografías del corazón humano.

Desde el comienzo del desarrollo de estas técnicas se puso especial empeño en involucrar a la comunidad médica y a los profesionales hospitalarios son el objetivo de lograr mejores sistemas de ultrasonidos. Con el tiempo se ha conseguido desarrollar sistemas más y más compactos, a la par que se ha desarrollado metodologías de uso más sencillas para estos aparatos. Hoy en día las imágenes de ultrasonidos pueden ser conseguidas en la propia consulta del médico o incluso los aparatos de medición pueden ser transportados por las diferentes salas de un hospital.

Esta relativa sencillez del procedimiento, junto con su naturaleza no invasiva, ha permitido que la técnica de generación de imágenes mediante señales de ultrasonidos sea reconocida por la comunidad médica como una herramienta imprescindible y se haya convertido en uno de los métodos más utilizados a la hora de diagnosticar patologías en nuestros días.

Las referencias [1], [2] and [22] permitirán al lector obtener una visión de conjunto de la historia de los ultrasonidos en el campo de la medicina, si desea profundizar en el tema.

C.2 Estado del arte

Las sondas o matrices de transductores han sido un área central de investigación en el campo de los ultrasonidos médicos durante años. Tanto matrices de transductores capacitivos como piezoeléctricos han sido estudiadas con diversos fines, tal y como demuestra la extensa literatura sobre el tema, investigándose distintos materiales piezoeléctricos, como el cuarzo, el titanato zirconato de plomo (PZT), el óxido de zinc o el nitruro de aluminio. Aunque el PZT es, generalmente, la elección más popular, estudios como el recogido en [5] han analizado transductores que utilizan otros materiales, que permiten reducir los costes de fabricación.

En los últimos 20 el interés en caracterizar transductores de ultrasonidos y matrices de ultrasonidos se ha centrado en los conocidos como *"Capacitive Micromachined Ultrasound Transducers"* (CMUTs) [4]-[7]. Desde su invención en 1994 en la Universidad de Standford [12], los CMUts se han convertido en una alternativa interesante a los transductores piezoeléctricos tradicionales. Pero *"La tecnología CMUT no es simplemente un reemplazo de bajo coste de la tecnología de transductores piezoeléctricos. Muchas de las características inherentes a la tecnología CMUT permiten avances revolucionarios en la generación de imágenes de ultrasonidos"*, [8]. En consecuencia, se han desarrollado estudios comparativos de ambas tecnologías en función de distintos parámetros. Por ejemplo en [4], Meyner et al. compararon dos matrices de transductores, una basada en CMUT y otra en *"Piezoelectric Micromachined Ultrasound Transducer"* (PMUT) con respecto a su impedancia eléctrica, su comportamiento electroacústico y sus patrones de radiación, concluyendo que las matrices CMUT presentan un mayor ancho de banda pero una sensibilidad menor a los impulsos.

Desde que se presentaron en los años noventa como una solución eficiente para construir transductores de ultrasonidos de banda ancha, se han conducido multitud de estudios para probar la viabilidad de los CMUTs como la evolución natural de las tecnologías de desarrollo de transductores. Haller et al. desarrollaron el

primer transductor micromecanizado, [12], y ya apuntaron a su futura proyección en términos de ancho de banda (unas cuatro veces mayor que la de los transductores piezoeléctricos) y a las posibilidades de integración con la electrónica de control. Otras ventajas descubiertas en estos primeros trabajos de investigación fueron la baja sensibilidad a la temperatura y la generación de pulsos más cortos por parte de este tipo de transductores.

Los CMUTs permiten la fabricación de grandes matrices de transductores con relativa facilidad y bajo coste, [10]. Consisten en electrodos de dos placas (celdas de condensadores) que son cargados con un voltaje continuo (DC). Cuando son excitados con una corriente alterna (AC) producen una vibración, que genera las ondas acústicas. El fenómeno reciproco también se produce, es decir, cuando el electrodo cargado recibe una señal de ultrasonidos genera una corriente de salida debida al cambio en su capacitancia, [8]. El proceso de diseñar y fabricar estos dispositivos ha sido recogido en multitud de artículos de los últimos años, centrados en distintos materiales y técnicas, [10]-[12].

En los años 2000 distintas investigaciones han probado la viabilidad de los CMUTs para generar imágenes con ultrasonidos. En [8] Oralkan et al. mostraron imágenes de un fantoma cableado usando matrices de transductores unidimensionales y utilizaron la función de dispersión de punto (PSF) para medir los efectos de los transductores de banda ancha en las imágenes B-Mode. También demostraron cómo la resolución axial (la habilidad del sistema para distinguir entre objetos próximos entre sí en la dirección axial) mejoraba con la utilización de pulsos de ultrasonidos más cortos; así como las mejoras significativas en la relación señal ruido (SNR) que se producían con el uso de este tipo de transductores.

Sin embargo, las imágenes resultantes no dependen solo de las características de los transductores, ya que están influidas por el tratamiento de señal que se aplique así como de la electrónica del conjunto del sistema de ultrasonidos. Es por ello que otro tipo de pruebas son ejecutadas para evaluar la calidad de las matrices de transductores, midiendo su impedancia eléctrica, su comportamiento electro-acústico, sus patrones de radiación o el sobrecalentamiento de la matriz, entre otros parámetros.

Estos experimentos han sido presentados para matrices completas en, entre otros, [4]. Otras investigaciones han evaluado tanto las características de la matriz completa como de cada uno de sus elementos de forma aislada. En [6], Jin et al. presentaron una serie de experimentos de caracterización de elementos de la matriz y compararon los resultados con modelos basados en el circuito equivalente de un CMUT. Este modelo fue también utilizado e investigado en profundidad en [11]. Ambas investigaciones mostraron una buena concordancia entre mediciones y modelos, apuntando a este modelo como una herramienta relevante para el diseño y la implementación de matrices de transductores.

Diferentes experimentos han sido utilizados para evaluar las características de las matrices de transductores: la generación de ecos usando superficies reflectoras para evaluar el comportamiento en modos de recepción y transmisión o el uso de hidrófonos para medir el campo de presión generado por el transductor, [4], [6], se encuentran entre las técnicas más utilizadas.

Otros estudios se han centrado en diferentes aplicaciones para estos transductores, como el funcionamiento dual a alta frecuencia [4], las aplicaciones subacuáticas [5], el funcionamiento en condiciones de alta presión [9] o la generación de imágenes volumétricas [11], entre otras. El diseño experimental para la caracterización del transductor no varía de manera excesiva entre estos estudios, incluso cuando el

funcionamiento último de los transductores es distinto. El proceso de diseño y caracterización haciendo uso de simulaciones con elementos finitos y modelos, se mantiene constante sin importar la aplicación final del dispositivo.

Otra línea de investigación en la que trabaja un número importante de investigadores en los últimos años es la del fenómeno de *"crosstalk"* o interferencia. Se refiere a la interacción entre los elementos de la matriz de transductores, y se ha demostrado que afecta tanto a la directividad como al patrón de radiación de la matriz. Este fenómeno incrementa también el ruido acústico en las mediciones con matrices de transductores así como en las imágenes resultantes. [23], [24]. [6]-[8], y [16] han sido capaces de mostrar las desviaciones producidas entre los resultados empíricos y los modelos teóricos en base a estas interferencias.

El proceso de diseño, fabricación, caracterización e integración de transductores de ultrasonidos ha sido investigado en profundidad en las últimas dos décadas, otorgándole especial relevancia a las posibilidades que la microelectrónica ha puesto sobre la mesa en el campo y a la construcción de modelos precisos para predecir el comportamiento de estos dispositivos, que son clave en el desarrollo de sistemas robustos de generación de imágenes a través de señales de ultrasonidos.

C.3 Motivación

Tal y como se ha visto en las secciones anteriores, los transductores de ultrasonidos han sido extensivamente estudiados y desarrollados desde una perspectiva multidisciplinar que ha involucrado diversos campos científicos, como la química, la electrónica, la acústica o la medicina, tanto en el siglo pasado como actualmente.

La literatura discutida previamente muestra, ante todo, la extrema importancia que se le ha dado a la adecuada caracterización de los transductores de ultrasonidos: Un análisis concienzudo de las características de este tipo de dispositivos es esencial para la adquisición de datos válidos que puedan traducirse en imágenes médicas de alta calidad. Por otro lado también pone de relieve la boga de esta área de investigación, con descubrimientos y artículos publicados de forma continuada en los últimos 20 años, y en la más cercana actualidad (2013).

La intención de este proyecto es, pues, profundizar en la investigación dentro de esta área con el objetivo de encontrar una metodología compacta para la caracterización de matrices de transductores de ultrasonidos. Debido a que el proceso de caracterización es difícil y costoso, requiriendo de profesionales altamente preparados y experimentados, como muestran [4]-[16] y otros, el presente estudio aspira a encontrar un procedimiento menos arduo que siga permitiendo la caracterización de transductores de ultrasonidos.

El Diccionario de Cambridge define caracterización como *"la manera en que algo es descrito mediante la exposición de sus principales características"*, [25]. Por lo tanto, cuando se ha de enfrentar un proyecto tal y como la caracterización de transductores de ultrasonidos, el primer paso que ha de ser tomado en consideración es, precisamente, el delimitar cuales son estas características principales, y como pueden ser determinadas y expuestas.

La caracterización de transductores de ultrasonidos es una tarea complicada, debido a que los

transductores son complejos dispositivos electromecánicos, que involucran una combinación de componentes eléctricos y mecánicos, [27]. Tal y como se muestra en la literatura hay multitud de parámetros que definen a los transductores, basados en sus propiedades eléctricas, acústicas o químicas. Este proyecto se centrará en las características acústicas de dichos dispositivos. Otros parámetros como la impedancia eléctrica, la repuesta en transmisión y recepción o el calentamiento de los transductores quedan fuera del ámbito del presente estudio. Se hace referencia a [4]-[16], [21] y [23]-[24], si el lector desea consultar investigaciones sobre la caracterización de transductores de ultrasonidos en función de otros parámetros.

C.4 Objetivos

La principal meta del presente proyecto es definir un procedimiento de caracterización de las propiedades acústicas de transductores de ultrasonidos basado en un único experimento consistente en la medición del campo de presión por ellos generado.

Con este fin se persiguen dos objetivos: El primero es encontrar cuánta información puede ser obtenida a través de una medición llevada a cabo sobre una matriz de transductores en emisión. Con esta finalidad se procesarán los datos obtenidos mediante una medición del campo de presión en Junio de 2012 para estimar, a partir de ellos, las posiciones de los elementos de la matriz, su directividad, patrón de radiación y ángulo de aceptación.

El segundo objetivo es desarrollar modelos que repliquen la configuración del experimento estudiado y evaluar su comportamiento en presencia de ruido. Se modificarán los distintos parámetros del experimento con el fin de diseñar una configuración óptima para el mismo que permita la obtención de los datos necesarios para la determinar de forma precisa las propiedades del transductor de ultrasonidos.

C.5 Estructura

Tras este capitulo introductorio, los conceptos teóricos necesarios para entender los métodos y resultados de este proyecto se explicarán en el **Capítulo 2**.

Tras ello, el **Capítulo 3** trata en profundidad los parámetros de caracterización, así como los métodos para obtenerlos a partir de mediciones del campo de presión.

El **Capítulo 4**, por su parte, está dedicado a presentar modelos teóricos de dichas mediciones con el objetivo de evaluar las posibilidades que distintos experimentos ofrecen en términos de eficiencia y precisión.

Finalmente el **Capítulo 5** (y el **apéndice D** en castellano) resume los resultados y conclusiones a las que se ha llegado en esta investigación, haciendo hincapié en en las posibilidades que abre de cara a futuras investigaciones en este campo.

APPENDIX **D**

Conclusión

La importancia del diagnóstico a través de ecografías en el campo de la medicina, y por extensión en la sociedad, se debe, entre otros factores, al hecho de que los sistemas de ultrasonidos son relativamente baratos comparados con otras técnicas de generación de imágenes médicas, así como fáciles de usar. Los transductores utilizados para emitir y recibir las señales de ultrasonidos son clave en el desarrollo de este tipo de sistemas y, por lo tanto, son un campo en el que se han desarrollado investigaciones continuas [4]-[13], tanto en los últimos años como todavía en la actualidad.

Este proyecto se ha centrado en la caracterización de estos transductores de ultrasonidos y, en particular, ha estudiado la viabilidad de utilizar un procedimiento experimental simplificado y condensado para caracterizar dichos dispositivos. Con este propósito, se ha considerado un experimento consistente en la medición del campo de presión generado por una matriz de transductores de 32x32 elementos, tal y como ha sido descrito en el capítulo 3.

Los datos de presión obtenidos en Junio de 2012 han sido analizados y a partir de ellos se han desarrollado métodos para derivar la directividad, el ángulo de aceptación, los patrones de radiación y la localización espacial de cada uno de los elementos de la matriz de transductores. En este proceso, la evaluación de la localización espacial de los elementos de transductor ha demostrado ser crucial para caracterizar sus propiedades, siendo de especial importancia para el análisis de los patrones de directividad.

La perfecta estimación de las coordenadas de los elementos de la matriz de transductores no ha sido lograda, aunque distintas estrategias, como el algoritmo RANSAC han sido investigadas para mejorarla. Se han diseñado métodos para superar el problema de estimaciones imprecisas, que han demostrado ser efectivos a la hora de evaluar los patrones de directividad y ángulos de aceptación de elementos con coordenadas inexactas.

A lo largo de este proyecto se han derivado valores para los ángulos de aceptación a distintos niveles y se ha mostrado como estos resultados concuerdan con los obtenidos, a través de otros métodos, por investigadores de la rama. Además, el comportamiento espacio-temporal de los campos de presión ha sido derivado a partir de las mediciones experimentales. También se ha desarrollado una metodología para suprimir la influencia que las características del dispositivo de medida, es decir del hidrófono, tienen sobre los resultados del experimento; así como un procedimiento para detectar aquellos elementos de la matriz de transductores que estén deteriorados o no emitan señales. En resumen, se ha demostrado que las características acústicas de los elementos de la matriz de transductores pueden ser derivadas, o al menos

aproximadas fielmente, a partir de los datos de un único experimento.

Cabe destacar que el proceso no carece de complejidad ni de inconvenientes. Han sido necesarias estimaciones precisas y un gran volumen de computación para optimizar los resultados, demostrando que el trabajar con grandes cantidades de datos puede resultar complicado y requiere tiempos de computación prolongados, por ello los esfuerzos han de ir destinado a reducir la cantidad de datos necesarios para ejecutar la caracterización.

En consecuencia, dos modelos teóricos han sido desarrollados para reproducir el experimento real, con la intención de mejorar la calidad de los datos obtenidos. El objetivo ha sido diseñar un experimento que pudiera producir datos relevantes para ser utilizados por investigadores y desarrolladores a la hora de obtener la información suficiente para caracterizar transductores de ultrasonidos de forma óptima.

Los efectos del ruido, del número de mediciones y de la posición espacial de los dispositivos involucrados en el experimento han sido estudiados usando un modelo simplificado basado en los tiempos de vuelo (tiempo que tarda la señal en propagarse desde el transductor hasta el hidrófono). Los resultados de investigar diferentes variaciones de las condiciones experimentales han permitido sugerir una serie de recomendaciones para llevar a cabo un experimento óptimo.

Con el objetivo de evaluar la metodología del cálculo de los tiempos de vuelo así como probar su resistencia a mediciones ruidosas, se ha desarrollado un modelo complejo que toma en consideración el proceso de estimación de dichos valores. El importante número de suposiciones utilizadas para desarrollar este modelo limitan la validez de sus resultados. Sin embargo, ha demostrado ser útil para valorar los efectos que el ruido tiene en la estimación de de las coordinadas de los elementos de la matriz de transductores así como para detectar las limitaciones del método utilizado para derivar estas coordenadas a partir de los datos experimentales.

La combinación del estudio de los modelos descritos con el análisis de los problemas observados en el proceso de obtención de los parámetros de caracterización, ha hecho posible delimitar las recomendaciones para ejecutar un experimento de medida del campo de presión óptimo: En este tipo de experimentos debe asegurarse, en base a los resultados obtenidos en las investigaciones desarrolladas en este proyecto, el utilizar un número adecuado de mediciones así como que estas mediciones se hagan en posiciones cercanas a la matriz de transductores. A la par que debe evitarse escoger posiciones del hidrófono con ángulos demasiado amplios respecto a la normal de la matriz, entre otras recomendaciones recogidas en la sección 4.17. Una continuación lógica de la presente investigación sería llevar a la práctica dicho experimento y verificar que, siguiendo estas recomendaciones, el conjunto de datos obtenidos permite una caracterización del transductor de ultrasonidos más sencilla y compacta.

Este proyecto ha puesto sobre la mesa la posibilidad de simplificar el proceso de caracterización de transductores de ultrasonidos, pero está lejos de ser es una línea de investigación cerrada. Nuevas posibilidades derivadas de esta investigación incluyen la optimización del método de estimación espacial de los elementos del transductor, la simplificación y automatización de las rutinas de caracterización o la expansión del número de parámetros a obtener de los datos del experimento descrito en esta memoria, entre otras.

Si la definición de Caracterización es consultada de nuevo en estas últimas líneas de la memoria como *"la manera en que algo es descrito mediante la exposición de sus principales características"* , [25], ha quedado manifiesto en este proyecto que el describir los transductores de ultrasonidos mediante sus características principales es una labor ardua y compleja en la que multitud de aspectos y parámetros han de ser considerados, ya que para describir estos dispositivos es necesario analizar sus propiedades tanto mecánicas, como eléctricas y acústicas.

El proceso de caracterización acústica llevado a cabo en este proyecto ha tratado de simplificar la obtención de los parámetros característicos de un transductor de ultrasonidos y ha mostrado que es posible, de hecho, conseguir los datos necesarios a partir de un único experimento. Queda abierta como futura línea de investigación la mejora de los métodos aquí desarrollados, así como la ampliación del número de características que podrían ser inferidas de una medición del campo de presión de un transductor.

APPENDIX **E**

Presupuesto

1) Ejecución Material	
• Compra de ordenador personal (Software incluido)	1.500 €
• Material de oficina	200 €
2) Honorarios Proyecto	
• 1200 horas a 18 €/ hora	21.600 €
3) Material fungible	
• Gastos de impresión	200 €
• Encuadernación	50 €
4) Subtotal del presupuesto	
• Subtotal Presupuesto	23.550 €
5) I.V.A. aplicable	
• 21% Subtotal Presupuesto	4.945,5 €
6) Total presupuesto	
• Total Presupuesto	28.495,5 €

Madrid, Abril 2014.
La Ingeniera Jefa de Proyecto

Fdo.: Helia Relaño Iborra
Ingeniera Superior de Telecomunicación

APPENDIX **F**

Pliego de condiciones

Pliego de condiciones

Este documento contiene las condiciones legales que guiarán la realización, en este proyecto, de una *Caracterización de Transductores de Ultrasonidos*. En lo que sigue, se supondrá que el proyecto ha sido encargado por una empresa cliente a una empresa consultora con la finalidad de realizar dicho sistema. Dicha empresa ha debido desarrollar una línea de investigación con objeto de elaborar el proyecto. Esta línea de investigación, junto con el posterior desarrollo de los programas está amparada por las condiciones particulares del siguiente pliego.

Supuesto que la utilización industrial de los métodos recogidos en el presente proyecto ha sido decidida por parte de la empresa cliente o de otras, la obra a realizar se regulará por las siguientes:
Condiciones generales.

1. La modalidad de contratación será el concurso. La adjudicación se hará, por tanto, a la proposición más favorable sin atender exclusivamente al valor económico, dependiendo de las mayores garantías ofrecidas. La empresa que somete el proyecto a concurso se reserva el derecho a declararlo desierto.

2. El montaje y mecanización completa de los equipos que intervengan será realizado totalmente por la empresa licitadora.

3. En la oferta, se hará constar el precio total por el que se compromete a realizar la obra y el tanto por ciento de baja que supone este precio en relación con un importe límite si este se hubiera fijado.

4. La obra se realizará bajo la dirección técnica de un Ingeniero Superior de Telecomunicación, auxiliado por el número de Ingenieros Técnicos y Programadores que se estime preciso para el desarrollo de la misma.

5. Aparte del Ingeniero Director, el contratista tendrá derecho a contratar al resto del personal, pudiendo ceder esta prerrogativa a favor del Ingeniero Director, quien no estará obligado a aceptarla.

6. El contratista tiene derecho a sacar copias a su costa de los planos, pliego de condiciones y presupuestos. El Ingeniero autor del proyecto autorizará con su firma las copias solicitadas por el contratista después de confrontarlas.

7. Se abonará al contratista la obra que realmente ejecute con sujeción al proyecto que sirvió de base para la contratación, a las modificaciones autorizadas por la superioridad o a las órdenes que con arreglo a sus facultades le hayan comunicado por escrito al Ingeniero Director de obras siempre que dicha obra se haya ajustado a los preceptos de los pliegos de condiciones, con arreglo a los cuales, se harán las

modificaciones y la valoración de las diversas unidades sin que el importe total pueda exceder de los presupuestos aprobados. Por consiguiente, el número de unidades que se consignan en el proyecto o en el presupuesto, no podrá servirle de fundamento para entablar reclamaciones de ninguna clase, salvo en los casos de rescisión.

8. Tanto en las certificaciones de obras como en la liquidación final, se abonarán los trabajos realizados por el contratista a los precios de ejecución material que figuran en el presupuesto para cada unidad de la obra.

9. Si excepcionalmente se hubiera ejecutado algún trabajo que no se ajustase a las condiciones de la contrata pero que sin embargo es admisible a juicio del Ingeniero Director de obras, se dará conocimiento a la Dirección, proponiendo a la vez la rebaja de precios que el Ingeniero estime justa y si la Dirección resolviera aceptar la obra, quedará el contratista obligado a conformarse con la rebaja acordada.

10. Cuando se juzgue necesario emplear materiales o ejecutar obras que no figuren en el presupuesto de la contrata, se evaluará su importe a los precios asignados a otras obras o materiales análogos si los hubiere y cuando no, se discutirán entre el Ingeniero Director y el contratista, sometiéndolos a la aprobación de la Dirección. Los nuevos precios convenidos por uno u otro procedimiento, se sujetarán siempre al establecido en el punto anterior.

11. Cuando el contratista, con autorización del Ingeniero Director de obras, emplee materiales de calidad más elevada o de mayores dimensiones de lo estipulado en el proyecto, o sustituya una clase de fabricación por otra que tenga asignado mayor precio o ejecute con mayores dimensiones cualquier otra parte de las obras, o en general, introduzca en ellas cualquier modificación que sea beneficiosa a juicio del Ingeniero Director de obras, no tendrá derecho sin embargo, sino a lo que le correspondería si hubiera realizado la obra con estricta sujeción a lo proyectado y contratado.

12. Las cantidades calculadas para obras accesorias, aunque figuren por partida alzada en el presupuesto final (general), no serán abonadas sino a los precios de la contrata, según las condiciones de la misma y los proyectos particulares que para ellas se formen, o en su defecto, por lo que resulte de su medición final.

13. El contratista queda obligado a abonar al Ingeniero autor del proyecto y director de obras así como a los Ingenieros Técnicos, el importe de sus respectivos honorarios facultativos por formación del proyecto, dirección técnica y administración en su caso, con arreglo a las tarifas y honorarios vigentes.

14. Concluida la ejecución de la obra, será reconocida por el Ingeniero Director que a tal efecto designe la empresa.

15. La garantía definitiva será del 4

16. La forma de pago será por certificaciones mensuales de la obra ejecutada, de acuerdo con los precios del presupuesto, deducida la baja si la hubiera.

17. La fecha de comienzo de las obras será a partir de los 15 días naturales del replanteo oficial de las mismas y la definitiva, al año de haber ejecutado la provisional, procediéndose si no existe reclamación alguna, a la reclamación de la fianza.

18. Si el contratista al efectuar el replanteo, observase algún error en el proyecto, deberá comunicarlo en el plazo de quince días al Ingeniero Director de obras, pues transcurrido ese plazo será responsable de la exactitud del proyecto.

19. El contratista está obligado a designar una persona responsable que se entenderá con el Ingeniero Director de obras, o con el delegado que éste designe, para todo relacionado con ella. Al ser el Ingeniero Director de obras el que interpreta el proyecto, el contratista deberá consultarle cualquier duda que surja en su realización.

20. Durante la realización de la obra, se girarán visitas de inspección por personal facultativo de la empresa cliente, para hacer las comprobaciones que se crean oportunas. Es obligación del contratista, la conservación de la obra ya ejecutada hasta la recepción de la misma, por lo que el deterioro parcial o total de ella, aunque sea por agentes atmosféricos u otras causas, deberá ser reparado o reconstruido por su cuenta.

21. El contratista, deberá realizar la obra en el plazo mencionado a partir de la fecha del contrato, incurriendo en multa, por retraso de la ejecución siempre que éste no sea debido a causas de fuerza mayor. A la terminación de la obra, se hará una recepción provisional previo reconocimiento y examen por la dirección técnica, el depositario de efectos, el interventor y el jefe de servicio o un representante, estampando su conformidad el contratista.

22. Hecha la recepción provisional, se certificará al contratista el resto de la obra, reservándose la administración el importe de los gastos de conservación de la misma hasta su recepción definitiva y la fianza durante el tiempo señalado como plazo de garantía. La recepción definitiva se hará en las mismas condiciones que la provisional, extendiéndose el acta correspondiente. El Director Técnico propondrá a la Junta Económica la devolución de la fianza al contratista de acuerdo con las condiciones económicas legales establecidas.

23. Las tarifas para la determinación de honorarios, reguladas por orden de la Presidencia del Gobierno el 19 de Octubre de 1961, se aplicarán sobre el denominado en la actualidad "Presupuesto de Ejecución de Contrata" y anteriormente llamado "Presupuesto de Ejecución Material" que hoy designa otro concepto.

Condiciones particulares.

La empresa consultora, que ha desarrollado el presente proyecto, lo entregará a la empresa cliente bajo las condiciones generales ya formuladas, debiendo añadirse las siguientes condiciones particulares:

1. La propiedad intelectual de los procesos descritos y analizados en el presente trabajo, pertenece por entero a la empresa consultora representada por el Ingeniero Director del Proyecto.

2. La empresa consultora se reserva el derecho a la utilización total o parcial de los resultados de la investigación realizada para desarrollar el siguiente proyecto, bien para su publicación o bien para su uso en trabajos o proyectos posteriores, para la misma empresa cliente o para otra.

3. Cualquier tipo de reproducción aparte de las reseñadas en las condiciones generales, bien sea para uso particular de la empresa cliente, o para cualquier otra aplicación, contará con autorización expresa y por escrito del Ingeniero Director del Proyecto, que actuará en representación de la empresa consultora.

4. En la autorización se ha de hacer constar la aplicación a que se destinan sus reproducciones así como su cantidad.

5. En todas las reproducciones se indicará su procedencia, explicitando el nombre del proyecto, nombre del Ingeniero Director y de la empresa consultora.

6. Si el proyecto pasa la etapa de desarrollo, cualquier modificación que se realice sobre él, deberá ser notificada al Ingeniero Director del Proyecto y a criterio de éste, la empresa consultora decidirá aceptar o no la modificación propuesta.

7. Si la modificación se acepta, la empresa consultora se hará responsable al mismo nivel que el proyecto inicial del que resulta el añadirla.

8. Si la modificación no es aceptada, por el contrario, la empresa consultora declinará toda responsabilidad que se derive de la aplicación o influencia de la misma.

9. Si la empresa cliente decide desarrollar industrialmente uno o varios productos en los que resulte parcial o totalmente aplicable el estudio de este proyecto, deberá comunicarlo a la empresa consultora.

10. La empresa consultora no se responsabiliza de los efectos laterales que se puedan producir en el momento en que se utilice la herramienta objeto del presente proyecto para la realización de otras aplicaciones.

11. La empresa consultora tendrá prioridad respecto a otras en la elaboración de los proyectos auxiliares que fuese necesario desarrollar para dicha aplicación industrial, siempre que no haga explícita renuncia a este hecho. En este caso, deberá autorizar expresamente los proyectos presentados por otros.

12. El Ingeniero Director del presente proyecto, será el responsable de la dirección de la aplicación industrial siempre que la empresa consultora lo estime oportuno. En caso contrario, la persona designada deberá contar con la autorización del mismo, quien delegará en él las responsabilidades que ostente.